QATAR UNIVERSITY

COLLEGE OF ENGINEERING

NUMERICAL SIMULATION OF DYNAMIC RESPONSE FOR MISALIGNMENT IN COUPLED SHAFTS

BY

MOHAMED DESOUKI DESOUKI

A Thesis Submitted to

the Faculty of the College of Engineering

in Partial Fulfillment of the Requirements for the Degree of

Masters of Science in Mechanical Engineering

June 2019

COMMITTEE PAGE

The members of the Committee approve the Thesis of
Mohamed Desouki Desouki defended on 16/04/2019.

Dr. Sadok Sassi
Thesis/Dissertation Supervisor

Name
Committee Member

Name
Committee Member

Name
Committee Member

Add Member

Approved:

Abdel Magid Hamouda , Dean, College of Engineering

ABSTRACT

DESOUKI,MOHAMED,D.,Masters:June:[2019:]

Masters of Science in Mechanical Engineering

Title: Numerical Simulation of Dynamic Response for Misalignment in Coupled Shafts

Supervisor of Thesis: Sadok, Sassi.

Preceded by unbalance, misalignment is the second most common fault in rotating machinery. The impact of misalignment fault on equipment can be severe and may considerably shorten the machine's lifetime. This dissertation discusses the unbalance, parallel and angular misalignment forces on rotative machines' vibration spectra. Numerical simulation model development is used to obtain the time and frequency responses of the rotor-coupling-bearing system. The parallel and angular misalignment response are synchronized with the 1X amplitude of the unbalance displacement. Moreover, the parallel misalignment fault magnifies the 2X amplitude while the angular misalignment response is captured at 2X and 4X amplitudes of the displacement response. Effects of changing the model's rotational speed, misalignment level, and coupling type are examined for both parallel and angular misalignments.

DEDICATION

This report is dedicated to the inspiration source of my journey through my Master's degree. Special thanks to my supervisor who always elevated my thrust whenever life circumstances were tough. Finally, this work is dedicated to my family, my wife, my best friend, and work colleagues for their support and believe in me.

TABLE OF CONTENTS

LIST OF TABLES

LIST OF FIGURES

CHAPTER 1: INTRODUCTION

Rotating machines are available in most of the industrial fields nowadays. They are available in almost all dimensions: from the gyroscopic level, like tuition bench-scale machines, up to the mega level like power plants. As industrial technology is growing, the need for higher speed and powerful equipment became an essential factor to cope up with the fast world transformations. Therefore, the rotor-dynamic filed had gained huge attention in recent years. One of the most important parts of any rotating machine is the coupling. Couplings are defined as the connecting elements between different shafts. A second purpose of using couplings are their ability to compensate for misalignment in the dynamic system. There are numerous types of couplings available today in the market which can be classified by more than one categorization as the method it accommodates misalignment. Misalignment can be defined as the rotation of the coupled shafts when the rotational axes of the shafts are not collinear. Increasing efforts to explain the misalignment behavior in the rotor-dynamic lead to the less usage of experimental approach in favor of the numerical simulation approach. The experimental methods include vibration analysis, temperature capturing, torque and motor current consumption while the simulation methods include structural analysis, finite element analysis, and mathematical derivations. Among all, the vibration spectrum is the most widely accepted method to capture misalignment fault. This study contributes to the state of art by developing a numerical program capable of evaluating the vibration response of misaligned shafts which is independent of the force derivation method. In other words, a numerical model is a simple tool which can be used with any other misalignment forces derivations (linear or nonlinear). In this chapter, types of couplings, misalignment faults and thesis objectives and outline will be discussed.

1.1.Types of couplings

There are numerous types of mechanical couplings classified based on the method of power transmission and the method of accounting for misalignment. The mechanical couplings are divided into two major types, depending on the ability of the coupling to perform any elastic behavior on the shafts. These two types are rigid and flexible couplings. The selection of the suitable shaft coupling type depends on numerous factors. In case some of these factors interact with each other (which is usually the case) decision should be made by prioritizing these factors. The main factors are: a) Torque limit of the system, b) Misalignment introduced in the system and its type, c) Torsional vibration dampening required in the coupling, d) Torsional stiffness required in the coupling, e) stresses on the supporting bearings by couplings (reactive) in case of misalignment, f) coupling maintainability and life period, g) coupling performance compared to its cost (Mancuso, Zilberman, Corcoran, & D'Ercole, 1994).

1.1.1. Rigid couplings

Rigid couplings are couplings that do not perform any (sometimes negligible effect) elastic behavior on the shafts. The coupling is connected to the shaft using a key or compression effect. Generally, rigid couplings are used when the misalignment of the shaft is precisely small as the increase in the misalignment will affect the coupling performance and its effective life. In other words, whenever the two shafts are expected to be near coaxial case, rigid couplings can be used. The critical disadvantages of a rigid coupling are: a) it doesn't account for shafts misalignment, b) it creates large bending stress on the shafts and bearings in case misalignment existed, c) it transmits the shock and impact loads. The main types of rigid couplings are:

- Flange Coupling.
- Sleeve or Muff Coupling.
- Clamp Coupling.
- Hirth coupling and other types.

1.1.1.1.Flange coupling

In this type of couplings, the rotating shafts are connected to flanges (one fixed to the end of the driving shaft and the other one joined to the end of the driven shaft by means of keys usually), and these two flanges are bolted together with a ring of bolts on a circle called bolt circle. Sometimes, the flanges are provided with spigot and recess to be located. Figure 1 illustrates the flange coupling assembly.

Figure 1: Flange coupling assembly.

As the figure shows, the two half couplings are bolted together (using six equiangular spaced bolts) for a given flange thickness. The number of bolts depends on the standard which has been followed (normally related to the shaft diameter). The two shafts are inserted in the coupling hubs of diameter D (each of the same width) and

locked with keys. The flange diameter is proportional to the shaft diameter as per engineering institutes. The power generated by the driving shaft is transferred to the driven shaft by force (load) on the bolts. Therefore, the most critical elements in the flange coupling are the bolts which have two general cases. The first case is when there is a clearance between the bolts and the flange holes. In this case, the distributed force generated from the applied torque on the flange will be transferred in a friction force (normal force from flanges on bolts) between the bolt and flange holes. The second case is when there is no clearance between the bolts and the flange holes. In this case, the failure is most likely to occur due to the shearing of bolts across the flanges mating surface (FESSLER, 2013).

1.1.1.2.Sleeve or muff coupling

In this type of couplings, the two rotating shafts are connected to one sleeve by means of keys or compression. The sleeve is basically a pipe which has a keyway on the internal surface (and sometimes keyway is not required). The sleeve coupling can be of different shapes as the well-known box coupling. Figure 2 illustrates the Sleeve coupling assembly.

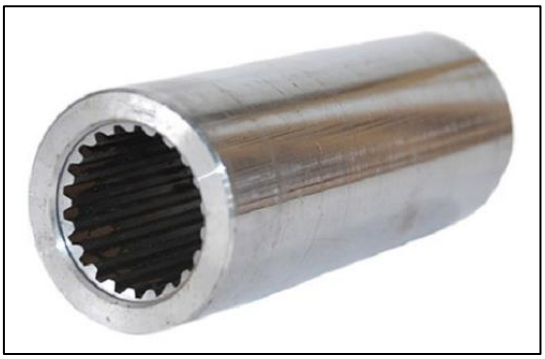

Figure 2: Sleeve coupling assembly.

The sleeve usually has a keyway on its bore to be of the same type and dimension of the keyway on the shafts. The bore size is of a high tolerance to allow the shaft to be fitted smoothly in case of a key to be used. The sleeve diameter is proportional to the shaft diameter as per standards. Usually, threaded holes are in the sleeve to allow for locking of coupling position. In case of not using a keyway, an interference fit is taking place between the shafts and the sleeve. In other words, the sleeve is pressed against the shaft and usually shrink fit process is followed. Shrink fit is (based on metals thermal expansion principle) to heat the sleeve to a certain temperature in special oven until it expands and then to place it in the proper location on shafts while cooling down. The power transmission from the drive shaft to the driven shaft depends on whether a key is used, or interference fit is used as a coupling element. In case of the interference fit, the stress will be generated on the sleeve bore in the radial and hoop directions (due to the high frictional force). In case of usage of a key to couple the shaft to the sleeve, the force will be applied on the sleeve's keyway side as the shaft rotates.

1.1.1.3.Clamp coupling

Clamp coupling is a muff coupling in two parts connected by bolts (split sleeve). The shafts are connected to the coupling by means of keys or sometimes compression type clamp is used. Clamp couplings are mainly used when the application requires no disturbance to the shafts' positions while installing and removing the coupling. Figure 3 illustrates the clamp coupling assembly.

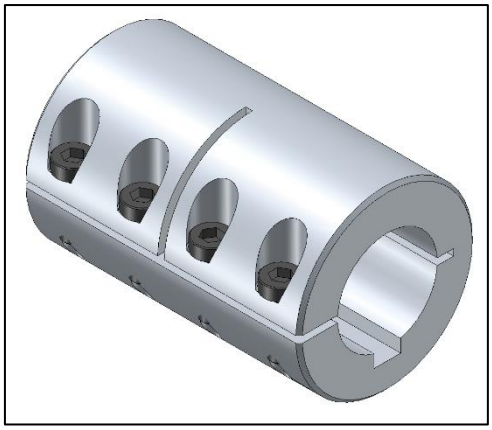

Figure 3: Clamp coupling assembly.

As shown, the two parts of the clamp are connected using bolts. A number of bolts, clamp diameter, and clamp length is related to the shaft diameter as per standards. The power transmission from the driver to the driven shafts depends on whether a key is used, or interference fit is used as a coupling element. In both cases, the forces and stresses introduced in the coupling and key are the same as explained for the sleeve couplings.

1.1.1.4.Other types

There are other coupling types and some of them are been used in industry while others are still under research development. One coupling type is Hirth coupling in which the rotating shafts are connected together by means of tapered teeth flanges that mesh together at the shafts end surface. As the power is transmitted from one shaft to the other by the meshed teeth, the material used for this type of coupling is usually of high toughness. Another coupling type which had been used in industry is a compression coupling. This coupling has a similar working principle as the clamp coupling but with two differences. First, the coupling consists of one part (not two parts as clamp coupling) to which a tightening bolt is connected (whenever bolts are

tightened, the clamping force is increased and hence increasing friction force). Second, a metallic wedge is inserted between the coupling sleeve and the shaft which the power is transmitted through.

1.1.2. Flexible couplings

Flexible couplings are couplings which perform an elastic behavior on the shafts. These couplings are mainly used to transfer power from one shaft to another when misalignment is presented. Flexible couplings can be considered as a securing element for the shafts beside its original function. It secures the shafts against any undesired or expected misalignment, shock loads or vibrations. It is a fact that not all misalignments can be maintained using flexible couplings. Depending on the type of the coupling which will be used in the system, the related axial, parallel (vertical or horizontal), angular misalignments could be sustained. A combination of different types of misalignments could occur in practice which will change the rating of the coupling for misalignments (Ming Xu & Marangoni, 2007). Flexible couplings can be classified into three types based on the flexibility source in the coupling as per various references in the machine's element field:

- Couplings with kinematic flexibility.
    - Cross sliding coupling.
    - Universal Joint.
    - Gear or toothed coupling.
    - Chain coupling and other types.
- Couplings with resilient members.
    - Elastomers.
    - Metallic membranes.
- Magnetic coupling.

1.1.2.1.Couplings with kinematic flexibility.

Kinematic flexible couplings are couplings that possess flexibility due to kinematic pairs inserted in the system. Kinematic pairs can provide an axial, parallel or angular flexibility. Depending on the coupling's degree of freedom and design parameters, the coupling sustains different types of misalignments. In most of the cases, kinematic flexibility couplings require the provision of lubrication in the system.

1.1.2.1.1. Cross sliding coupling

As the name of these types of couplings states, couplings of this type have sliding members which are sliding perpendicular to each other. The sliding motion of the coupling members provides parallel flexibility to the shaft's rotation. Oldham coupling is the most well-known coupling of this type. In this type of coupling, the rotating shafts are connected to two discs (one fixed to the driving shaft and the other one fixed to the driven shaft). The two discs connected to the shafts are then connected to each other by means of the third disc which can slide vertically in one side and horizontally on the other side. Figure 4 illustrates the Oldham coupling assembly.

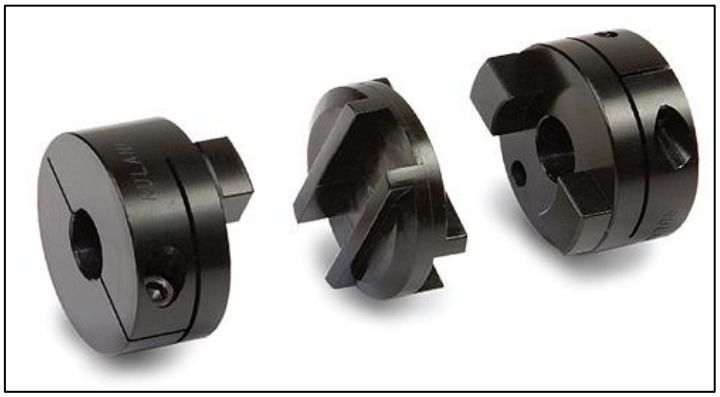

Figure 4: Oldham coupling assembly.

As shown, the middle disc is connected to the shafts' discs by means of groove and tongue. The middle disc tongue on one side is perpendicular to the tongue on the other side. Once the coupling is compacted, the middle disc will have the same rotational speed as the shafts' discs, but its center of rotation is a circular orbit around the midpoint between the driver and driven shafts. Oldham couplings are used when angular misalignment doesn't exist in the system (or exists in a small range) as it can accommodate for large parallel (radial) misalignment but not angular. Power is transferred from the driving shaft to the driven shaft by applying the torque first to the driver shaft key (as discussed in rigid couplings) and then to the middle disc of the coupling. The middle floating disc contact with the other two discs has two arrangement. It can be connected with clearance or with no clearance. In case there is no clearance, the total torque load generated by the driver shaft is acting on the middle disc tongue. The tongue will have the maximum load on the edges (as one edge is driven by the driver shaft and the other is driving the driven shaft) and minimum in the middle. As the load is minimum on the middle, sometimes the discs are hollow. In the other case where the clearance exists between the contacting tongues and grooves, a higher safety factor should be considered. It is significant to note that due to the eccentric rotation of the middle disc, a centrifugal force is resulting in a bending moment on shafts (therefore, the weight of the floating member should be kept as light as possible).

There are many types other than Oldham couplings that have cross sliding members to provide some parallel flexibility to the shaft. American flexible coupling is a coupling of similar kinematics as Oldham coupling but the main difference is its shape. American flexible coupling has half square recess on each half of the shafts' discs. The third disc (floating disc) is of a square cross-section which is sliding at the shaft discs edges to provide parallel flexibility to the shafts (FESSLER, 2013).

1.1.2.1.2. Universal joint

The universal joint is also known as hook's joint, Cardan joint and U-joint. In this type of couplings, the rotating shafts are connected to each other by a special kind of pin – cross pin (or sometimes two pins are used). Each shaft is connected to a sleeve of a solid hinge shape. Figure 5 illustrates the universal joint assembly.

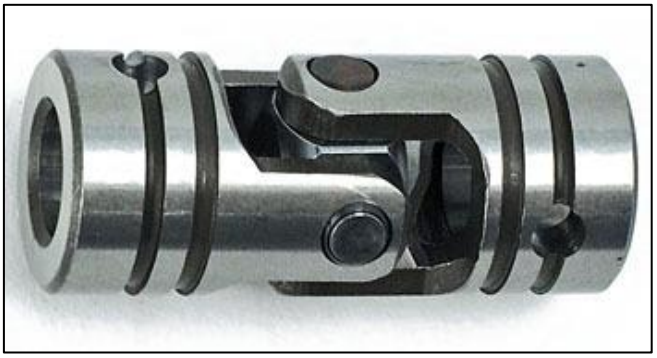

Figure 5: Universal joint coupling assembly.

As illustrated in the figure, the two hinges are connected to the rigid cross pin. This arrangement allows the shafts to have large angular flexibility (up to 45 degrees). The main drawback using this type of couplings that it could not be used in the applications where the constant speed of the shafts is required. In each quarter cycle of the driving shaft, the driven shaft angular position lacks behind the driver shaft (lower velocity) and then it speeds up to catch the driver shaft angular position by the end of the quarter cycle (higher velocity). In other words, the single U joint is classified to be a non-constant velocity joint as the driven shaft doesn't have the same speed of the drive shaft where the drive shaft has a constant velocity, and the driven shaft has an alternating velocity. To overcome the shafts velocity problem, double U joint can be used in a certain arrangement to have a constant velocity shaft.

1.1.2.1.3. Gear or toothed coupling

In this type of couplings, the rotating shafts are connected to with a geared hub taking advantage of gears flexibility. Figure 6 illustrates the gear coupling assembly.

Figure 6: Gear coupling assembly.

As shown in the figure, sleeve with teethed bores is connected to the two shafts' hubs. The flexibility member in this coupling is the tooth design and the amount of backlash introduced in the design. Increasing the backlash to a certain level increases the angular flexibility as well. Gear couplings allow for axial flexibility as the sleeve is designed to accommodate some axial movement of the shafts.

1.1.2.1.4. Chain coupling and other types

There are various other types of couplings that exert flexibility to the shafts by inserting kinematic pairs. Chain coupling is coupling with a similar working idea to the gear coupling but with a chain-sprocket been used as the flexibility pair instead of gears. Figure 7 illustrates the chain coupling assembly.

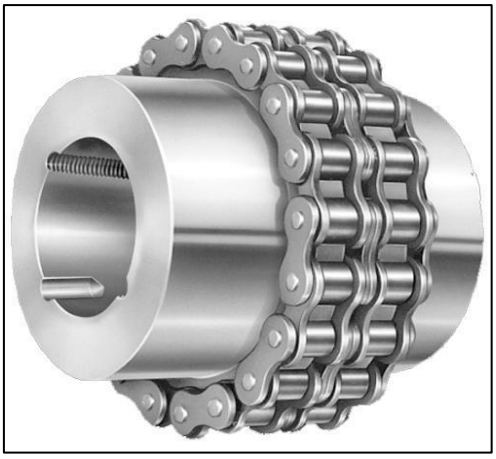

Figure 7: Chain coupling assembly.

As shown in the figure, each shaft is connected to a hub with sprockets on its external surface (usually connected by a key). Chains are connected to the sprockets and then covered by a grooved split sleeve which is usually connected by bolts. In some applications, a Nylon chain is used in order to introduce damping in the system. Another type of kinematic flexibility coupling is Schmidt coupling that is designed to account for large radial misalignments. Figure 8 illustrates the Schmidt coupling assembly which consists of three discs connected in series by means of links.

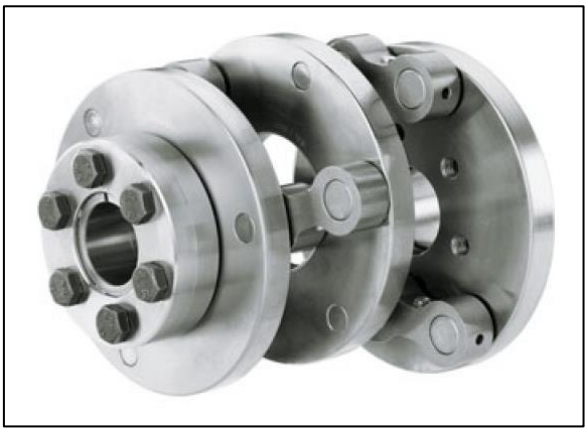

Figure 8: Schmidt coupling assembly plain and section.

1.1.2.2.Couplings with resilient members

Resilient member flexible couplings are couplings that possess flexibility due to a resilient member inserted in its system. The resilient member can provide an axial, parallel or angular flexibility. The major advantage of this type of coupling compared to other types is its shock loads absorbability. This type of flexible couplings requires no provision of lubrication in the system.

1.1.2.2.1. Elastomer members

In this type of couplings, the shafts are connected by a system of elements including an elastomer. The most widely used elastomer is rubber. They can be of any shape such as ring, bush, spider or sometimes more complex shapes. Elastomers can be used in many designs to be affected by shear force, compression force or both. Shock loads are absorbed by the inserted elastomer element. There are many types of elastomer couplings such as pin bush coupling, Jaw coupling, tyre coupling, and other types. Jaw coupling is one of the elastomeric couplings that is widely used in medium duty power transmission systems. This coupling consists of two metallic hubs (connected to the shafts by means of a key) and an elastomeric member called a spider. Figure 9 illustrates the jaw coupling assembly.

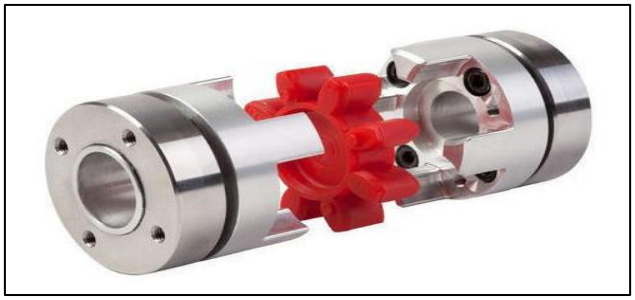

Figure 9: Jaw coupling assembly (FESSLER, 2013).

As shown, the spider element can have a different number of lobes to accommodate a different type of applications with its misalignment and vibration. One important notice about jaw coupling that in case a straight compression spider element fails, then the hubs will continue transmitting the torque till the next maintenance period. If the shear spider is used, then in case of its failure there will be no torque transmission by the hubs.

1.1.2.2.2. Metallic membrane

These types of couplings are a metallic coupling that possesses flexibility by using it in a thin (membrane) form. There are many types of metallic membranes used in these couplings such as spring grid, disc, and diaphragm. Figure 10 illustrates the metallic spring and spiral coupling assemblies.

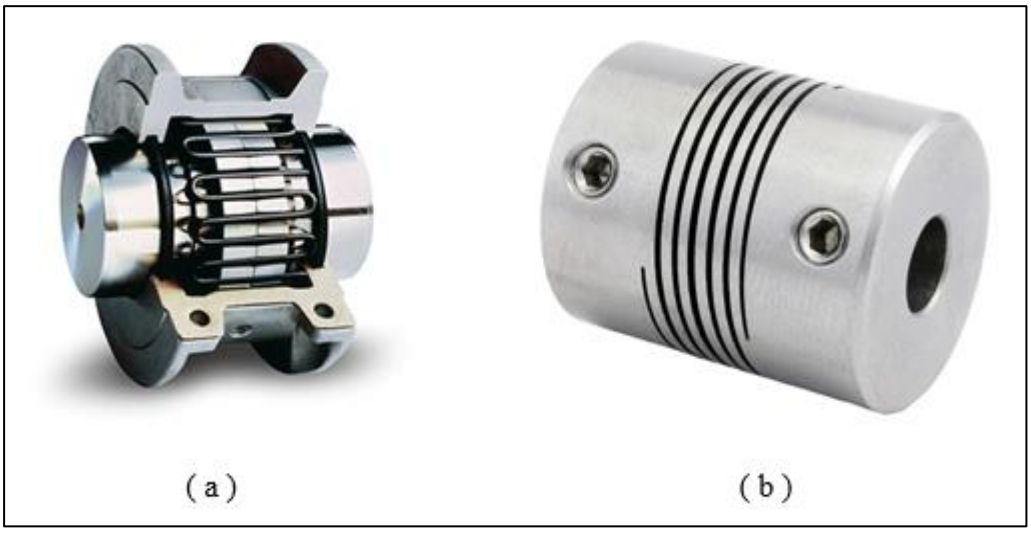

Figure 10: Metallic membrane couplings, a) spring coupling and b) spiral coupling.

As shown, the metallic spring coupling consists of two hubs slotted in a specific manner to allow the insertion of the spring through them. The spiral coupling is basically a pipe which has some material removal in a specific shape to give flexibility.

These types of couplings transmit high power rates compared to other resilience couplings due to the strength of the flexing membranes. Failure of this type of couplings is due to either excessive angular or radial misalignment or excessive torque.

1.1.2.3. Magnetic coupling

Magnetic coupling is a type of coupling where there is no physical contact between the driver and driven shafts; rather it is using the magnetic field to couple the shafts together. This type of coupling eliminates many mechanical failures such as mechanical seal failure, wearing of coupling elements and maintenance difficulties. Magnetic couplings allow for large parallel misalignment of shafts. Some of the difficulties using this type of coupling that it requires soft start, can't handle high torque applications and its large diameter. Figure 11 illustrates the magnetic coupling assembly.

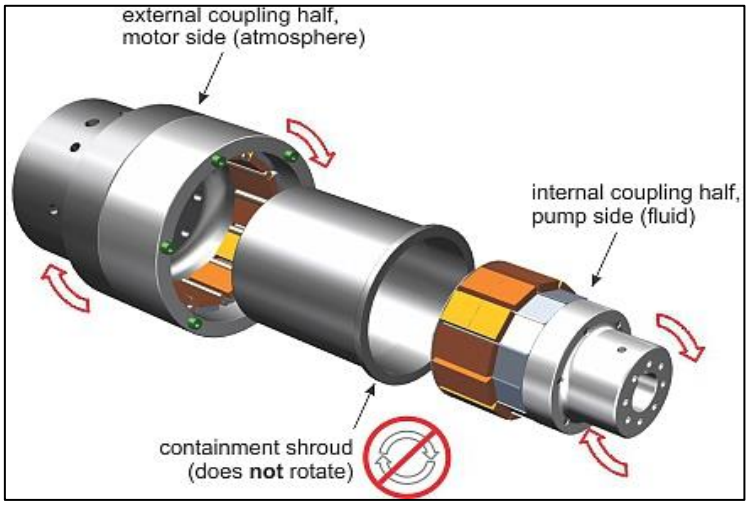

Figure 11: Magnetic coupling assembly.

As shown in the figure, the coupling is connected to the shafts by means of key or screws. The two magnetic flanges can be parallel to each other or to form a hub-

sleeve arrangement as shown. A series of magnets are located to the surface of each flange to allow for torque transfer between shafts. The clearance between the two flanges and the size of the flanges depend on the required torque transmission of the coupling (Engineer, Division, Corporation, Misalignment, & Misalignment, n.d.).

1.2. Misalignment in rotating shafts

Alignment is said to be the geometrically perfect combination of the rotating parts as described by the German engineers' society. However perfect alignment can't be achieved in practical situations. This is a result of the misalignment causes which can occur during operation. Misalignment is the condition at which the two coupled rotating drive and driven shafts don't rotate on the same centerline. Misalignment is the second most common fault in rotating machines after mass unbalance ("Shaft Alignment Handbook by John Piotrowski [Books and Reports]," 2005). In the current time, 60 to 70 percent of the failure of the rotating machine is because of misalignment faults. Moreover, misalignment fault leads to forces and moments development in the rotating system. Over the span of the last decade, misalignment detection techniques had developed due to technological improvements. However, modern technological tools availability is not the only factor needed to thoroughly understand misalignment behavior; it is also required to have a detailed mechanism to describe the misalignment phenomena. There are many experimental methods of predicting misalignment fault in the research state of the art such as motor current signals, torque signals, acoustics and vibration signals. The vibration-based diagnostic is the most common technique as its signals are of great mechanical information and more convenient to collect (Elbhbah & Sinha, 2013). Vibration response of the rotor-coupling-bearing system under misalignment fault had not yet been fully developed. Generally, a typical misalignment response can be considered to be a multiple of the shaft rotating speed especially the excessive 2X RPM amplitude. Recently, the numerical modeling of the misalignment fault had been increased such as mathematical derivation-based method, component mode method and finite element analysis method (Vermolen, 2005). Types, causes, and effects of misalignment will be discussed in this chapter.

1.2.1. Types of misalignment

There are two basic types of shafts misalignment in rotodynamic, namely parallel and angular misalignments. The misalignment in the industry is of a combined type of parallel and angular in both vertical and horizontal directions. Figure 12 shows the different types of misalignment.

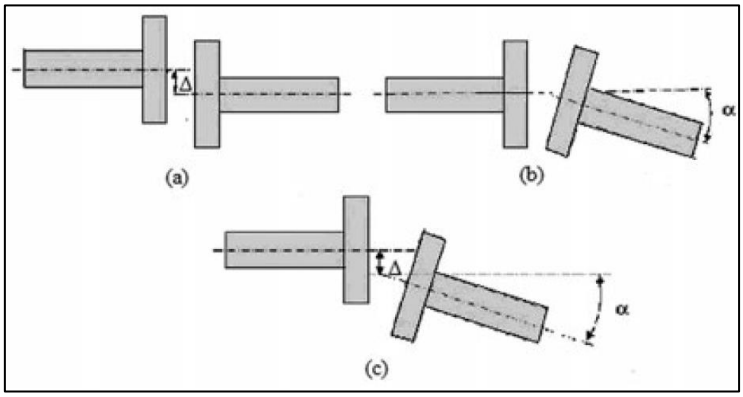

Figure 12: Types of misalignment, a) parallel, b) angular and c) combined.

As it is shown, parallel misalignment is when the axes of rotation are not colinear and does not intersect with each other. The parallel misalignment can be in both vertical and horizontal directions. On the other hand, angular misalignment is when the axes of rotation are not colinear and intersect each other. The combined misalignment is the existence of parallel and angular misalignments simultaneously. In the case of parallel misalignment, the vibration spectrum amplitudes are excessive in the radial direction (vertically and horizontally). Whereas, in the case of angular misalignment, the vibration spectrum amplitudes are excessive in the axial direction as well as the radial direction. It is predicted that in case of combined misalignment, the vibration amplitudes will be more than for any of the two types. Usually, the misalignment of the rotating shafts affects the system's balance and the vibration spectrum diagnosis ("Shaft Alignment Handbook by John Piotrowski [Books and Reports]," 2005).

1.2.2. Causes and effects of misalignment

There are many sources of misalignment in rotating machines. The major causes of shafts misalignment are installation errors, foundation settling or soft foot, lack of preventive maintenance and thermal expansion. Installation errors can be at the bearings (inner bearing to the shaft or outer bearing to the casing), improper welding of machine parts or at the coupling location. Likewise, foundation settling can be due to the age of the machine or the bad compaction of building ground. Furthermore, lack of preventive maintenance can always threaten the alignment of the shaft as it needs to be checked periodically. Thermal expansion is usually a common problem for the long shafts under the sunlight due to the seasonal temperature changes ("Shaft Alignment Handbook by John Piotrowski [Books and Reports]," 2005).

The important effects of shafts misalignment in rotating machines are equipment failure, energy loss, increased vibration, excessive heat, and noise. Firstly, when the machine is rotating under excessive misalignment, it will generate loads that can damage the equipment such as mechanical seal, coupling, and bearings. Secondly, when the machine is rotating under misalignment, the friction force at the bearings will increase which results in wasted energy and less efficient system. Thirdly, under high misalignment fault, the vibration response of all other machine faults will be hidden which leads to machine unreliability. Finally, as the machine heat increases, it will increase casing temperature and result in high lubrication oil discharge which can lead to increased oil replacement frequency ("Shaft Alignment Handbook by John Piotrowski [Books and Reports]," 2005).

Forces and moments due to misalignment of rotating machines depends on the type of coupling used in the system. If a rigid coupling is used, then the loads will be maximum on the system while flexible couplings compensate for part of these loads.

The machine shafts are at risk of damage or bowing due to the coupling restoring moment under misalignment condition.

1.3.Objectives and thesis outline

The objective of this thesis is to develop a numerical model capable to define parallel and angular misalignment faults and unbalanced rotating machine systems. This will be carried out by firstly, studying one type of flexible coupling (spiral) to predict its stiffnesses using (ABAQUS). Secondly, conducting an experimental work namely modal analysis to predict the coupling damping coefficients. Finally, to build-up a numerical simulation program to evaluate the time and frequency vibration response of the system using (MATLAB).

The report outline starts with chapter 1 - introduction about the types of couplings and misalignment faults. Then in chapter 2 – literature review for previous studies in this regard is studied by showing the numerical simulation models and experimental work done along with their vibration analysis. And then a discussion about the existing mathematical modeling of parallel and angular misalignment forces is presented. Chapter 3 discusses the model used in the current study and the mathematical derivation of the forces and moments exerted on the system due to misalignment. After that chapter 4 previews, the results of each type of misalignment and discusses its effect on the model. Finally, chapter 5 highlights the conclusions and future work of this study.

CHAPTER 2: LITERATURE REVIEW

Modeling of a rotor-coupling-bearing system (rigid or flexible) has gained an increasing interest in the past few years. Accurate modeling of the rotor-bearing-coupling system and its components is an indispensable factor in predicting the system dynamics (Chatelet, D'Ambrosio, & Jacquet-Richardet, 2005). Although the coupling misalignment is a common fault in rotating machines, the coupling misalignment forces and moments ambiguity hindered the growth of research in this field. Vibration response of misaligned coupled shafts had been studied through both experimental and numerical approaches. In this chapter, the experimental and numerical studies of the misalignment fault (both parallel and angular misalignments) were discussed. The vibration response of various models was investigated in order to relate it to the study results. Finally, the forces and moments in the rotor-coupling-bearing system due to misalignment fault were presented.

2.1. Vibration response of experimental and numerical simulation of the rotor-coupling-bearing system

The vibration spectrum of rotating machines was examined in some researches experimentally and numerically, but the results found were not always consistent. It is generally accepted for parallel misalignment to be the main source of 2X amplitude increase in the vibration spectrum. The 1X RPM was related to the parallel and angular misalignment in some studies, but on the contrary, it was not affected by misalignment in other studies. The effect of increasing rotational speed of system on the vibration spectrum was examined and found to affect the part of the spectrum amplitudes for parallel and angular misalignment. In addition, the angular misalignment was synchronized with 4X peaks and sometimes with even multiples of the RPM. Not only the low-frequency vibration spectrum was affected but the high-frequency spectrum also. The type of flexible coupling was found to affect the vibration spectrum.

2.1.1. Importance of flexible coupling modeling and its effect on vibration response

Most of the researchers had based their numerical coupling modeling publications work on the fundamental models which were enunciated by Kramer in 1993 (Krämer, 2013) and Nelson and Crandall in 1992 (Sekhar & Prabhu, 1995). Kramer suggested two different models for the coupling. The first model of Kramer considered the coupling as a rigid element (in the radial direction) with mass and inertia located at the nearest beam element node (i.e., 1 and 2). In this model, the shafts had been considered as a beam element (each of 8 DOF). The coupling modeling constrained the translational motion in i and j directions (hence $u_i = u_j$ and $v_i = v_j$). In other words, the shafts had been connected axially by the flexible coupling. The below figure illustrates Kramer's first model of a coupling:

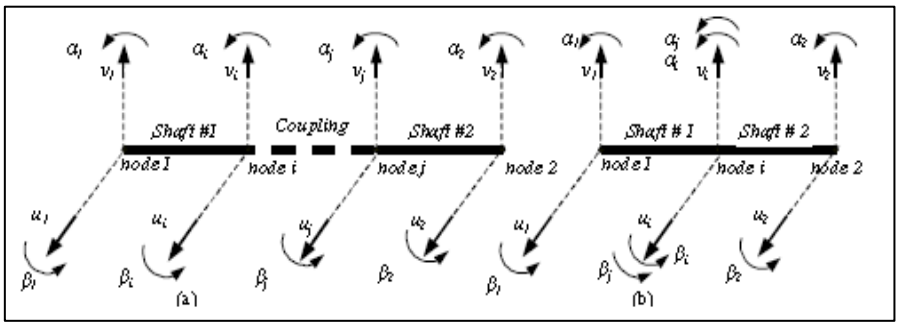

Figure 13: (a) Mechanical system of two shafts connected by a coupling, (b) Kramer's first model of the system (Krämer, 2013).

The governing equation of motion of Kramer's first coupling model is given as follows:

$$M_c \begin{Bmatrix} \ddot{q}_\iota \\ \ddot{q}_J \end{Bmatrix} + \Omega\, G_c \begin{Bmatrix} \dot{q}_\iota \\ \dot{q}_J \end{Bmatrix} = f_{ext} + f_{con} \qquad \text{Equation 1}$$

Where M_c is the mass matrix of components, $\ddot{q}_\iota$ and $\ddot{q}_J$ are the acceleration at nodes i and j, Ω is the shaft speed, $\dot{q}_\iota$ and $\dot{q}_J$ are the velocity at nodes i and j, G_c is the gyroscopic matrix of components and f_{ext} , f_{con} are the external forces and connecting forces vectors, respectively. Kramer's second model considered rotational stiffness K_r and rotational damping C_r while the restrictions on the first model is still present (constraint on the i and j translational movement). As the flexible coupling is represented by a flexible element with the mass distributed to the nearest nodes (i.e. i and j), the total degrees of freedom for this system is 8. Kramer's second model is illustrated below:

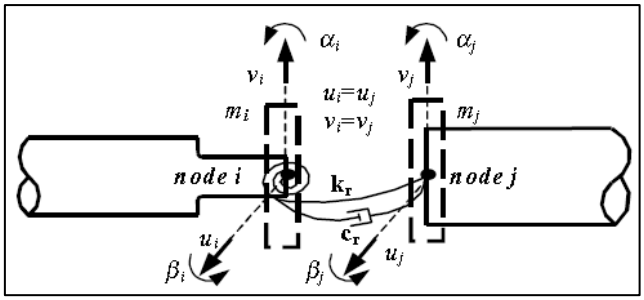

Figure 14: Kramer's second model of flexible coupling (Krämer, 2013).

The governing equation of motion of Kramer's second coupling model is given as follows:

$$M_a \begin{Bmatrix} \ddot{q}_i \\ \ddot{q}_j \end{Bmatrix} + (\Omega\, G_a + C_a) \begin{Bmatrix} \dot{q}_i \\ \dot{q}_j \end{Bmatrix} + K_a \begin{Bmatrix} q_i \\ q_j \end{Bmatrix} = f_{ext} + f_{con} \qquad \text{Equation 2}$$

Where C_a is the coupling damping matrix and K_a is the coupling stiffness matrix. The coupling mass, damping, gyroscopic and stiffness matrices for Kramer's second model is given in appendix 1.

Nelson and Crandall's first coupling model considered the flexible coupling as an elastic component with isotropic translational and rotational stiffnesses K_T and K_R, respectively. The coupling model didn't include inertia and mass effect. This model also has 8 degrees of freedom (4 translational and 4 rotational). The governing equation of motion of Nelson and Crandall's first coupling model is given as follows:

$$K_c \begin{Bmatrix} q_i \\ q_j \end{Bmatrix} = f_{ext} + f_{con} \qquad \text{Equation 3}$$

The second coupling model by Nelson and Crandall is similar to their first model but incorporating the translational and rotational damping in the system C_T and C_R, respectively. Moreover, the inertia effect had been added in this model as two rigid components. The governing equation of motion of Nelson and Crandall's second coupling model is given as follows:

$$M_a \begin{Bmatrix} \ddot{q}_i \\ \ddot{q}_j \end{Bmatrix} + (\Omega\, G_a + C_a) \begin{Bmatrix} \dot{q}_i \\ \dot{q}_j \end{Bmatrix} + K_a \begin{Bmatrix} q_i \\ q_j \end{Bmatrix} = f_{ext} + f_{con} \qquad \text{Equation 4}$$

The 1st and 2nd coupling models of Nelson and Crandall are illustrated in figure 15:

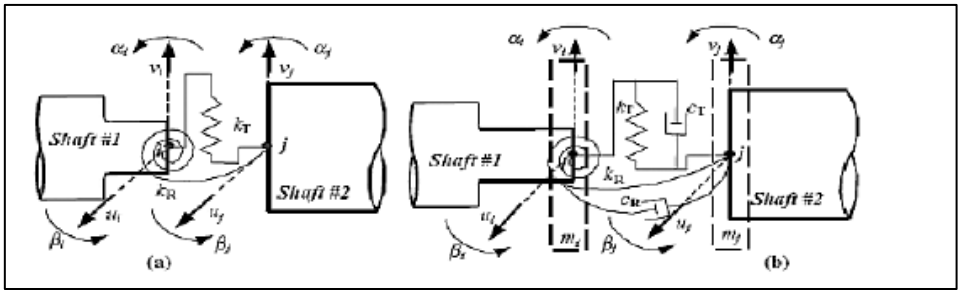

Figure 15: Nelson and Crandall's Flexible Coupling models (a) with stiffness, (b) with stiffness, damping, and inertia (Sekhar & Prabhu, 1995).

The coupling stiffness and damping matrices of Nelson and Crandall's models are given in appendix 2 (both included translational terms compared to Kramer's matrices) while the mass and gyroscopic matrices are the same as Kramer's model.

Experimental work was done by Tadeo et al. aimed to compare the magnitudes of the frequency response functions (FRF) of Kramer, Nelson, and Crandall coupling models (Tadeo, Cavalca, & Brennan, 2011). The system used in this experiment is a rotor-bearing-coupling and pedestal system with four hydrodynamic bearings, neoprene coupling (to isolate the motor vibrations) and Vulkan Tormin L-3R coupling (high torsional stiffness and flexible in bending). Finite element model of the system is shown in figure 16.

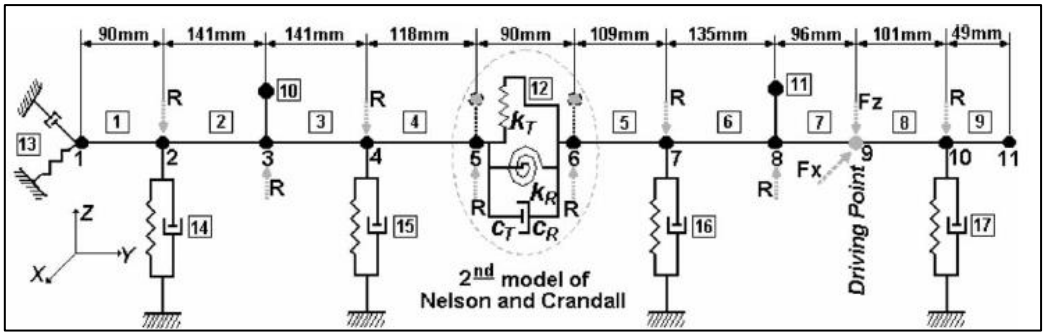

Figure 16: Finite element model of the rotor system used by Tadeo et al. (Tadeo et al., 2011).

The rotor system was modeled by 11 nodes and 17 elements (all the elements and nodes were kept the same with all models while changing the coupling model to follow one of the four tested models). Tadeo et al. defined an objective function of the magnitudes of the FRF to evaluate each model. The objective function is defined as the weighted squared differences between the experimental FRF and the numerical FRF. The test was done with shaft rotational speed of 420 RPM, and magnitudes of frequency response functions were obtained at nodes 3,5,6,8 and 9 in the vertical direction as it had shown better coherence than the horizontal direction. It was found that the second Nelson-Crandall's model is the most accurate model based on the objective function results in table 1.

Table 1

The objective function of the FRF for the four models studied

	1st Kramer	**2nd Kramer**	**1st Nelson-Crandall**	**2nd Nelson-Crandall**
Objective function	225.88	46.02	54.86	38.6
Iterations	64	5	26	8

Tadeo et al. had revealed another work to enrich the content of flexible coupling modeling. The same four models (1st and 2nd Kramer and 1st and 2nd Nelson and Crandall) were compared to the traditional modeling of coupling as a rigid disk. The main force of the shaft's vibration was considered to be the residual unbalance. The study considered bending vibrations only in the rotor-bearing-coupling system. One coordinate system XYZ was used to define inertia of the system while another coordinate system xyz was fixed to the shaft to describe the system's equation of motion. The equation of motion for the rigid disk and the shaft were obtained by applying the Lagrange equation as done by Lalanne (Lalanné, 1991). It was found that the first natural frequency depends on the model type while the second natural frequency is not model dependent. The same behavior was recorded for the third (model dependent) and fourth (model independent) natural frequencies. This is because the systems modal shape as the first and third natural frequencies are mainly due to the deformations in the coupling while the second and fourth natural frequencies are mainly due to other system components. This study concluded that the coupling type in a rotating system affects the vibration amplitudes and natural frequencies (Tadeo & Cavalca, 2005).

Ronak and Anand studied the effect of the couplings types on the vibration analysis by modeling 3D model for the rotor-bearing system and obtain its modal analysis then determining the vibration trends experimentally using machinery fault simulator (Walden, 2000). These analyses were done for three types of couplings which were rigid coupling (machined set screw coupling), elastomeric coupling (3-jaw coupling) and flexible coupling (spiral coupling). The figure illustrates the rotor-bearing 3D model. The three coupling types were tested in the 3D model to obtain each natural system frequency. The natural frequency of the machined set screw coupling

system was found to be 20.428 Hz, the natural frequency of the 3-jaw coupling system was found to be 17.381 Hz, and the natural frequency of the spiral coupling system was found to be 8.0428 Hz. Moreover, experimental acceleration spectrum concluded that the coupling potential to compensate for misalignment is in order of – as expected – spiral coupling, 3-jaw coupling and then machined set screw coupling as expected.

2.1.2. Vibration response of parallel and angular misaligned coupled shafts

A model for the rotor-bearing system was developed using higher order finite elements with displacement and its first three derivatives (slope, bending moment and shear force). The model was constructed of elements with eight degrees of freedom at each node. The derived reaction forces and moments were introduced in the model to evaluate the imbalance response for two harmonics as will be discussed in section 2.2. Figure 17 shows the theoretical model used in their paper with its mode shapes.

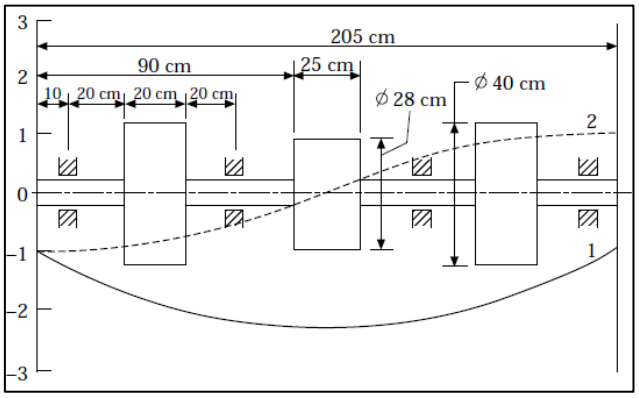

Figure 17: Rotor-coupling-bearing system used by Sekhar and Prabhu with its mode shapes (Sekhar & Prabhu, 1995).

The model consisted of four bearings (two inner and two outer bearings), two rotors and a diaphragm coupling. The outer bearing stiffness and damping were considered to

be 10^8 N/m and 0.5×10^3 N.s/m, respectively while the inner bearing stiffness and damping were considered to be 10^7 N/m and 1×10^3 N.s/m, respectively. The discs imbalance was considered to be 0.01 mm eccentricity. The parallel misalignment in the system was 0.5842 mm in the x-direction and -0.7874 mm in the y-direction while the angular misalignment was considered to be 0.2 degrees. Based on the mentioned conditions, the first two harmonics response with parallel and angular misalignment was obtained as in figure 18.

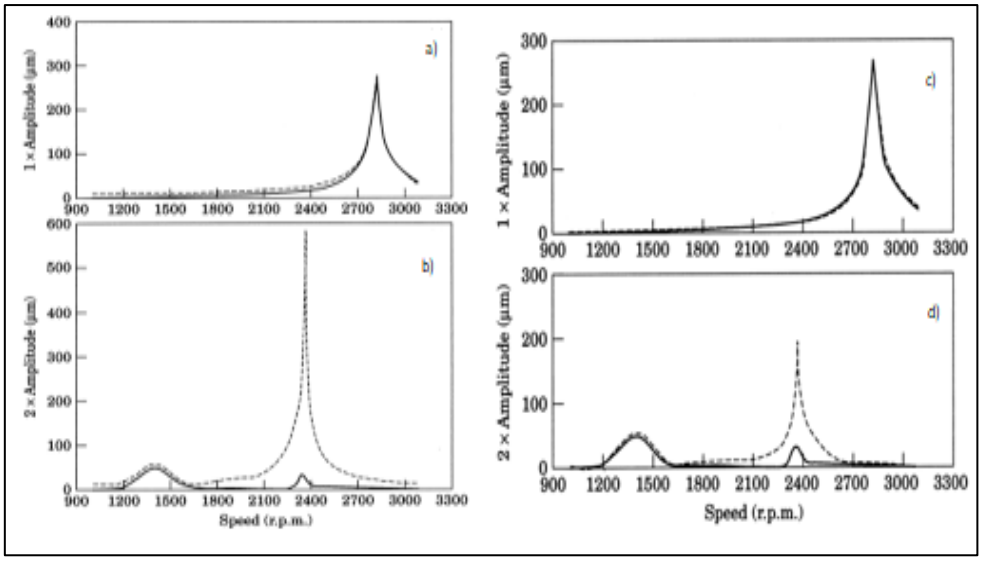

Figure 18: Imbalance response with parallel misalignment of (0.5842, -0.7874) mm. a) 1X amplitude and b) 2X amplitude, and angular misalignment of 0.2 degrees. c) 1X amplitude and d) 2X amplitude. Solid line – without misalignment and dashed line – with misalignment (Sekhar & Prabhu, 1995).

It can be noticed that the 1X RPM amplitude had increased with the increase of rotational up to a certain speed and then started decreasing again while the 2X RPM amplitude had two peaks for both parallel and angular misalignment. In addition, the 1X RPM amplitude had not affected due to the parallel and angular misalignment. On

the other hand, the 2X RPM amplitude had increased significantly at 2400 RPM. In addition, the vibration response of the system was examined while changing the parallel misalignment values from 0-2.03 mm and the angular misalignment form 0-6 degrees. It was found that the first vibration response 1X was not affected by misalignment introduction in the rotor-bearing- coupling system except when it is running with the RPM responsible for the peak on the previous graph while the second vibration response 2X illustrates clearly the misalignment effect on the system's response in all RPM values. Figure 19 summarizes the effect of each type of misalignment on the rotor-coupling-bearing system response. The angular misalignment was converted to millimeters by using the center of articulation.

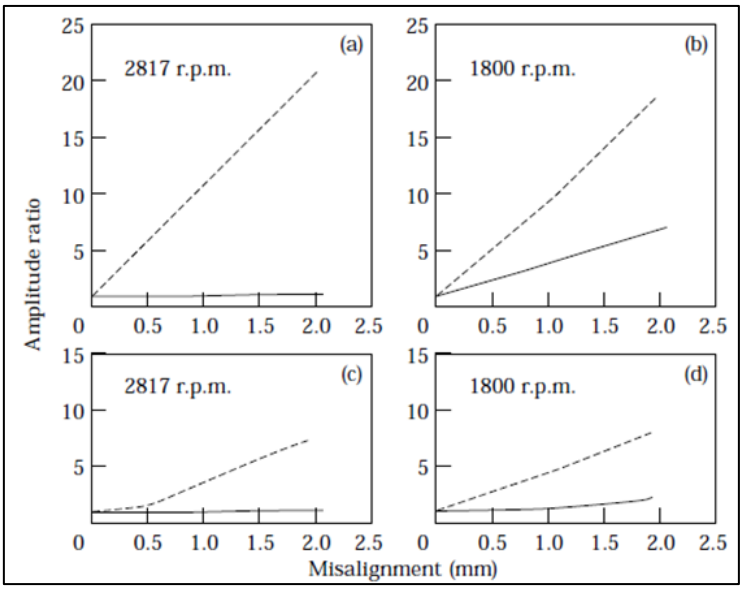

Figure 19: Vibration response with misalignment a) and b) with parallel misalignment, c) and d) with angular misalignment. Solid line – 1X response and dashed line – 2X response (Sekhar & Prabhu, 1995).

A theoretical model of the rotor-coupling-motor system was developed by Xu and Marangoni to describe the vibration response of the angular misaligned and

imbalanced system. Component synthesis method was used to describe the model by dividing it into three components (rotor, flexible coupling, and motor). In order to solve the model and compare the vibration results to experimental outcomes, necessary assumptions were made such as only angular misalignment was considered, angular velocity of the motor was constant while the torque was changing with misalignment, damping and friction were neglected, gyroscopic effect was neglected and finally the ball bearing was treated as rigid support as its stiffness was much higher than the flexible coupling's stiffness (Xu & Marangoni, 1994). Flexible coupling force and torque were derived (as will be discussed in section 2.2) for two situations namely, coupling loads due to misalignment only and coupling loads due to misalignment and unbalance. ANSYS was used to model the system components and to calculate the system's natural frequency. The equations of motion of the system were obtained using component mode synthesis program (CMSP). The frequencies due to shaft angular misalignment were estimated numerically and experimentally to result in even multiple frequencies of the motor speed with an error of 0.1542%.

Zhao et al. publication discussed the meshing forces in misaligned spline coupling and its vibration response. The spline meshing force in x and y directions was proved to be formed of the single spline transmission force due to applied torque and the dynamic force due to vibration displacement. Several factors affecting the single spline meshing force were examined including dynamic vibration misalignment in x and y directions. Numerical simulation considered a spline coupling with 14 splines, alignment meshing distance (AMD) of 3.375 mm, the width of 100 mm, spline thickness of 16 mm and radius of 69.5 mm. A model of 14 nodes (with four degrees of freedom at each node, two translational and two rotational) was examined in the paper. Spline misalignment was increased from zero to 0.4 mm and then 0.8 mm in the positive

x-direction while the spline misalignment angle was 45 degrees anticlockwise at a rotating speed of 5000 rpm (Zhao, Liu, & Chen, 2008). Figure 20 shows the vibration spectrum at the coupling location for the rotating rotor-spline coupling system in the x-direction.

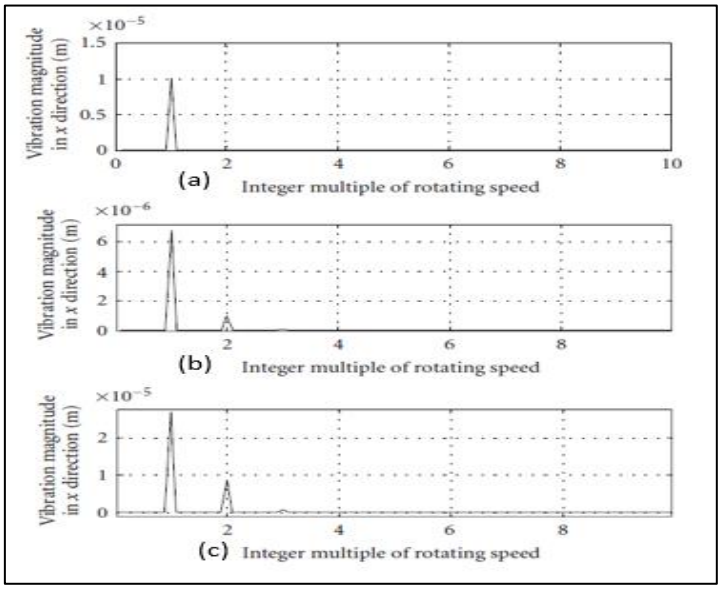

Figure 20: Vibration response in the x-direction of the rotor-spline coupling system. a) response of the aligned system, b) response of 0.4 mm misaligned coupling at misalignment angle of 45 degrees and c) response of 0.8 mm misaligned coupling at misalignment angle of 45 degrees (Zhao et al., 2008).

It can be noticed that the 1X rotating speed was the main response frequency at the aligned system situation. When the misalignment was introduced, 1X and 2X were the main frequencies of the response with the 2X rotating speed increasing rapidly when the static misalignment increased. It is also noticed that the 1X RPM had decreased and then increased again while increasing the misalignment.

Parallel misalignment effect was studied by Hariharan and Srinivasan through a model of misalignment in pin coupling. Finite element method was used (ANSYS) and compared to an experimental test which was done using motor-rotor system. The

pin coupling was modeled as cast-iron flanges and natural rubber bushes. The natural rubber material properties were considered as a linear model for the initial stage (Poisson ratio of 0.49) and then it was considered as nonlinear material with Mooney Rivlin model for natural rubber. Vibration spectrum was obtained from both model and experiment for various shaft speeds (500, 1000, 1500 and 2000 RPM) without introducing misalignment in the system to formulate the baseline response. Then the vibration spectrum was obtained experimentally and numerically as well while introducing 0.2mm parallel misalignment in the system for the same shaft speeds. Both measured and model results showed that parallel misalignment could be categorized by twice the shaft rotating speed 2X (Hariharan & Srinivasan, 2009).

In a recent study, Sawalhi et al. compared the numerical and experimental vibration spectrum for the rotor-coupling-bearing system under parallel misalignment fault. The model was considered to be FE beams with 18 elements. Motor, coupling, inner bearing, outer bearing, rotor, and pedestal were modeled. Each element beam had five degrees of freedom (two translational in X and Y directions and three rotational in X, Y and Z directions) except for the pedestal which was considered to be rigid against rotation. The total DOF of the system was calculated to be 84. Moreover, an experimental procedure was done in the research to estimate the coupling stiffness as a function of rotational angle. It was done to predict two types of couplings bending stiffnesses, namely 3-jaw coupling and spiral coupling. Bending stiffness 3-jaw and spiral couplings were found to be 179,236 N/m and 119259 N/m, respectively. Furthermore, simulation and experimental vibration spectrum were obtained for the 3-jaw coupling. Experimentally, a 29 Hz shaft speed for the aligned and misaligned shaft-system was considered (misaligned at 0.635mm or 25 mils) while in simulation 40 Hz shaft speed for the aligned and misaligned shaft-system was considered (misaligned

shaft (0.889 mm or 35 mils). Simulation results were obtained using variable step solver on the system's equation of motion. Residual unbalance effect was noticed in the 1X component in all misalignment levels. It was noticed that parallel misalignment affected both low and high-frequency orders. Experimentally, the main low frequency affected orders were 6X, 9X, 10X and in simulation showed similar orders (Sawalhi, Ganeriwala, & Tóth, 2019).

A study by Tuckmantel and Cavalca aimed to compare forces and moments on disc coupling of the rotor-bearing-coupling system under angular misalignment for two models. The first model was a linear bending model of the disc introduced by Sekhar and Prabhu while the second model was FEM using ABAQUS introduced by Tuckmantel. The model used in this study consisted of two shafts, two rigid discs, four journal bearings and Vulkan Tormin coupling (disc coupling). The forces and moments from Sekhar and Prabhu model were assumed to be the summation of the 1X to 4X harmonics (Tuckmantel & Cavalca, 2019). The displacement spectrum of Tuckmantel model at the coupling in vertical and horizontal directions with the rotational speed of 12.05Hz (one-fourth of the natural frequency of the system) is shown in figure 21.

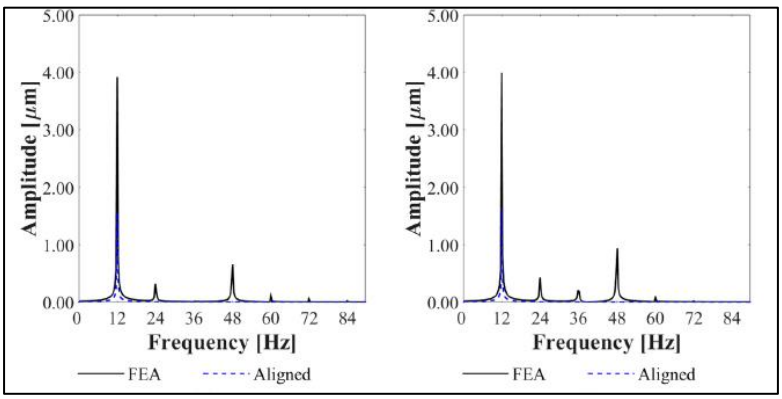

Figure 21: Displacement spectrum of Tuckmantel model at the coupling with 12.05Hz. a) horizontal and b) Vertical (Tuckmantel & Cavalca, 2019).

It was noticed that the angular misalignment response was synchronized with the 1X and 4X peaks with the existence of the 2X and 3X in very small values. For Sekhar and Prabhu model, the coupling displacement response in the horizontal and vertical directions was also obtained at 12.05 Hz rotational speed as shown in figure 22.

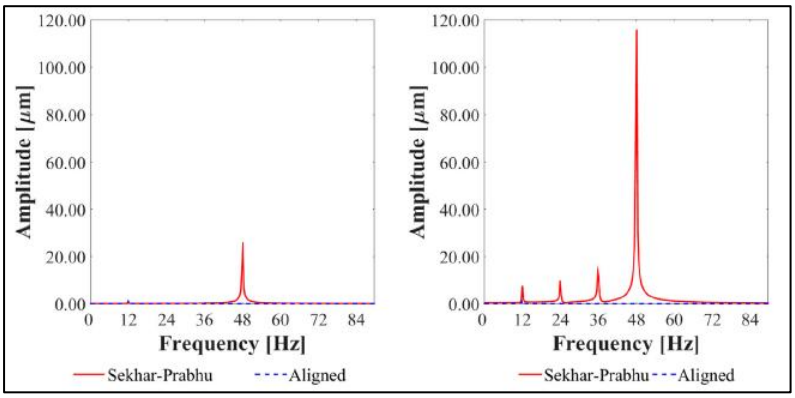

Figure 22: Displacement spectrum of Sekhar and Prabhu model at the coupling with the rotational speed of 12.05Hz a)horizontal and b) Vertical (Tuckmantel & Cavalca, 2019).

It can be noticed that the angular misalignment response was synchronized with the 1X, 2X, 3X and 4X with maximum amplitude at 4X. Moreover, the amplitudes resulted from the mathematical linear bending model of Sekhar and Prabhu (in range of 20 to 100 µm) was higher than the amplitudes obtained from FEM of Tuckmantel (in range of 1 to 4 µm) which could be a result of the summation assumption of the first four harmonics in the mathematical model.

Another recent study on the vibration response of rigid coupling parallel misalignment in a rotor-bearing-coupling system with the aluminum shaft was done experimentally and through simulation by Hujare and Karnik (Hujare & Karnik, 2018). The experimental setup used for this research was machinery fault simulator (MFS)

with FFT analyzer while the simulation was done using ANSYS software with beam elements for the response function and force model developed by A.W.Lees (Lees.A.W., 2007). The experimental results of the vibration amplitude with changing the parallel misalignment value (at 1800 RPM) and with changing the rotational speed for various misalignment values are shown in figure 23.

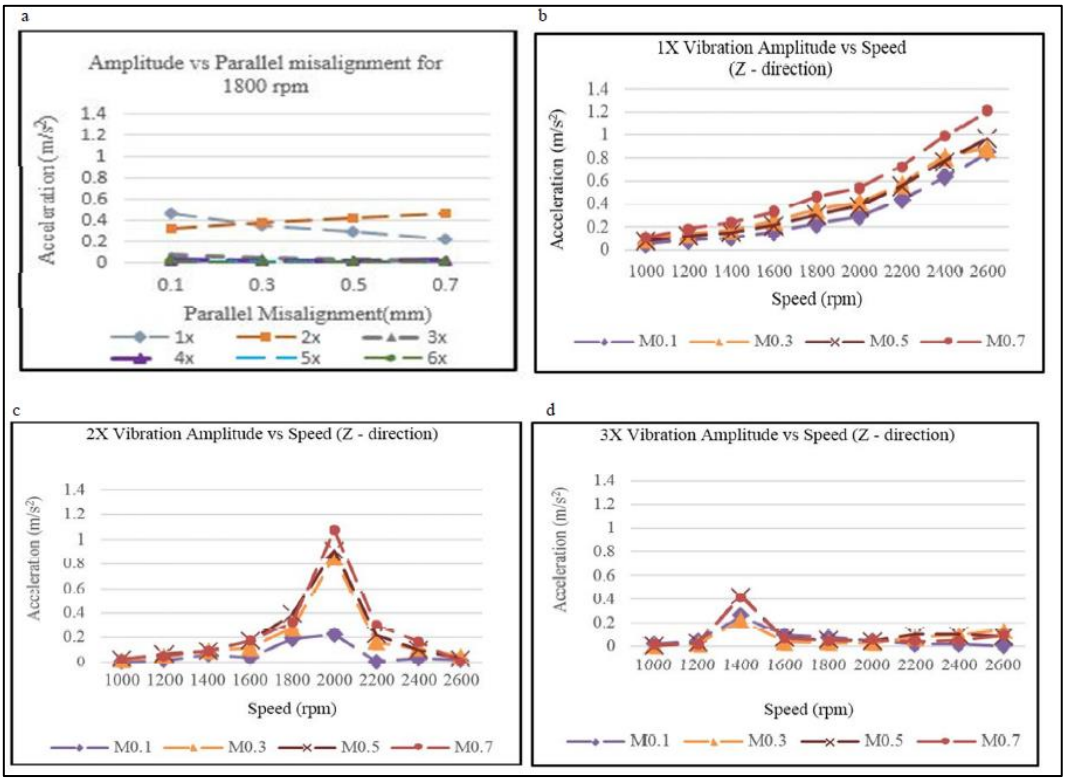

Figure 23: Experimental results for Hujare and Karnik study, a) Amplitude Vs. parallel misalignment at 1800 RPM, b) 1X vibration response against RPM, c) 2X vibration response against RPM and d) 3X vibration response against RPM (Hujare & Karnik, 2018).

It can be noticed that the 1X and 2X acceleration responses were dominant than other vibration harmonics at all parallel misalignment levels. The 3X to 6X acceleration amplitudes were constant with the change in parallel misalignment value. Moreover,

the 1X amplitude had shown an increasing trend with the increase of rotational speed at all misalignment levels while the 2X and 3X had increased up to a peak value at 2000 RPM and 1400 RPM respectively and then decreased. The simulation results of the vibration amplitude with changing the parallel misalignment value (at 1800 RPM) and with changing the rotational speed for various misalignment values are shown below.

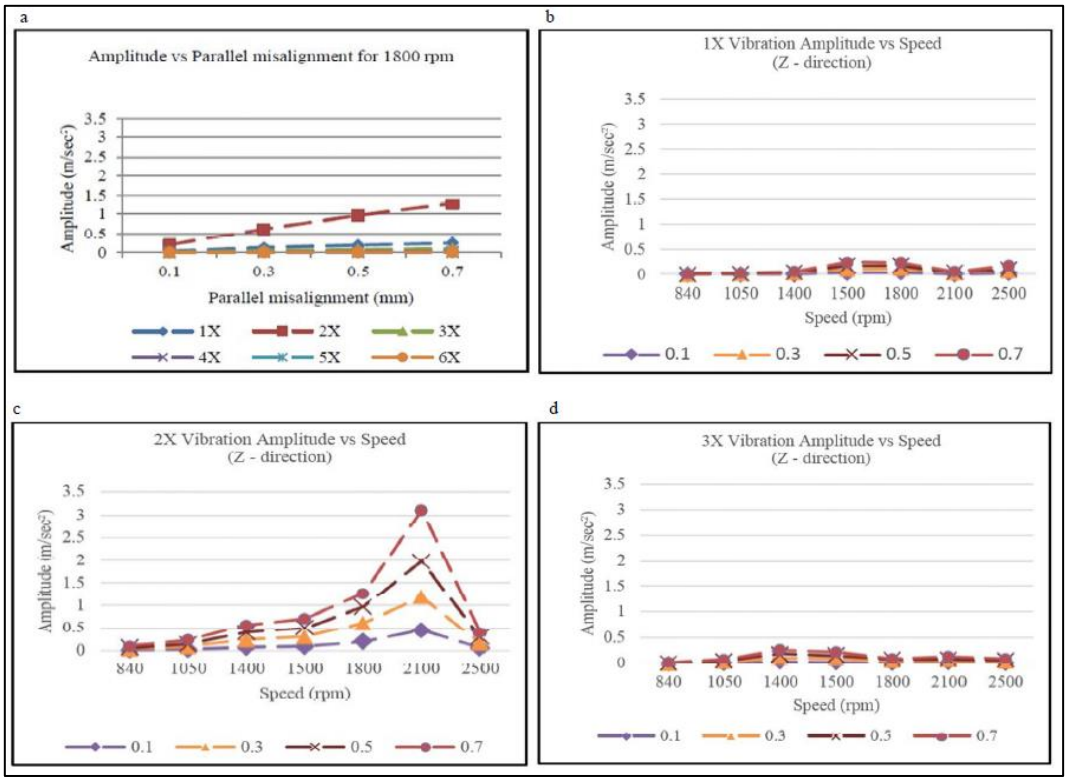

Figure 24: Simulation results for Hujare and Karnik study, a) Amplitude Vs. parallel misalignment at 1800 RPM, b) 1X vibration response against RPM, c) 2X vibration response against RPM and d) 3X vibration response against RPM (Hujare & Karnik, 2018).

Simulation results showed that the 2X acceleration responses were dominant than other vibration harmonics at all parallel misalignment levels. The rest of the acceleration amplitudes were constant with the change in parallel misalignment value. Moreover,

the 2X response had increased up to a peak value at 2100 RPM and then decreased for the rest of the values while the 1X and 3X amplitudes had shown not changed significantly with the change of the RPM.

Another numerical simulation model was developed by Wang and Gong to study the parallel and angular misalignment dynamics of the rotor-bearing-coupling system. FEM was used to model a system consisting of two shafts, four bearings, three disks and a coupling connecting the rotating shafts with 6 DOF. The parallel and angular misalignment forces were derived mathematically as it will be explained in section 2.2. (H. Wang & Gong, 2019). The displacement response of parallel misalignment of 1 mm at 3800 rotational speed in horizontal and vertical directions are shown in figure 25.

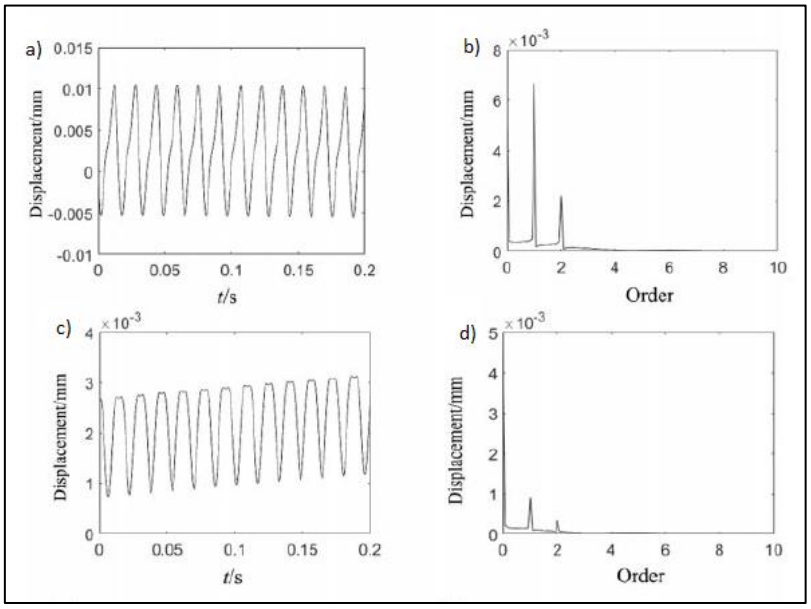

Figure 25: Displacement response of 1 mm parallel misalignment at 3800 RPM, a) time response in the horizontal direction, b) frequency response in the horizontal direction c) time response in the vertical direction and d) frequency response in the vertical direction (H. Wang & Gong, 2019).

It can be noticed that the time response is periodic with the response in the vertical direction in a positive range. In spectrum graphs, the 1X and 2X were clear with higher amplitudes in the horizontal direction. Moreover, parallel misalignment orbit was found to be a triangular shape. The displacement response of angular misalignment of 5 degrees at 6400 RPM in horizontal and vertical directions are shown in figure 26.

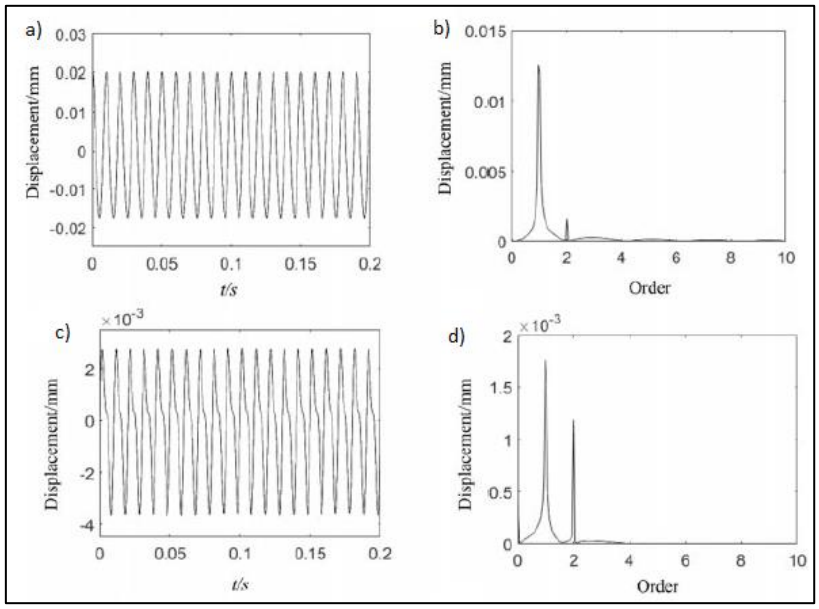

Figure 26: Displacement response of 5 degrees angular misalignment at 6400 RPM, a) time response in the horizontal direction, b) frequency response in the horizontal direction c) time response in the vertical direction and d) frequency response in the vertical direction (H. Wang & Gong, 2019).

It can be noticed that the time response is periodic with the response in the vertical direction in a positive range. In spectrum graphs, the 1X and 2X were clear with higher amplitudes in the horizontal direction. The 2X was dominant in the vertical direction. Moreover, angular misalignment orbit was found to be like moon shape.

2.1.3. Vibration and torque signals of parallel and angular misaligned coupled shafts

The misalignment was detected experimentally using vibration spectrum as well as torque spectrum by Sekhar and Reddy. Rotor-bearing set-up used in that experiment consisted of a motor (0-5000 rpm), rotor shafts (Steel material), four ball bearings (with the stiffness of 8×10^7 N/m), disk, two couplings, pedestal, accelerometer, and torque sensor as it is illustrated in figure 27.

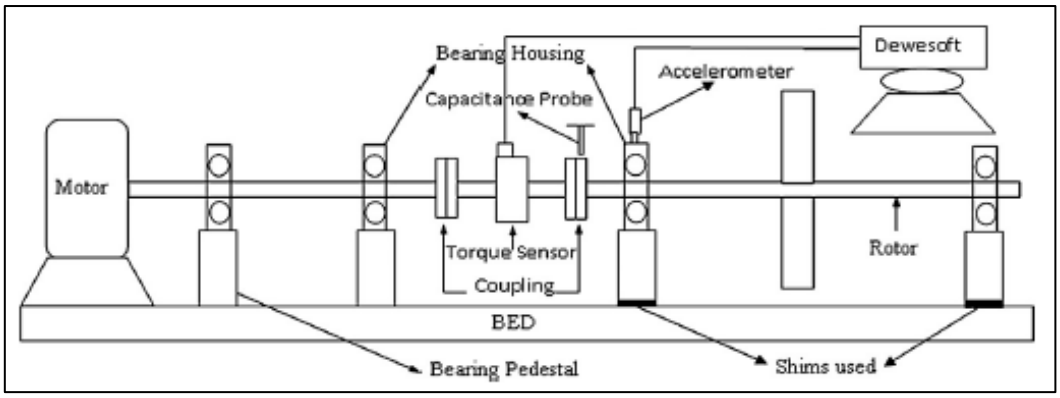

Figure 27: Schematic diagram of the rotor-bearing system used by Sekhar and Reddy (Chandra Sekhar Reddy & Sekhar, 2015).

Parallel and angular misalignments were introduced in the rotor-bearing system by means of shims. The examined parallel misalignment values were 0, 150, 250, 400, 550 µm while the angular misalignment values were 0.001, 0.022, 0.034, 0.048 radians with a rotating speed of 20, 25, 40 Hz. The obtained vibration acceleration and reaction torque in the time domain were analyzed using both Fourier transform. It was observed in the FFT result plots for the case of parallel misalignment 250 µm at 20 Hz rotational speed that the 2X vibration component increased which was evident in the torque spectrum as well but not as significant as the vibration response in figure 28.

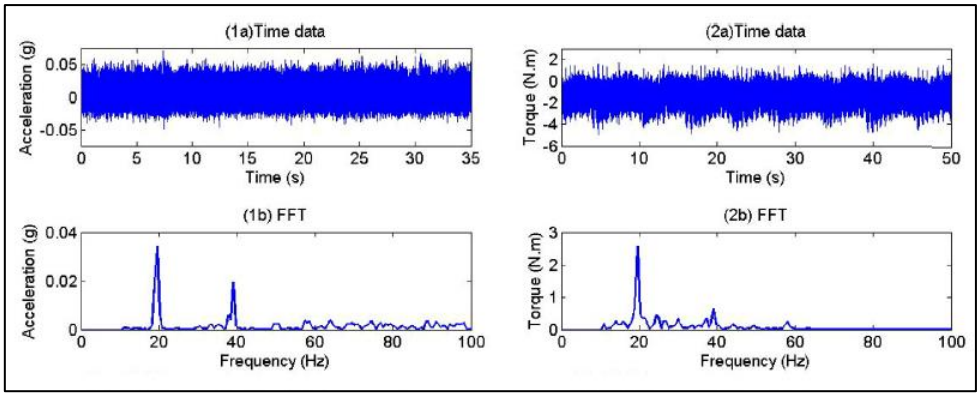

Figure 28: Accelerometer and torque sensors responses for the case of parallel misalignment 250 µm at 20 Hz rotational speed. 1) vibration and 2) torque. a) time domain and b) frequency domain (Chandra Sekhar Reddy & Sekhar, 2015).

The amplitude of the frequency response of both acceleration and torque with the increase in the parallel misalignment level was found to be increasing for both 1X and 2X RPM.

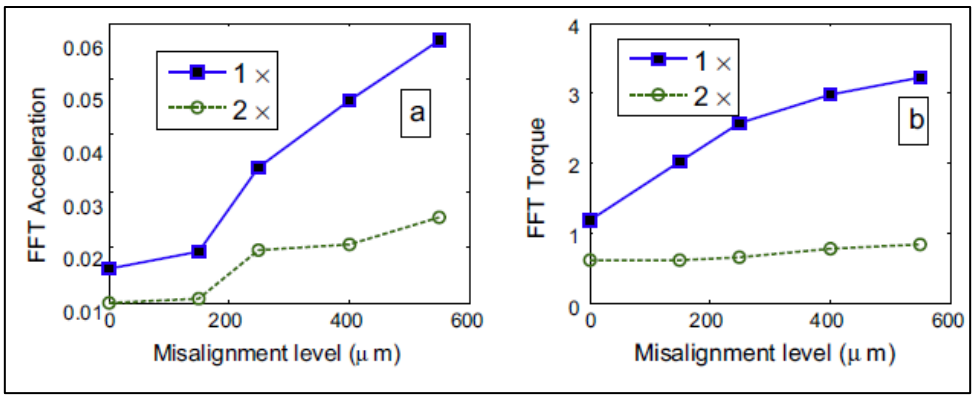

Figure 29: Parallel misalignment effect on 1X and 2X amplitudes of signals at 20 Hz rotational speed (a) FFT acceleration and (b) FFT torque (Chandra Sekhar Reddy & Sekhar, 2015).

Analyzing the angular misalignment FTT results, a similar trend of the 1X and 2X increased harmonics was noticed. However, it was observed that the torque spectrum

is clearer in amplitude than the acceleration spectrum which was not consistent. The angular misalignment spectrum for acceleration and torque is shown in figure 30 for the case of 0.022 radians angular misalignment at 20 Hz shaft rotational speed.

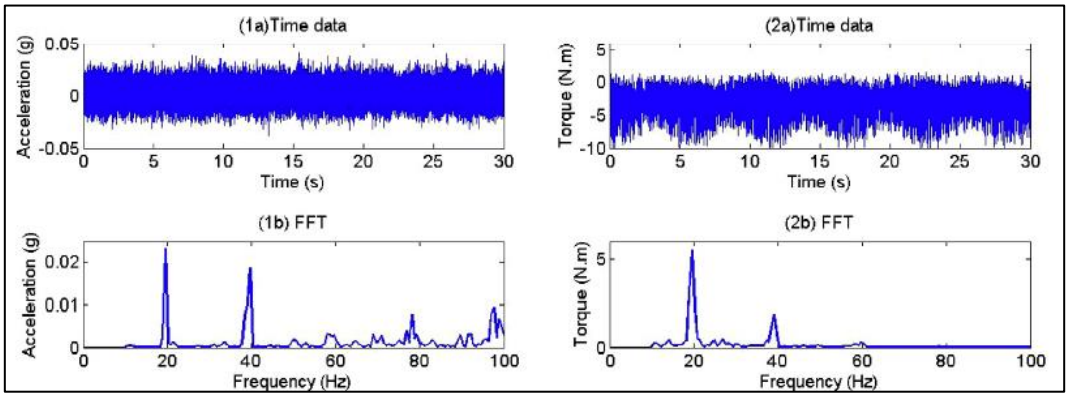

Figure 30: Accelerometer and torque sensors responses for the case of angular misalignment 0.022 radians at 20 Hz rotational speed. 1) vibration and 2) torque. a) time domain and b) frequency domain (Chandra Sekhar Reddy & Sekhar, 2015).

The torque signals were better monotonic than the acceleration signals in case of angular misalignment. The amplitude of the frequency response of both acceleration and torque with the increase in the angular misalignment level was found to be increasing for both 1X and 2X RPM.

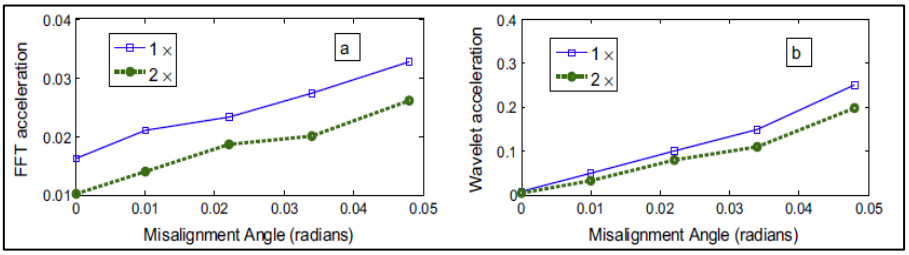

Figure 31: Angular misalignment effect on 1X and 2X amplitudes of signals at 20 Hz rotational speed (a) FFT acceleration and (b) FFT torque (Chandra Sekhar Reddy & Sekhar, 2015).

2.2. Unbalance and misalignment forces

Mechanical unbalance is the most common fault in rotating machinery as it can't be avoided in the majority of equipment. The existence of unbalance can also be due to the appearance of some other faults such as misalignment, looseness and fractured parts. Therefore, unbalance reaction forces on rotating machines shafts had been developed to be as below which was considered in various researches such as Sawalhi et al. and Xu and Marangoni.

$$F = m\, e\, \omega^2\, sin(\omega\, t) \qquad \text{Equation 5}$$

Where m is the mass of the rotor-bearing-coupling system. e is the eccentricity of the rotor-bearing-coupling system. ω is the rotational speed of the shafts and t is the time.

On the other hand, the misalignment forces and moments on the shafts of the rotating machine had not yet fully understood. Gibbons studied the coupling forces and moments for four different types of couplings after noticing that replacing gear coupling with a diaphragm coupling in a steam turbine cooling pump had reduced the parallel misalignment moment from 7120 N.m to 192 N.m and reduced the vibration level from 5 mils to 1 mil. The four types of couplings used in that study were gear coupling, multi-disk diaphragm coupling, disk coupling and diaphragm coupling with contoured thickness. The reaction forces and bending moments due to parallel misalignment were derived for the four couplings (Engineer et al., n.d.). Figure 32 explains the forces and moments in coupled shafts due to parallel misalignment using a flexible coupling.

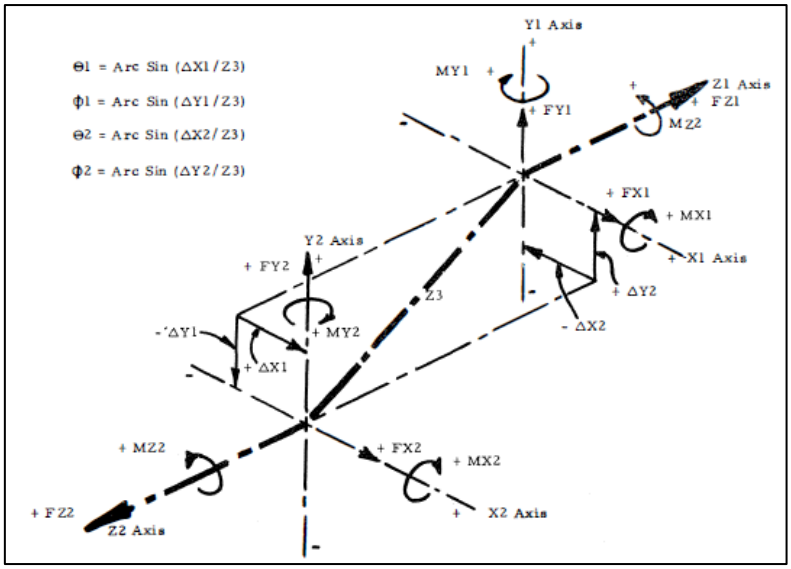

Figure 32: Forces and moments in coupled shafts due to parallel misalignment using flexible coupling as per Gibbons (Engineer et al., n.d.)

The forces and moments of parallel misalignment were defined as follows.

$$\begin{cases} MX1 = T_q\, sin\theta_1 + K_b\Phi_1\ , & MX2 = T_q\, sin\theta_2 - K_b\Phi_2\ , \\ MY1 = T_q\, sin\Phi_1 - K_b\theta_1, & MY2 = T_q\, sin\Phi_2 - K_b\theta_2, \\ MZ1 = T_q, & MZ2 = -T_q, \\ FX1 = (-MY1 - MY2)/Z3\,, & FY1 = (MX1 + MX2)/Z3\,, \\ FX2 = -FX1, & FY2 = -FY1, \\ FZ1 = K_a\,\Delta Z + K_a\,(\Delta Z)^3\,, & FZ2 = -FZ1 \end{cases}$$

Equation 6

Where X1, Y1, Z1 are the coordinates for the first shaft, X2, Y2, Z2 are the coordinates for the second shaft. Z3 is the distance between the two coupled systems centers of articulation. T_q is the torque applied at shaft 1. M is the moment exerted by the coupling on the system. F is the force exerted by the coupling on the system. $\theta_1\ and\ \theta_2$ are the angles between the Z3 and the first and second shafts' displacements in the x-direction, respectively. $\Phi_1 and\ \Phi_2$ are the angles between the Z3 and the first and second shafts' displacements in the y-direction, respectively.

In a continuation to the identification of the reaction forces and bending moments, Sekhar and Prabhu derived the reaction forces and bending moments due to

angular misalignment using the same procedure which had been used in various works. The forces and moments of angular misalignment were defined as follows.

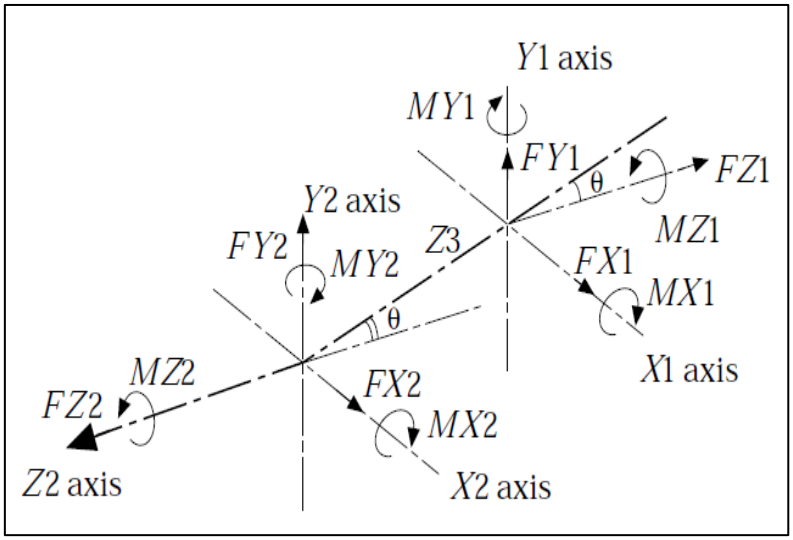

Figure 33: Forces and moments in coupled shafts due to angular misalignment as per Sekhar and Prabhu (Sekhar & Prabhu, 1995).

The forces and moments of angular misalignment were defined as follows.

$$\begin{Bmatrix} MX1 = 0.0\ , & MX2 = -K_b\theta\ , \\ MY1 = 0.0, & MY2 = Tqsin\theta, \\ MZ1 = T_q/cos\theta\ , & MZ2 = -T_q, \\ FX1 = (-MY1 - MY2)/Z3\ , & FY1 = (MX1 + MX2)/Z3\ , \\ FX2 = -FX1, & FY2 = -FY1 \\ FZ1 = (K_a\,\Delta Z + K_a\,(\Delta Z)^3)/cos\theta\ , & FZ2 = -FZ1 \end{Bmatrix} \quad \text{Equation 7}$$

Parallel misalignment forces were derived in numerous ways. Sawalhi et al. defined parallel misalignment forces based on variable coupling stiffness with rotational angle. Parallel misalignment forces on the rotor were given as follows.

$$\begin{Bmatrix} F_e = K^c(\alpha)d^c + F_m \\ F_m = K_A^c(\alpha)\begin{Bmatrix} 0 \\ d_{0B} \end{Bmatrix} + K_B^c(\alpha)\begin{Bmatrix} d_{0B} \\ 0 \end{Bmatrix} \end{Bmatrix} \quad \text{Equation 8}$$

Where F_e is the excitation force. F_m is the misalignment force. $K_A^c(\alpha)$ and $K_B^c(\alpha)$ are the top and bottom halves of the stiffness matix for coupling. α is the angle of rotation. d_{0B} is the misalignment vector at the coupling (Sawalhi et al., 2019).

Moreover, another study on the parallel and angular misalignment forces was done by Wang and Jiang in their study of the misalignment effect on a dual-rotor system. Figure 34 shows the misaligned duel-rotor system and its misalignment fault schematic.

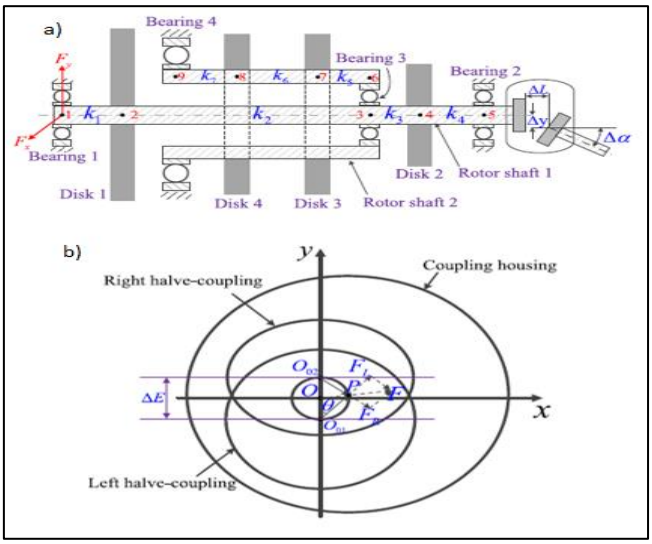

Figure 34: Parallel and angular misalignment forces as per Wang and Jiang study. a) misaligned duel-rotor system and b) misalignment fault schematic (N. Wang & Jiang, 2018).

The rotating shafts had a geometric center O and dynamic center P due to the relative motion of the shafts. The parallel and angular misalignment forces were derived as in appendix 3 and found to be as follows.

$$\begin{Bmatrix} F_x = m_o\,\omega^2(\Delta y + \Delta L\tan(\frac{\Delta\alpha}{2}))\sin 2\omega t \\ F_y = m_o\,\omega^2(\Delta y + \Delta L\,tan(\frac{\Delta\alpha}{2}))cos2\omega t \end{Bmatrix} \quad \text{Equation 9}$$

Where ΔE is the combined misalignment amount, Δy is the parallel misalignment distance, α is the angular misalignment angle. m_o is the mass of the coupling. ω is the rotational speed.

Angular misalignment forces of coupled shafts were also derived by Xu and Marangoni using the fact that the misaligned shafts attain a universal joint pattern. It was assumed that the two shafts were angularly misaligned by an angle α and that they were connected by a flexible coupling. This angular misalignment mathematical derivation was used later in other researches such as Wang and Gong study. Figure 35 shows the schematic diagram of the misaligned shafts and its torque components.

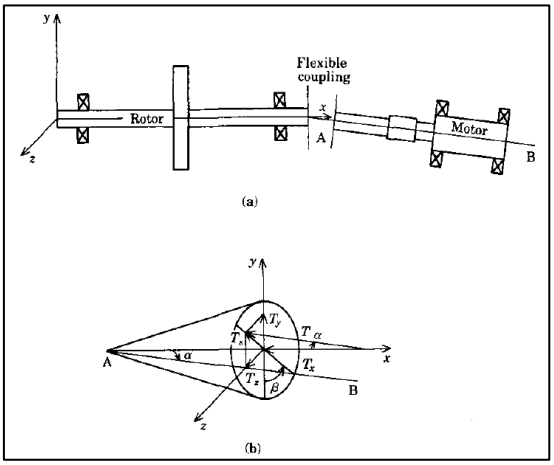

Figure 35: Angular misalignment forces as per Xu and Marangoni. A) misalignment schematic and b) torque components (Xu & Marangoni, 1994).

The angular misalignment forces derivation is given in Appendix 4 and the obtained results were as following.

$F = \sum_{n=1}^{\infty} F_{2n} sin2n\Omega t$ Equation 10

where $F_{2n} = [0, \ldots, E_{2n}, G_{2n}]^T$

$E_{2n} = (-1)^{n+1} J_R \Omega^2 B_{2n} tan\alpha cos\beta$ and $G_{2n} = (-1)^{n+1} J_R \Omega^2 B_{2n} tan\alpha sin\beta$

K_b is the bending stiffness, J_R is the polar moment of inertia, Ω is the rotational speed, α is the misalignment angle with the axial direction, β is the misalignment angle with the radial direction and B_{2n} is an even multiple of the rotational speed.

2.3. Modeling techniques of the rotor-coupling-bearing system

As it had been illustrated in section 2.1 that there are various types of modeling techniques of the rotor-coupling-bearing system. FEA method is the most widely used method to model the system's components and derive the EOM and then the numerical solving method was used to obtain the system's response. The system of EOM was solved by various methods such as Newmark-Beta stepping integration, direct stiffness method and self-built programs using Matlab and FORTAN. Moreover, the component mode synthesis method is also another technique to model the system which had been also well established. The FEA modeling techniques used included nodes, beam elements, 3D modeling and higher order elements (displacement, slope, bending moments, shear force). The system's DOF throughout the literature was varying significantly depending on the modeling elements type and its quantity. Most of the publications didn't elaborate on the number of elements used in the modeling process but the number of DOF at each node was well presented. Firstly, the shafts of the rotating system were usually modeled as a beam element with different number of DOF at each node. As the bending vibration was usually the targeted study outcome, the translational and rotational radial degrees of freedom was always incorporated in the mass, stiffness and damping matrices while the axial DOF was incorporated with dissimilar degrees. In some cases, the mass of the shafts was ignored as they were assumed to be very small compared to discs mass. Secondly, the discs were usually modeled as rigid with mass and inertia matrices derived using Lagrange equations. In some models, the discs gyroscopic matrix was introduced as well. Thirdly, in case of ball bearings, translational viscous damping and stiffness were used at the bearing node while the influence of rotation, bending moments and oil film were ignored. In other

cases, the bearings were modeled as Hertzian contact stiffness force formula. On the other hand, in case of journal bearings, hydrodynamic linear forces were defined as the first order Taylor series of the journal bearing which was derived by numerical integration of oil film's Reynolds equation in axial and circumferential directions. In some studies, the bearings were simplified by a string element to support the system. The system's damping matrix was developed by modal analysis or as a ratio of the stiffness and mass matrices. Fourthly, coupling modeling was done in many ways using FEA or by deriving the forces and moments due to misalignment at the coupling location and introducing it to the system's excitation forces. The general model to represent the coupling forces and moments established by Gibbons was of 2 nodes with 6 DOF at each node (3 translational and 3 rotational). Finally, the system's pedestals were usually ignored and not included in the system as they considered to be rigid and the systems boundary conditions were applied at the bearings locations. Table 2 illustrates the modeling method of each system component and its nodes DOF.

Table 2

Summary of modeling techniques for each system component

Bibliography			**Modeling**			
#	**Year**	**Authors' Name**	**Shaft nodes**	**Coupling nodes**	**Bearing node**	**Discs nodes**
1	1976	Gibbons	2 nodes - 6 DOF (3T,3R)	2 nodes - 6 DOF (3T,3R)	Not included	Not included
2	1994	Xu and Marngoni	FEA: 11 nodes – 6 DOF	FEA: 14 nodes – 6 DOF	Rigid support	Not included

3	1995	Sekhar and Prabhu	Beam element of 2 nodes – 4 DOF (displacement, slope, bending moments, shear force)	Forces and moments in diaphragm coupling were introduced as excitation forces	Translational viscous damping and stiffness - 2 DOF (2T) in bending	Rigid disk of mass, gyroscopic matrices - 4 DOF (displacement, slope) in bending
4	2000	Ronak and Anand	3D FE model	3D FE model	Not included	3D FE model
5	2005	Tadeo and Cavalca	Beam element of 2 nodes - mass, stiffness, gyroscopic - 4 DOF (2T,2R) in bending	2 nodes of mass, stiffness, damping - 4 DOF (2T,2R) in bending	Translational viscous damping and stiffness - 2 DOF (2T) in bending.	Rigid disk of mass, gyroscopic matrices - 6 DOF (3T,3R)
6	2008	Zhao et al.	Beam elements - 4 DOF (2T,2R)	Forces were introduced as excitation forces.	Linear springs supporting the system	Not included
7	2009	Hariharan and Srinivasan	3D FE model	3D FE model	3D FE model and boundary conditions	Not included
8	2018	Hujare and Karnik	3D FE model and no damping introduced.	3D FE model and forces due to parallel misalignment	3D FE model and BCs with no damping	Not included

9	2018	Wang and Jiang	The system was divided into lumped masses and stiffnesses with 2 DOF at each segment (x, y)	Included as excitation forces due to misalignment	Hertzian contact stiffness force and relative bearing cage displacement stiffness and damping	Rigid disk of mass – 2 DOF in x and y directions
10	2019	Sawalhi et al.	Beam element – 5 DOF (2T,3R)	Included as excitation forces due to unbalance and misalignment	Stiffness and damping- 2 DOF in x and y directions	Not included
11	2019	Tuckmantl and Cavalca	Beam elements - 4DOF (2T,2R) in bending	3D FE model was developed to evaluate the stiffness	Numerical integration of oil film's Reynolds equation	Rigid disk of mass, gyroscopic - 4 DOF (2T,2R)
12	2019	Wang & Gong	Beam elements with 6 DOF at each node	Included as excitation forces due to unbalance and misalignment	String element to support the system	Rigid disk of mass and inertia

In the current study, the rotor-coupling bearing system was modeled as two nodes of mass, stiffness and damping of 6 DOF at each node (3 translational and 3 rotational) to capture the effect of the radial, axial and angular system parameters on the vibration response. The shafts were modeled of radial, axial and torsional stiffness and lumped masses. The mass and inertia matrices were constructed to be diagonal as the misalignment was assumed to be caused equally by each node of the system. This

modeling method simplifies the needed matrices calculations. The system's stiffness behavior was linear for all its components as the geometry and material were having linear properties. In addition, viscous damping modeling was followed for simplicity. The coupling was modeled as an elastic element of mass, damping, and stiffness in axial, radial and rotational directions. The discs were assumed to cause a certain level of eccentricity at each node in the excitation force vector. Finally, pedestals were ignored in the current study and the system was assumed to be rigidly supported at the bearing locations.

CHAPTER 3: MODELING OF ROTOR-COUPLING-BEARING SYSTEM

The system under observation was modeled using Lagrange energy method. The system was divided into two elements of mass, stiffness and damping matrices with 12 DOF. The two shafts were modeled as measured from the machinery fault simulator in Qatar University. The shafts material was AISI-1045 steel – cold drawn and the two shafts were not identical in length. Moreover, shaft 1 – longer - is the driven side shaft and shaft two – shorter – is the motor side shaft. Shaft 2 keyway was neglected in the current study to simplify the simulation analysis. Figure 36 illustrates the two subsystems with the center of gravity of each system representing the simulation node.

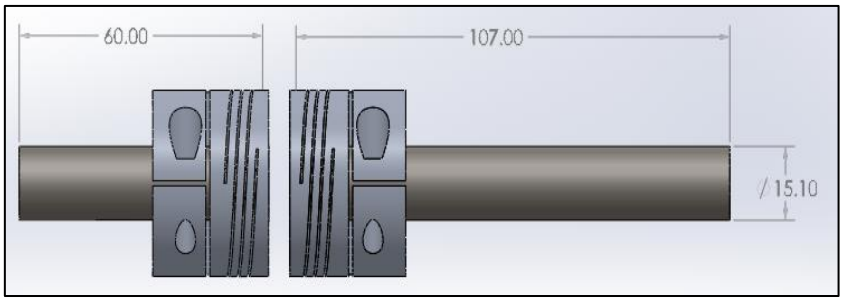

Figure 36: 3D model and dimensions of spiral coupling – shafts system in millimeters.

In this chapter, modeling of the rotor-coupling-bearing system using Lagrange energy method will be done, and then the unbalance and misalignment forces will be derived. Moreover, the determination of two flexible couplings stiffness will be done using Solidworks for modeling and Abaqus for FEA. To integrate all the system components' parameters in the stiffness, damping and mass matrices, determination of two flexible couplings damping coefficients will be done using the logarithmic decrement method. Bearings and shaft stiffness and damping will be discussed, and the system of equations will be solved numerically using Matlab.

3.1. Modeling of the rotor-coupling-bearing system using Lagrange energy method

The system under observation was divided into two elements of mass, stiffness and damping matrices of 12 DOF. Figure 37 illustrates the modeled two half's coupling masses and the set of stiffness and damping.

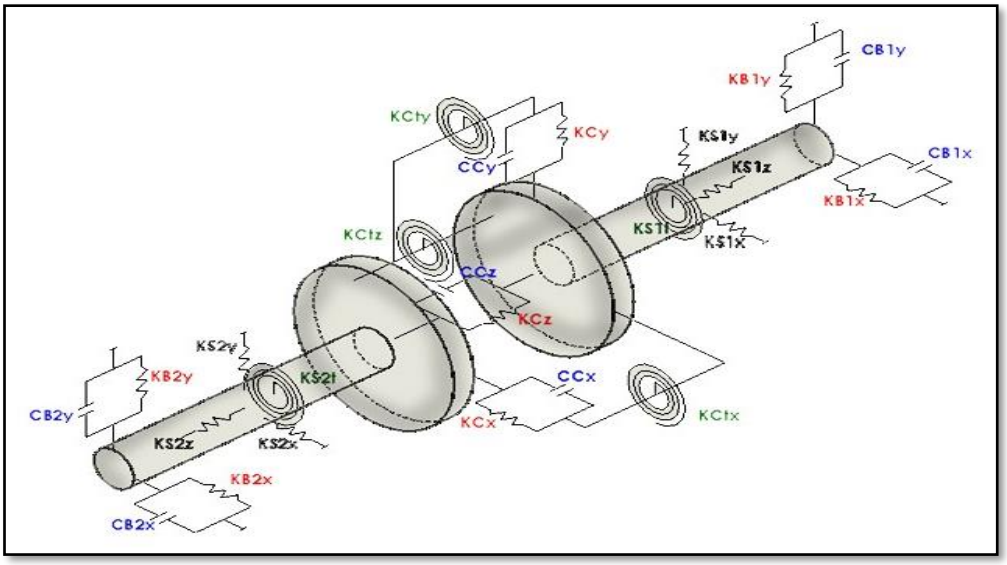

Figure 37: Model of coupling, shafts, and bearings.

The system is of 12 degrees of freedom (DOF) with six DOF for each mass as below:

$$\{x\} = \begin{Bmatrix} X_1 \\ X_2 \\ Y_1 \\ Y_2 \\ Z_1 \\ Z_2 \\ \theta_1 \\ \theta_2 \\ \beta_1 \\ \beta_2 \\ \alpha_1 \\ \alpha_2 \end{Bmatrix}$$

Where:

X_1 is the displacement in the radial horizontal direction for mass 1
X_2 is the displacement in the radial horizontal direction for mass 2
Y_1 is the displacement in the radial vertical direction for mass 1
Y_2 is the displacement in the radial vertical direction for mass 2
Z_1 is the displacement in the axial direction for mass 1
Z_2 is the displacement in the axial direction for mass 2
θ_1 is the rotation around Z-axis for mass 1
θ_2 is the rotation around Z-axis for mass 2
β_1 is the rotation around X-axis for mass 1
β_2 is the rotation around X-axis for mass 2
α_1 is the rotation around Y-axis for mass 1
α_2 is the rotation around Y-axis for mass 2

Using Lagrange energy method

$$\frac{d}{dt}\left(\frac{\partial T}{\partial \dot{q}_i}\right) + \frac{\partial V}{\partial q_i} + \frac{\partial D}{\partial \dot{q}_i} = F_i \qquad \text{Equation 11}$$

Where: T is the Kinetic energy of the system.
V is the Potential energy of the system.
D is the Dissipation energy of the system.
F is the external force vector acting on the system.
q is the independent generalized displacement vector.
t is the time.

The kinetic energy equation is developed as follows:

$$T = \frac{1}{2}m_1\dot{X_1}^2 + \frac{1}{2}m_2\dot{X_2}^2 + \frac{1}{2}m_1\dot{Y_1}^2 + \frac{1}{2}m_2\dot{Y_2}^2 + \frac{1}{2}m_1\dot{Z_1}^2 + \frac{1}{2}m_2\dot{Z_2}^2 + \frac{1}{2}I_{z1}\dot{\theta_1}^2 +$$

$$\frac{1}{2}I_{z2}\dot{\theta_2}^2 + \frac{1}{2}I_{x1}\dot{\beta_1}^2 + \frac{1}{2}I_{x2}\dot{\beta_2}^2 + \frac{1}{2}I_{y1}\dot{\alpha_1}^2 + \frac{1}{2}I_{y2}\dot{\alpha_2}^2 \qquad \text{Equation 12}$$

The potential energy equation is developed as follows:

$$V = \frac{1}{2}(KB1_x \,//\, KS1_x)X_1^2 + \frac{1}{2}\left(KB1_y \,//\, KS1_y\right)Y_1^2 + \frac{1}{2}(KB2_x \,//\, KS2_x)X_2^2 +$$

$$\frac{1}{2}\left(KB2_y \,//\, KS2_y\right)Y_2^2 + \frac{1}{2}KC_x(X_1 - X_2)^2 + \frac{1}{2}KC_y(Y_1 - Y_2)^2 + \frac{1}{2}KC_z(Z_1 - Z_2)^2 +$$

$$\frac{1}{2}KCT_x(\beta_1 - \beta_2)^2 + \frac{1}{2}KCT_y(\alpha_1 - \alpha_2)^2 + \frac{1}{2}KCT_z(\theta_1 - \theta_2)^2 + \frac{1}{2}KS1_zZ_1^2 +$$

$$\frac{1}{2}KS2_zZ_2^2 + \frac{1}{2}KS1T_z\theta_1^2 + \frac{1}{2}KS2T_z\theta_2^2 \qquad \text{Equation 13}$$

The dissipation energy equation is given as follows.

$$D = \frac{1}{2}CB1_x\dot{X_1}^2 + \frac{1}{2}CB1_y\dot{Y_1}^2 + \frac{1}{2}CB2_x\dot{X_2}^2 + \frac{1}{2}CB2_y\dot{Y_2}^2 + \frac{1}{2}CC_x\left(\dot{X_1} - \dot{X_2}\right)^2 +$$

$$\frac{1}{2}CC_y(\dot{Y_1} - \dot{Y_2})^2 + \frac{1}{2}CC_z(\dot{Z_1} - \dot{Z_2})^2 \qquad \text{Equation 14}$$

The mass, stiffness and damping matrices were derived as per Appendix 5 and found to be as follows.

The mass matrix [M] is given as below. Equation 15

m_1	0	0	0	0	0	0	0	0	0	0	0
0	m_2	0	0	0	0	0	0	0	0	0	0
0	0	m_1	0	0	0	0	0	0	0	0	0
0	0	0	m_2	0	0	0	0	0	0	0	0
0	0	0	0	m_1	0	0	0	0	0	0	0
0	0	0	0	0	m_2	0	0	0	0	0	0
0	0	0	0	0	0	I_{z1}	0	0	0	0	0
0	0	0	0	0	0	0	I_{z2}	0	0	0	0
0	0	0	0	0	0	0	0	I_{x1}	0	0	0
0	0	0	0	0	0	0	0	0	I_{x2}	0	0
0	0	0	0	0	0	0	0	0	0	I_{y1}	0
0	0	0	0	0	0	0	0	0	0	0	I_{y2}

The stiffness matrix [K] is given as below. Equation 16

$KBS1_x + KC_x$	$-KC_x$	0	0	0	0	0	0	0	0	0	0
$-KC_x$	$KBS2_x + KC_x$	0	0	0	0	0	0	0	0	0	0
0	0	$KBS1_y + KC_y$	$-KC_y$	0	0	0	0	0	0	0	0
0	0	$-KC_y$	$KBS2_y + KC_y$	0	0	0	0	0	0	0	0
0	0	0	0	$KC_z + KS1_z$	$-KC_z$	0	0	0	0	0	0
0	0	0	0	$-KC_z$	$KC_z + KS2_z$	0	0	0	0	0	0
0	0	0	0	0	0	$KCT_z + KS1T_z$	$-KCT_z$	0	0	0	0
0	0	0	0	0	0	$-KCT_z$	$KCT_z + KS2T_z$	0	0	0	0
0	0	0	0	0	0	0	0	KCT_x	$-KCT_x$	0	0
0	0	0	0	0	0	0	0	$-KCT_x$	KCT_x	0	0
0	0	0	0	0	0	0	0	0	0	KCT_y	$-KCT_y$
0	0	0	0	0	0	0	0	0	0	$-KCT_y$	KCT_y

The damping matrix [D] is given as below. Equation 17

$$\begin{bmatrix} CB1_x + CC_x & -CC_x & 0 & 0 & 0 & 0 & 0 & 0 & 0 & 0 & 0 & 0 \\ -CC_x & CB2_x + CC_x & 0 & 0 & 0 & 0 & 0 & 0 & 0 & 0 & 0 & 0 \\ 0 & 0 & CB1_y + CC_y & -CC_y & 0 & 0 & 0 & 0 & 0 & 0 & 0 & 0 \\ 0 & 0 & -CC_y & CB2_y + CC_y & 0 & 0 & 0 & 0 & 0 & 0 & 0 & 0 \\ 0 & 0 & 0 & 0 & CC_z & -CC_z & 0 & 0 & 0 & 0 & 0 & 0 \\ 0 & 0 & 0 & 0 & -CC_z & CC_z & 0 & 0 & 0 & 0 & 0 & 0 \\ 0 & 0 & 0 & 0 & 0 & 0 & 0 & 0 & 0 & 0 & 0 & 0 \\ 0 & 0 & 0 & 0 & 0 & 0 & 0 & 0 & 0 & 0 & 0 & 0 \\ 0 & 0 & 0 & 0 & 0 & 0 & 0 & 0 & 0 & 0 & 0 & 0 \\ 0 & 0 & 0 & 0 & 0 & 0 & 0 & 0 & 0 & 0 & 0 & 0 \\ 0 & 0 & 0 & 0 & 0 & 0 & 0 & 0 & 0 & 0 & 0 & 0 \\ 0 & 0 & 0 & 0 & 0 & 0 & 0 & 0 & 0 & 0 & 0 & 0 \end{bmatrix}$$

Assumptions made to model the rotor-coupling-bearing system are given hereafter:

- The two shafts were connected to the coupling by interference fit and no keys were introduced in the system.
- The bearings used in the current system does not impose any stiffness or damping in the axial direction.
- The discs of the system are responsible for unbalance (introduced into the system as eccentricity in the excitation force equation).
- The coupling stiffness is independent of the rotational angle.
- The stiffness and damping coefficient of the coupling can be fully described by three directions of which two are radial and one axial.
- Unbalance and misalignment are the only two excitation forces exist in the system.

3.2. Modeling of unbalance and misalignment forces

The unbalance force in the coupling can be defined to be the dynamic eccentricity of the system at the two parts of the coupling. The imbalance force in the radial direction is defined as follows.

$$\begin{Bmatrix} F_{x1} = m_1 e_1 \omega^2 \sin(\omega t) \\ F_{x2} = m_2 e_2 \omega^2 \sin(\omega t) \\ F_{y1} = m_1 e_1 \omega^2 \cos(\omega t) \\ F_{y2} = m_2 e_2 \omega^2 \cos(\omega t) \\ F_{\theta 1} = I_{z1} \frac{e_1}{r} \omega^2 \sin(\omega t) \\ F_{\theta 2} = I_{z2} \frac{e_2}{r} \omega^2 \sin(\omega t) \end{Bmatrix} \quad \text{Equation 18}$$

Where m_1 is the mass of subsystem 1 of the rotor-bearing-coupling system.

m_2 is the mass of subsystem 2 of the rotor-bearing-coupling system.

e_1 is the eccentricity of subsystem 1 of the rotor-bearing-coupling system.

e_2 is the eccentricity of subsystem 2 of the rotor-bearing-coupling system.

ω is the rotational speed of the shafts.

t is the time

r is the radius of the coupling.

The misalignment forces between two coupled shafts had been modeled using mathematical formulation. Figure 38 shows the general arrangement of the parallel and angular misaligned coupled shafts.

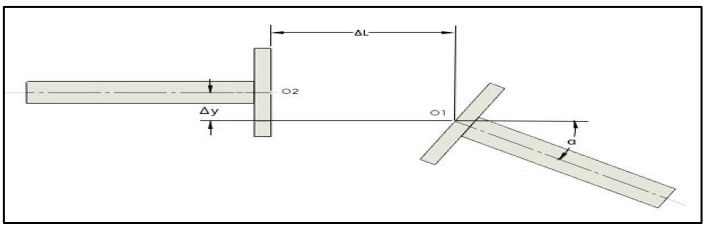

Figure 38: Misalignment modeling between coupling subsystem 1 and 2.

The total misalignment ΔE can be defined as the summation of parallel misalignment Δy and angular misalignment α where O1 and O2 are the center of articulation for subsystem 1 and 2:

$$\Delta E = \Delta y + \Delta L \tan(\alpha)$$ Equation 19

For parallel misalignment, the forces were derived in continuation to Wang and Jiang methodology. The relative motion diagram of coupling subsystems under parallel misalignment fault is given in figure 39.

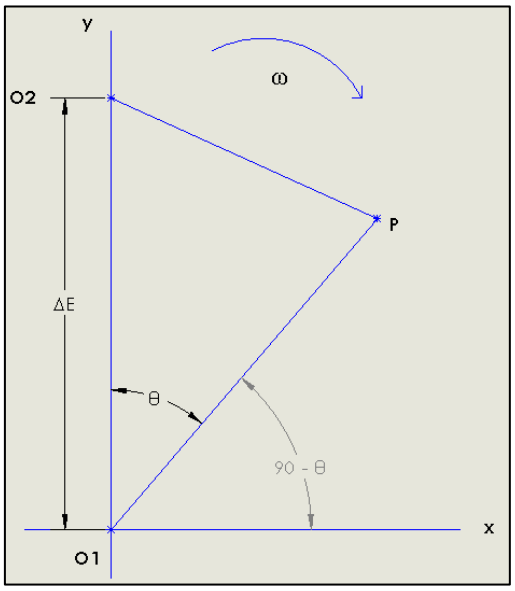

Figure 39: Relative motion diagram of coupling subsystems under parallel misalignment fault.

The coupling dynamic center P can be defined as:

$$x = O_1P \sin\theta = \Delta E \sin\theta \cos\theta = \Delta E \sin(\omega t) \cos(\omega t)$$

$$y = O_1P \cos\theta = \Delta E \cos\theta \cos\theta = \Delta E \cos(\omega t) \cos(\omega t)$$

The deformation of the coupling is O_1P where the deformations of the shafts caused by subsystem can be defined as $\frac{O_1P}{2}$.

Deformation in the radial direction is $d = \frac{O_1P}{2} = \frac{\Delta E}{2} cos(\omega t)$

The force acting on the coupling is then defined as follows.

$F = K\,d = K\,\frac{\Delta y}{2} cos\,(\omega t)$ Equation 20

Equation 20 can be decomposed to in X_1 and Y_1 directions to estimate the forces in radial direction at part 1 of the coupling F_{X1} , F_{Y1} as following.

$F_{X1} = F\,sin(\omega t) = K_x\,\frac{\Delta y}{2} cos(\omega t)\,sin(\omega t)$ Equation 21

Using half trigonometric angle identity $\sin 2\theta = 2sin\theta\,cos\theta$ in equation 21, the parallel misalignment force in X_1-direction can be rewritten as:

$F_{X1} = K_x \frac{\Delta y}{4} sin(2\omega t)$ Equation 22

And similarly, for the parallel misalignment force in Y_1-direction.

$F_{Y1} = F\,cos(\omega t) = K_y\,\frac{\Delta y}{2}\,cos(\omega t)\,cos(\omega t)$ Equation 23

Using double angle trigonometric identity $cos^2\theta = \frac{1+cos2\theta}{2}$ in equation 23, the parallel misalignment force in Y_1-direction can be rewritten as:

$F_{Y1} = K_y\,\frac{\Delta y}{2}\,(\frac{1+cos(2\omega t)}{2})$ Equation 24

And finally, for the parallel misalignment forces in $X_2\ and\ Y_2$ directions are:

$F_{X2} = -F_{X1}$ Equation 25

$F_{Y2} = -F_{Y1}$ Equation 26

For angular misalignment, the forces were derived in continuation to Wang and Gong methodology. The torque decomposition schematic of coupling subsystems under parallel misalignment fault is given in figure 40.

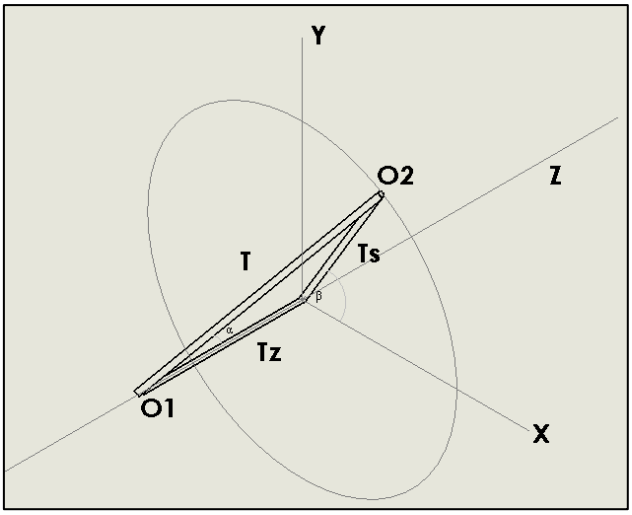

Figure 40: torque decomposition schematic for coupled shafts under angular misalignment fault.

The torque due to angular misalignment can be decomposed to T_Z and T_S as follows:

$T_Z = T\cos\alpha$ Equation 27

$T_S = T\sin\alpha$ Equation 28

As mentioned by Xu and Marangoni, the relative velocity ratio between two misaligned shafts can be expressed as:

$$\frac{\omega_2}{\omega_1} = \frac{\frac{4\cos\alpha}{3+\cos 2\alpha}}{1+\frac{1-cos\alpha}{3+\cos 2\alpha}\cos 2\omega t}$$ Equation 29

Equation 29 can be differentiated to obtain angular misalignment in $\ddot{\theta}_2$ as following.

$$\ddot{\theta} = \frac{-(8\omega^2 \sin 2\omega t\ \cos\alpha(\cos\alpha-1)}{(\frac{\cos 2\omega t\,(\cos\alpha-1)}{(2\,cos^2\alpha+2)-1})^2(2\,cos^2\alpha+2)^2}$$ Equation 30

And finally, the torque due to angular misalignment can be obtained using Newton's second law as follows.

$$T_Z = I_Z\ddot{\theta} = \frac{-I_Z(8\omega^2 \sin(2\omega t)\ \cos(\alpha)(\cos(\alpha)-1)}{(\frac{\cos(2\omega t)\,(\cos(\alpha)-1)}{(2\,cos^2(\alpha)+2)-1})^2(2\,cos^2(\alpha)+2)^2}$$ Equation 31

3.3. Determination of flexible coupling stiffness

Using Solidworks software, a 3D model was developed of the two spiral couplings. The coupling type used in this study is Ruland PCR24 - 10 - 10 – A which stands for “A” is Aluminum coupling, “PCR” is clamp type relief, “24” is 24/16 outer diameter in inches (38.1 mm) and “10” is 10/16 both bores in inches (15.875 mm) as per the supplier catalog (Forsthoffer, 2017). It should be noticed that the two spiral couplings used are similar in all aspects except for length, spiral grooves degree and a slight change in radius. The white coupling grooves are of 380 degrees while the black coupling grooves are of 525 degrees. Figure 41 illustrates the dimensions of the two spiral couplings – which had been named as white and black couplings due to its coating color.

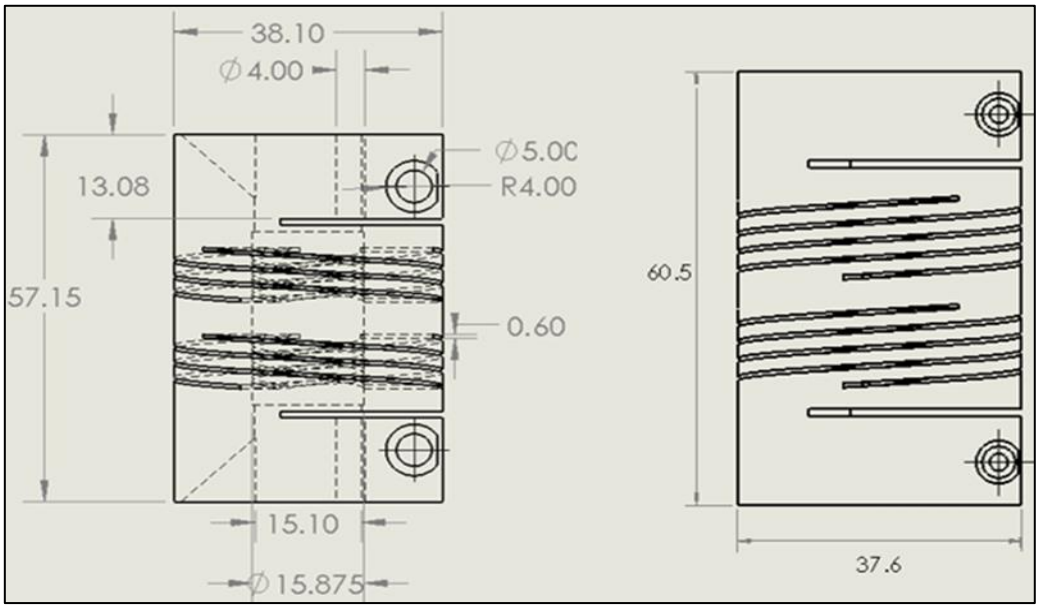

Figure 41: Dimensions of the two spiral couplings in millimeters. a) white and b)black.

The manufacturer properties of the white spiral coupling are listed below in table 3.

Table 3

Mechanical properties for white spiral coupling

Mechanical Property	**Commercial values by the supplier**
Material	Aluminum 7075- T651 Extruded and Drawn
Mass without bolts	130 g
Static torque	10.73 N.m
Torsional stiffness	0.38 Deg/N.m
Parallel misalignment	0.762 mm
Moment of inertia	2.9937×10^{-5} Kg.m^2

To evaluate the SolidWorks model of the couplings, a comparison of the mass and the moment of inertia in z-direction was made with the supplier values. It was found that the modeled mass of the white coupling is 134 g which represents 3% error. Moreover, it was found that the modeled moment of inertia in the z-direction is 2.8185×10^{-5} Kg.m^2 which represents a 5.8% error. It should be noted that the black coupling does not have a manual as it is an old version. The actual mass was measured to be 120 g while the modeled mass was 122 g which represents 1.67% error. The analysis mentioned in this section will illustrate the determination of white coupling stiffness procedure.

In order to determine the spiral coupling stiffness, Abaqus software was used to apply a static load in one direction (at one end of the coupling while fixing the other end) and to measure the static deflection in the same direction. Prior to starting of Abaqus analysis, modeling requirements were introduced to the software as follows:

- Geometry (part): spiral coupling was imported from Solidworks software.
- Material (property): material properties for spiral coupling Aluminum 7075-

T651 was used:

- Density (general): 2810 kg/m^3.
- Elastic modulus (Mechanical): 72,000 MPa.
- Poisson ratio (Mechanical): 0.33.

- Simulation (step): linear geometry model with a time period of 4 seconds and increment size of 1 second.
- Connections(interaction): connect the surface of the applied load to the center point to allow for point load application on that surface.
- Load: a uniform force applied in the three directions (x, y, and z) separately as well as a uniform moment about each of the three axes.
- Mesh: Tetrahedral element mesh was used due to the complexity of the spiral coupling geometry.

With the intention to determine the best mesh size for the spiral coupling, a series of compression simulation was done with a 100 N load applied at one end of the coupling while the other end was fixed. The mesh size was changed from 6 to 1.5 to visualize the effect of the mesh size on the compression deflection (the minimum mesh size was chosen to be 1.5 as the mesh size of 1 couldn't be simulated due to the huge time needed). Table 4 shows the mesh convergence analysis and simulation time.

Table 4

Mesh size analysis and simulation time

Mesh size	Deformation at Point Load (mm)	Relative Error %	Time (s)
6	0.46160	-----	33
5	0.50246	8.13	36
4	0.55800	9.95	40
3	0.57836	3.52	45
2	0.58787	1.62	103
1.5	0.59261	0.80	224

As it can be noticed that the relative error of the mesh size had been reduced to less than 2 % with a mesh size of 2 which was the optimum mesh size by the auto-meshing function in Abaqus. Moreover, figure 42 visualizes the mesh size behavior of the spiral coupling geometry.

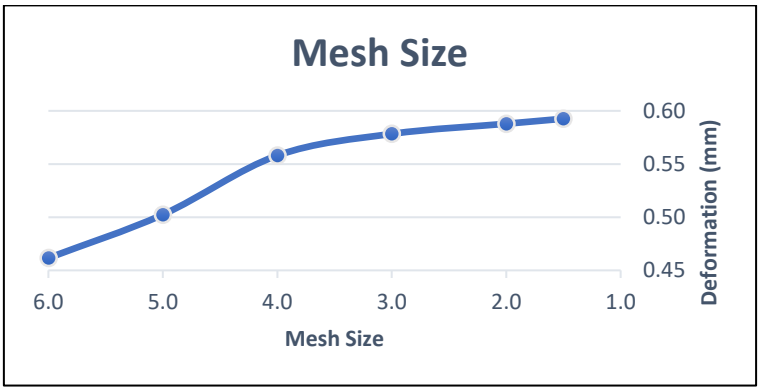

Figure 42: Mesh size behavior of the spiral coupling geometry.

Applying a load of 100 N in the axial direction for both compression and tension load conditions, figure 43 visualizes the deflection in the z-direction at the final step corresponding to the full load.

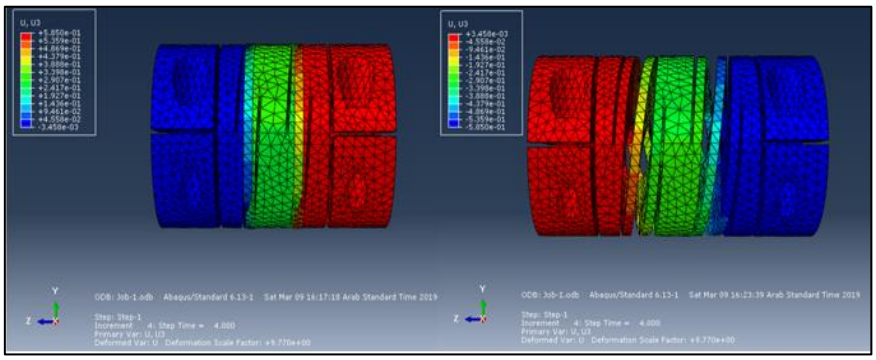

Figure 43: Spiral coupling tension and compression FEA deflection in the z-direction

The stiffness of the coupling was determined by correlating the applied uniform load in the z-direction to the deflection in the same direction. Figure 44 shows the stiffness of the spiral coupling in tension and compression.

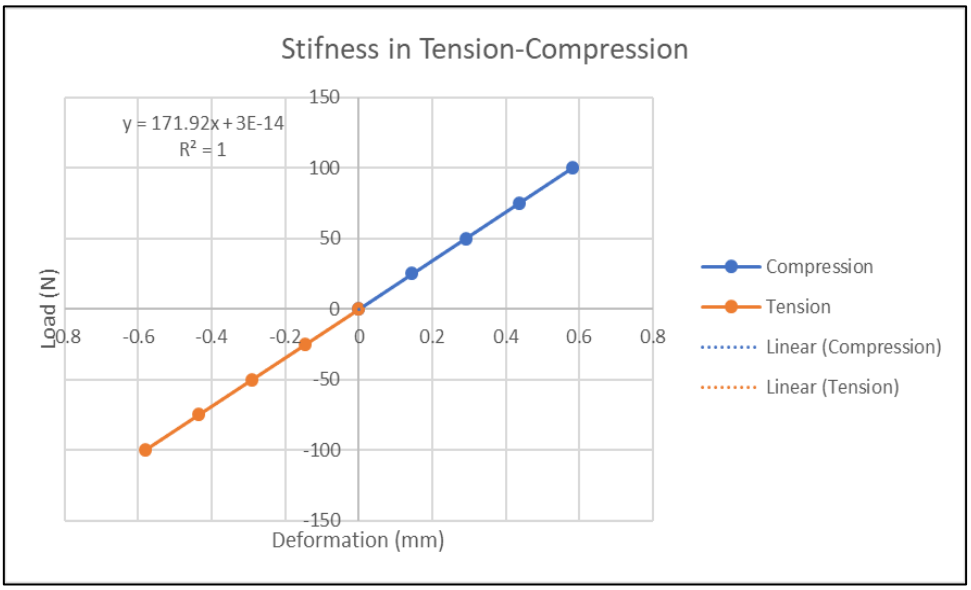

Figure 44: Stiffness of spiral coupling in tension and compression (z-direction) for the four steps.

From the graph's slope, it can be noticed that the stiffness in the positive and negative z-direction are the same and equals 171.92 KN/m.

Applying a load of 100 N in the positive and negative radial direction, figure 45 visualizes the deflection in the x-direction at the final step corresponding to the full load.

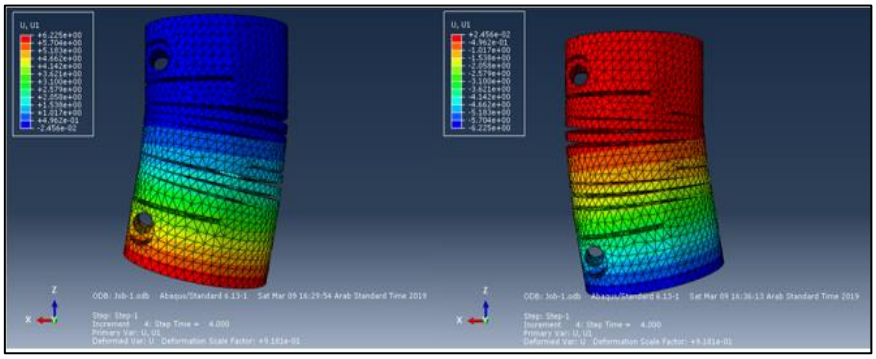

Figure 45: Spiral coupling FEA deflection in the positive and negative x-direction.

The stiffness of the coupling was determined by correlating the applied uniform load in the x-direction to the deflection in the same direction. Figure 46 shows the stiffness of the spiral coupling in the positive and negative x-direction.

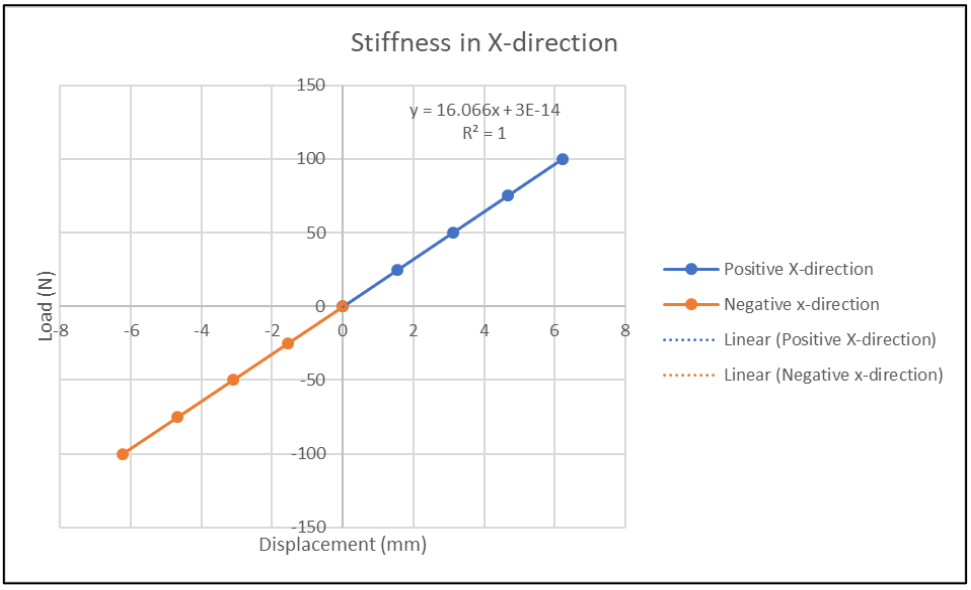

Figure 46: Stiffness of spiral coupling in positive and negative x-direction for the four steps.

From the graph's slope, it can be noticed that the stiffness in positive and negative x-directions are the same in and equals 16.066 KN/m.

Applying a load of 100 N in the positive and negative radial direction, figure 47 visualizes the deflection in the y-direction at the final step corresponding to the full load.

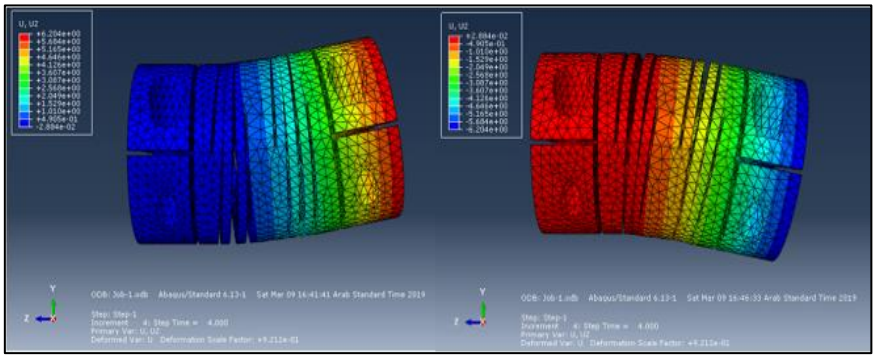

Figure 47: Spiral coupling FEA deflection in the positive and negative y-direction.

The stiffness of the coupling was determined by correlating the applied uniform load in the y-direction to the deflection in the same direction. Figure 48 shows the stiffness of the spiral coupling in the positive and negative y-direction.

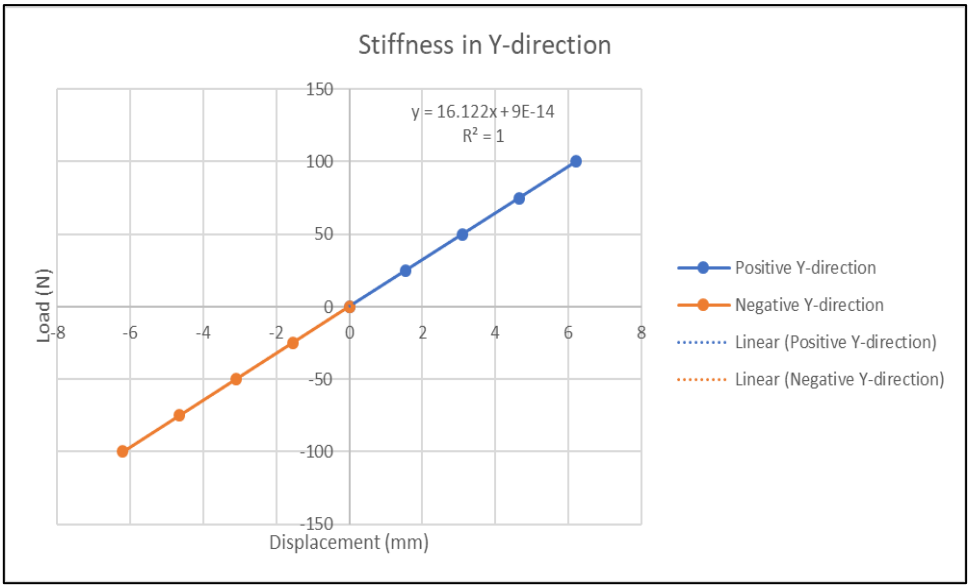

Figure 48: Stiffness of spiral coupling in the positive and negative y-direction for the four steps.

From the graph's slope, it can be noticed that the stiffness in positive and negative y-directions are the same in and equals 16.122 KN/m.

Applying a couple load of 100 N at any opposite positions of one end of the spiral coupling while fixing the other end, it would result in a moment load of 3810 N.mm. Figure 49 visualizes the angular deflection around the z-axis in both directions (clockwise and counter-clockwise) at the final step corresponding to the full load.

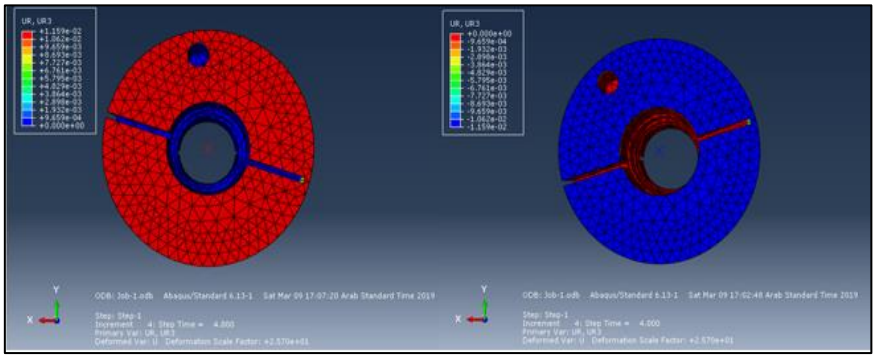

Figure 49: Spiral coupling FEA angular deflection in clockwise and counterclockwise around the z-axis.

The stiffness of the coupling was determined by correlating the applied uniform load to the angular deflection in the same direction. Figure 50 shows the stiffness of the spiral coupling around the z-axis.

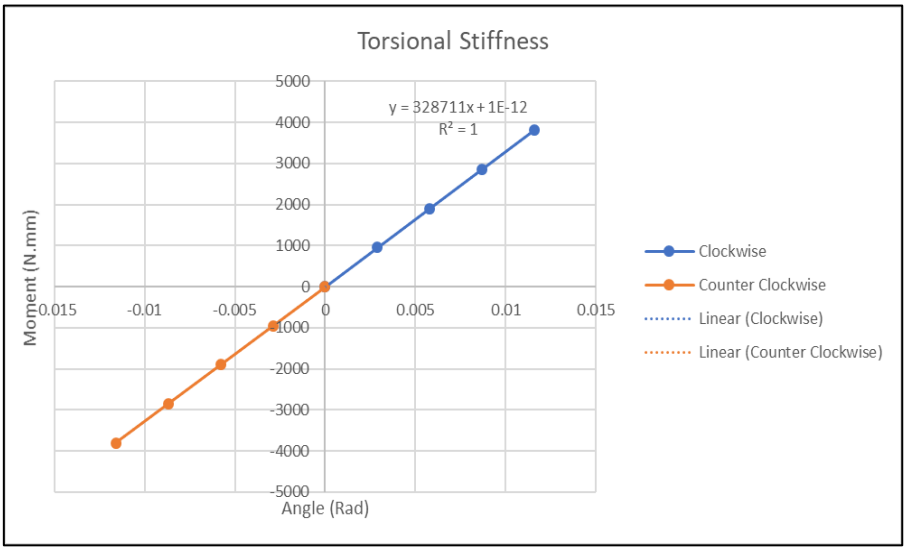

Figure 50: Angular stiffness of spiral coupling clockwise and counter-clockwise around z-axis for the four steps.

From the graph's slope, the spiral coupling angular stiffness around the z-axis in positive and negative directions are the same and equals 328.711 N.mm/rad.

Applying a load of 100 N at 90,270 positions of one end of the spiral coupling while fixing the other end, it would result in a moment load of 5715 N.mm. Figure 51 visualizes the angular deflection around the x-axis in both directions (clockwise and counter-clockwise) at the final step corresponding to the full load.

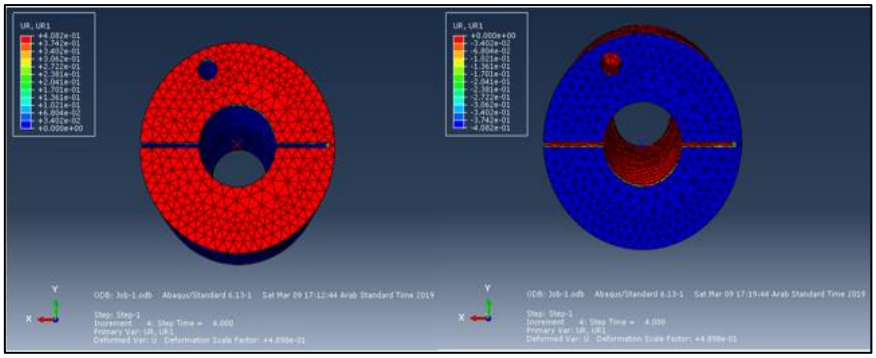

Figure 51: Spiral coupling FEA angular deflection in clockwise and counterclockwise around the x-axis.

The stiffness of the coupling was determined by correlating the applied uniform load around the x-axis to the angular deflection in the same direction. Figure 52 shows the stiffness of the spiral coupling around the x-axis.

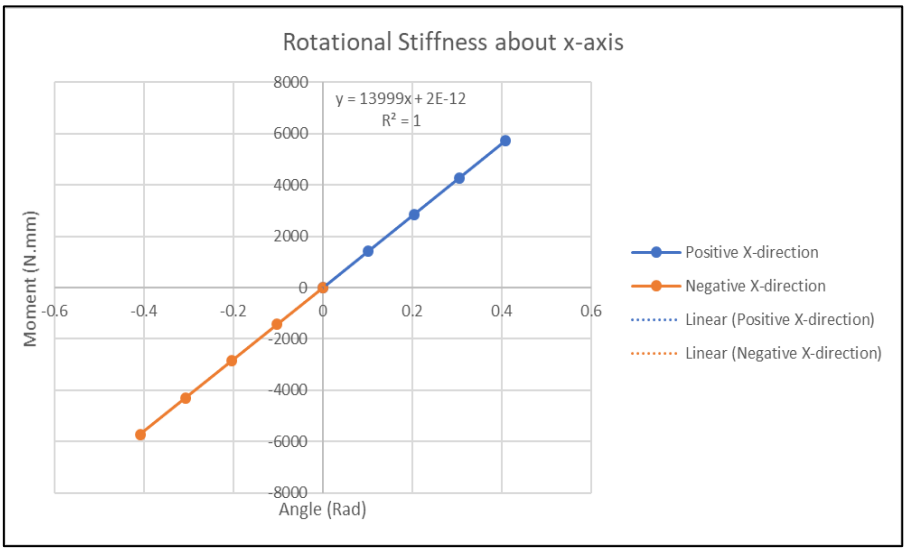

Figure 52: Angular stiffness of spiral coupling clockwise and counter-clockwise around x-axis for the four steps.

From the graph's slope, the spiral coupling angular stiffness around x-axis in positive and negative directions are the same and equals 13.999 N.mm/rad.

Applying a load of 100 N at 0,180 positions of one end of the spiral coupling while fixing the other end, it would result in a moment load of 5715 N.mm. Figure 53 visualizes the angular deflection around the y-axis in both directions (clockwise and counter-clockwise) at the final step corresponding to the full load.

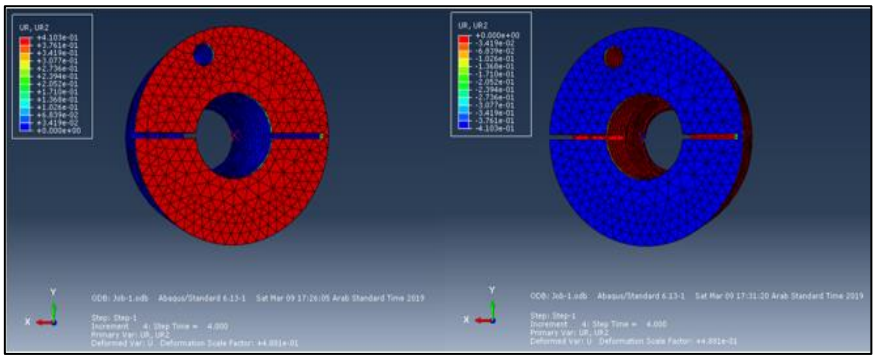

Figure 53: Spiral coupling FEA angular deflection in clockwise and counterclockwise around the y-axis.

The stiffness of the coupling was determined by correlating the applied uniform load around the y-axis to the angular deflection in the same direction. Figure 54 shows the stiffness of the spiral coupling around the y-axis.

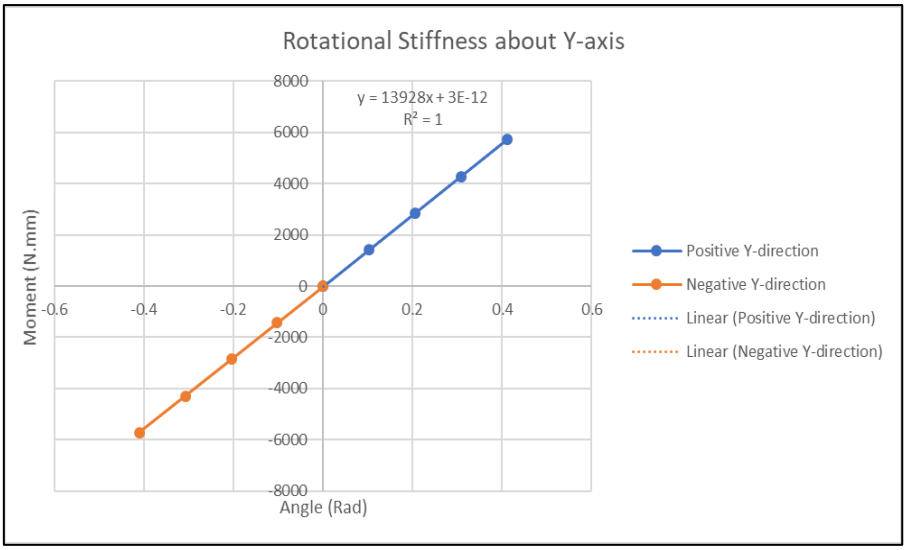

Figure 54: Angular stiffness of spiral coupling clockwise and counter-clockwise around y-axis for the four steps.

From the graph's slope, the spiral coupling angular stiffness around y-axis in positive and negative directions are the same and equals 13.928 N.mm/rad.

3.4. Determination of flexible coupling damping coefficients

An experimental method was used to estimate the coupling damping in the three translational directions X, Y, and Z. Logarithmic decrement method is usually used to measure the under-damped systems damping coefficient (Büchholdt, 2012). Figure 55 shows the motion of a damped system:

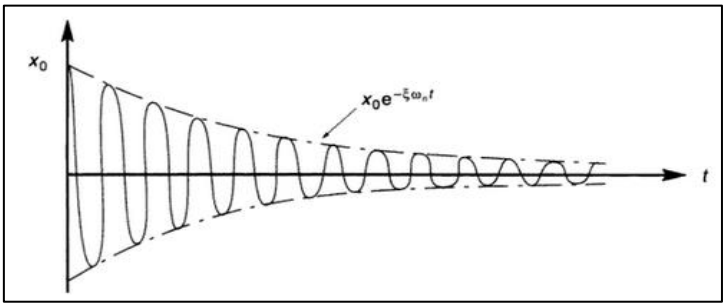

Figure 55: Motion of a damped system (Büchholdt, 2012).

Equation 32 was used to estimate the damping coefficient by knowing the exponent of the systems damped motion.

$$C = 2\zeta\sqrt{Km} \qquad \text{Equation 32}$$

Where ζ is the damping ratio of the coupling, k and m are the stiffness (in the desired direction) and mass of the coupling.

Impact test for spiral couplings was done using PCB PIZOTRONICS tools (hammer and accelerometer) and BETAVIB data acquisition unit. The first step was to set the hammer and accelerometer sensitivity based on their model 2.25 mv/N and 10.2 mv/(m/s^2), respectively. After fixing the coupling, the accelerometer was in the direction of interest. Fifty impacts were applied in the direction understudy to result in averaged time-response of the coupling. In this section, the determination of white spiral coupling was shown. Figure 56 shows the experimental tools used.

Figure 56: PCB PIZOTRONICS tools and BETAVIB data acquisition used for coupling damping experiment.

Figures 57, 58 and 59 show the experimental logarithmic decrement result of the modal analysis for X, Y and Z directions.

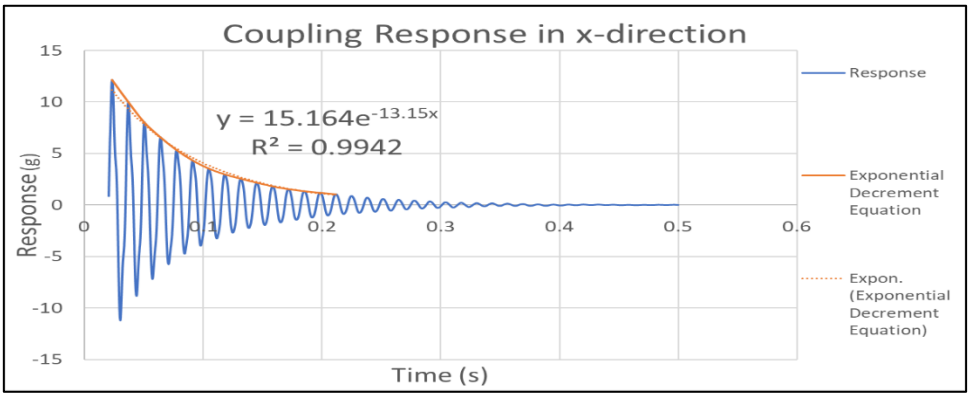

Figure 57: Coupling Impact Test Response in X-direction.

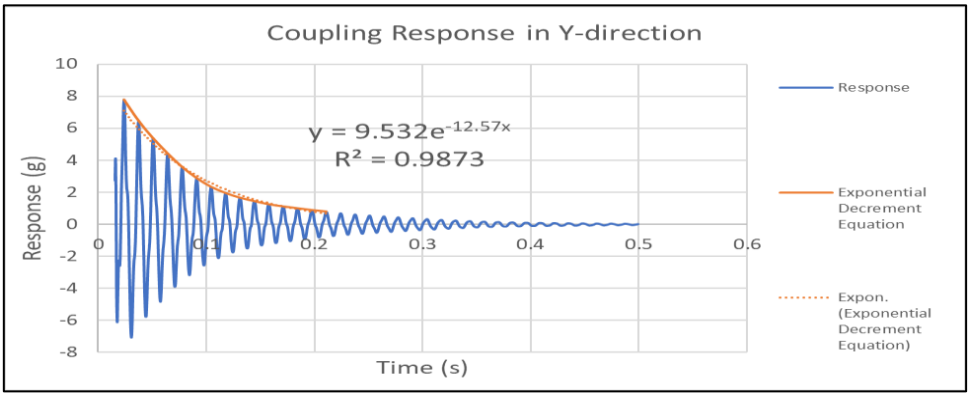

Figure 58: Coupling Impact Test Response in Y-direction.

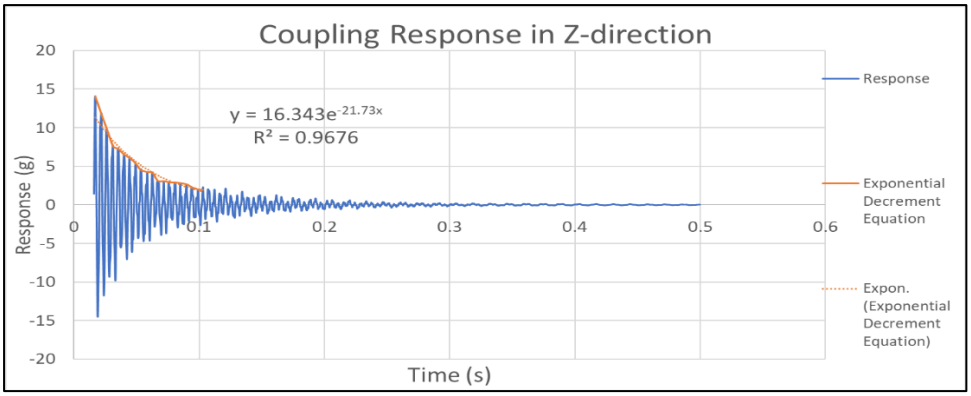

Figure 59: Coupling Impact Test Response in Z-direction.

It should be noted that the first 0.01 (s) of the coupling impact test response was not included as it is of a high amplitude due to the impact. Moreover, the exponential decrement equation in the Z direction was found to be more monotonic. The exponents of the exponential decrement equation were found to be -13.15, -12.57 and -21.73in the X, Y and Z directions, respectively. Consecutively, the damping coefficients of the coupling in X, Y and Z directions were found to be 3.42 (N.s/m), 3.27 (N.s/m) and 5.65 (N.s/m), respectively.

3.5. Bearings and shaft stiffness and damping

The bearing stiffness and damping values were taken from the Qatar university student's thesis to be 6.56×10^8 N/m radial stiffness and 1.8×10^3 N.s/m damping coefficient in the radial direction.

The shafts stiffness in radial and axial directions was estimated using laws of solid mechanics. The shafts material was AISI-1045 cold drawn steel with an elastic modulus (E) of 205,000 N/mm^2 and Shear modulus (G) of 79,457 N/mm^2.

For Shaft 1:

$$k_{radial} = \frac{3}{4}\frac{\pi\, r^4 E}{{L_1}^3} = \frac{3}{4}\frac{\pi\,(7.55)^4(205\times10^3)}{107^3} = 1{,}281.15\ N/mm$$

$$k_{axial} = \frac{AE}{L_1} = \frac{\pi\, r^2 E}{L_1} = \frac{\pi\,(7.55)^2(205\times10^3)}{107} = 343{,}094.58\ N/mm$$

$$k_{rotational} = \frac{J\,G}{L_1} = \frac{\pi\, r^4 G}{2\,L_1} = \frac{\pi\,(7.55)^4(79457)}{2\,(107)} = 3{,}790{,}147.13\ N.mm/rad$$

For Shaft 2:

$$k_{radial} = \frac{3}{4}\frac{\pi\, r^4 E}{{L_2}^3} = \frac{3}{4}\frac{\pi\,(7.55)^4(205\times10^3)}{60^3} = 7{,}266.06\ N/mm$$

$$k_{axial} = \frac{AE}{L_2} = \frac{\pi\, r^2 E}{L_2} = \frac{\pi\,(7.55)^2(205\times10^3)}{60} = 611{,}852\ N/mm$$

$$k_{rotational} = \frac{J\,G}{L_2} = \frac{\pi\, r^4 G}{2\,L_2} = \frac{\pi\,(7.55)^4(79457)}{2\,(60)} = 6{,}759{,}095.72\ N.mm/rad$$

Where r is the radius of both shafts; A is the area of the shaft cross section. J is the polar moment of inertia. L_1 and L_2 are the length of shaft 1 and shaft 2, respectively.

3.6. Numerical solving of rotor-coupling bearing system equations of motion

The system of the equation of motion matrixes as derived in section 3.1 was solved numerically using Matlab software. The software program was divided into subprograms to allow for easy control of the simulation parameter. The numerical solver strategy was to use the Matlab built-in Simulink tool to solve the system of equations of motion of the rotor-coupling-bearing system in a matrices form. The simulation parameters such as simulation time and simulation step were chosen to provide a suitable time range stepping for the system to be solved. Moreover, the sampling frequency was chosen to be around 50 times larger than the system's running frequency to produce accurate response except when the natural frequency test was examined. Figure 60 shows a summary of the programming software functionality and the full program is provided in Appendix 6.

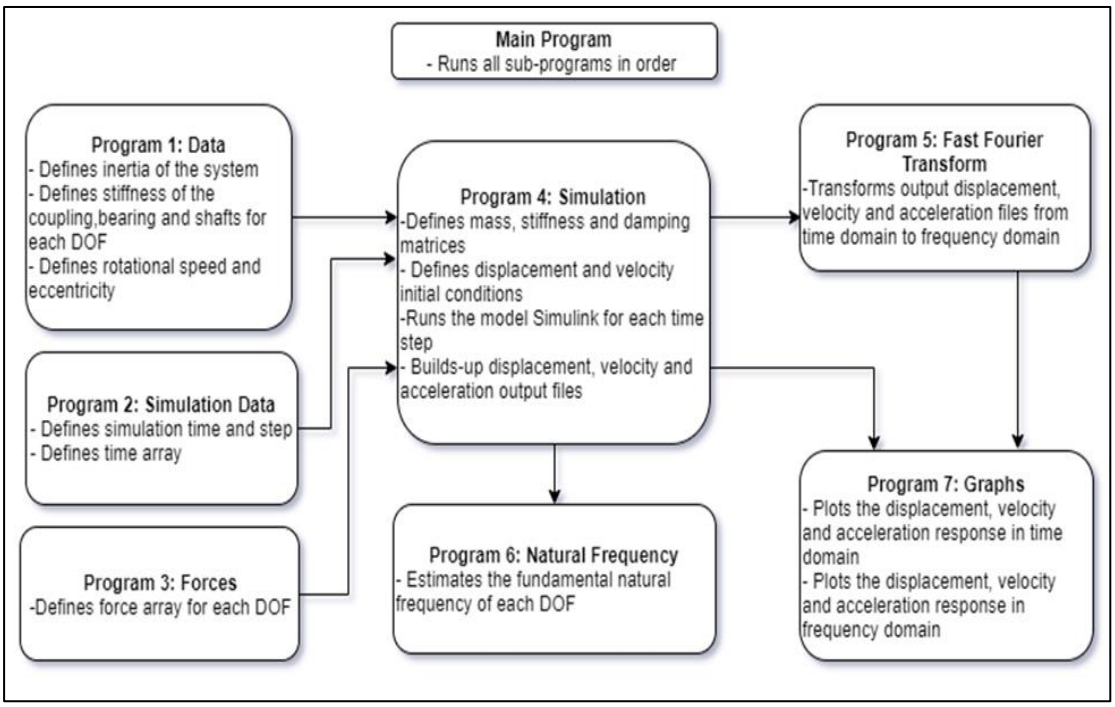

Figure 60: Summary of numerical solver programming software functionality.

Moreover, Table 5 summarizes all the rotor-coupling-bearing system parameters required for the numerical solver using the white coupling.

Table 5

Summary of the white coupling-rotor-bearing system parameters

Parameter	**Value**	**unit**	**Parameter**	**Value**	**unit**
m_1	0.21745	Kg	$KS2_z$	6.12×10^{8}	N/m
m_2	0.15138	Kg	$KS1T_z$	3790.15	N.m/rad
I_{x1}	2.33×10^{-4}	$Kg.m^2$	$KS2T_z$	6759.10	N.m/rad
I_{x2}	4.90×10^{-5}	$Kg.m^2$	KC_x	16066	N/m
I_{y1}	2.33×10^{-4}	$Kg.m^2$	KC_y	16122	N/m
I_{y2}	4.88×10^{-5}	$Kg.m^2$	KC_z	171920	N/m
I_{z1}	1.84×10^{-5}	$Kg.m^2$	KCT_x	13.999	N.m/rad
I_{z2}	1.66×10^{-5}	$Kg.m^2$	KCT_y	13.928	N.m/rad
$KB1_x$	6.56×10^{8}	N/m	KCT_z	328.711	N.m/rad
$KB1_y$	6.56×10^{8}	N/m	$CB1_x$	1.8×10^{3}	N.s/m
$KB2_x$	6.56×10^{8}	N/m	$CB1_y$	1.8×10^{3}	N.s/m
$KB2_y$	6.56×10^{8}	N/m	$CB2_x$	1.8×10^{3}	N.s/m
$KS1_x$	1.28×10^{6}	N/m	$CB2_y$	1.8×10^{3}	N.s/m
$KS1_y$	1.28×10^{6}	N/m	CC_x	3.42	N.s/m
$KS1_z$	3.43×10^{8}	N/m	CC_y	3.27	N.s/m
$KS2_x$	7.27×10^{6}	N/m	CC_z	5.65	N.s/m
$KS2_y$	7.27×10^{6}	N/m			

In addition, table 6 summarizes black coupling parameters required for the numerical solver.

Table 6

Summary of the black coupling parameters

Parameter	**Value**		**Parameter**	**Value**	
m_1	0.21247	Kg	KC_x	6422.6	N/m
m_2	0.1464	Kg	KC_y	6472.4	N/m
I_{x1}	2.24×10^{-4}	$Kg.m^2$	KC_z	52315	N/m
I_{x2}	4.68×10^{-5}	$Kg.m^2$	KCT_x	6.577	N.m/rad
I_{y1}	2.24×10^{-4}	$Kg.m^2$	KCT_y	6.506	N.m/rad
I_{y2}	4.66×10^{-5}	$Kg.m^2$	KCT_z	125.923	N.m/rad
I_{z1}	1.74×10^{-5}	$Kg.m^2$	CC_x	1.62024	N.s/m
I_{z2}	1.55×10^{-5}	$Kg.m^2$	CC_y	1.59528	N.s/m
			CC_z	1.39776	N.s/m

CHAPTER 4: RESULTS AND DISCUSSION

In this chapter, the rotor-coupling-bearing system simulation results will be presented and discussed. The white spiral coupling was used in the simulation to examine the model's response due to unbalance and misalignment forces. The simulation time was chosen to be 1 second divided to 1-millisecond intervals which are equivalent to 50 times the 1X frequency. The scale of the vibration spectrum was truncated at 100 Hz as the low-frequency range is of interest. The study of vibration analysis of the rotor-coupling-bearing system included a) the effect of the parallel and angular misalignment in time domain and vibration spectrum, b) the effect of increasing the parallel and angular misalignment levels in time domain and vibration spectrum, c) the effect of changing the RPM for parallel and angular misaligned systems in time domain and vibration spectrum and finally d) the effect of changing the flexible coupling type on both time domain and vibration spectrum.

4.1. The natural frequency of the system

The natural frequency of the rotor-coupling-bearing system was estimated in the excited degrees of freedom which are X_1, X_2, Y_1, Y_2, θ_1 and θ_2. Table 7 shows the natural frequency of the rotor-coupling-bearing system in the radial and angular directions.

Table 7

The natural frequency of the rotor-coupling-bearing system in the radial and angular directions

DOF	$\boldsymbol{X_1}$	$\boldsymbol{X_2}$	$\boldsymbol{Y_1}$	$\boldsymbol{Y_2}$	$\boldsymbol{\theta_1}$	$\boldsymbol{\theta_2}$
Natural frequency (Hz)	8750.3	10535	8750.3	10535	2384.5	3302.3

Generally, the natural frequencies of the system were found to be high due to the inclusion of the shafts' stiffness (Metal) in the stiffness matrix. Therefore, the rotor-coupling-bearing system operation RPM in the range of 1200 to 3000 RPM won't induce any resonance in the system. It should be noted that the natural frequency in X_1 *and* Y_1 directions are the same and this is since the stiffness of bearings are dominant in the radial direction. The same explanation applies for the natural frequencies in X_2 *and* Y_2 directions. In θ_1 *and* θ_2 directions, the bearings didn't imply any stiffness on the system as mentioned in the model assumptions which lead to the changes in the natural frequencies.

4.2. Vibration response of the unbalanced rotor-coupling-bearing system

The unbalance forces effect on the rotor-coupling-bearing system response was investigated in radial and angular directions.

4.2.1. Unbalanced response of the system in a radial direction

The unbalanced response of the system in a radial direction (X_1, X_2, Y_1, Y_2) was obtained with a rotating speed of 1200 RPM equivalent to 20 Hz at the 1X frequency. Eccentricity of 1 mm was introduced to the system in both radial directions (vertical and horizontal). Figures 61 and 62 present the time and frequency domains response of the unbalanced system in a radial direction.

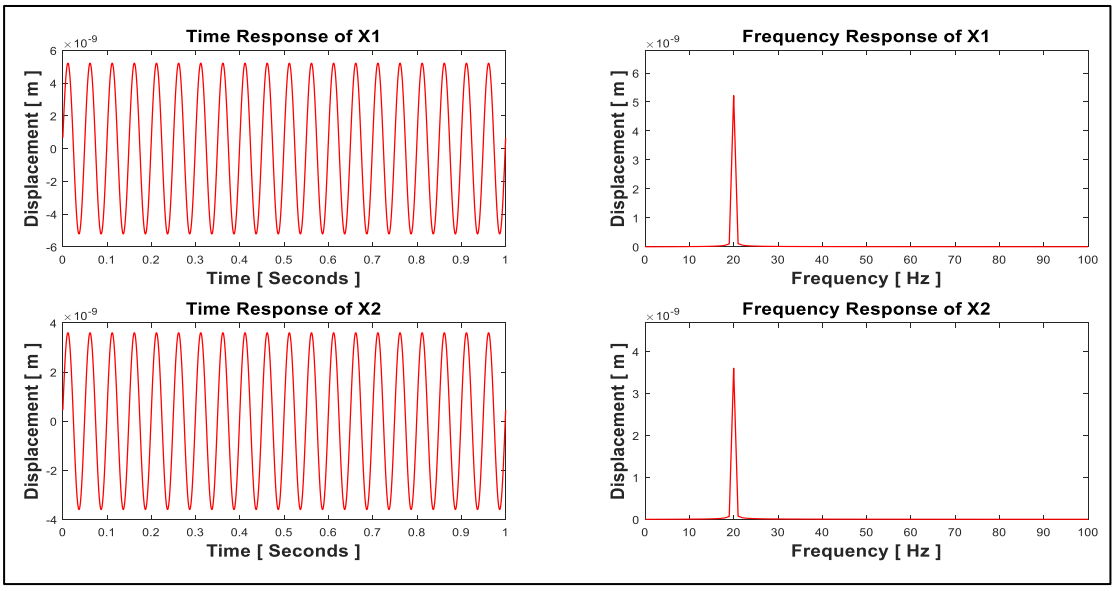

Figure 61: Time and frequency domains response of the unbalanced system in the x-direction.

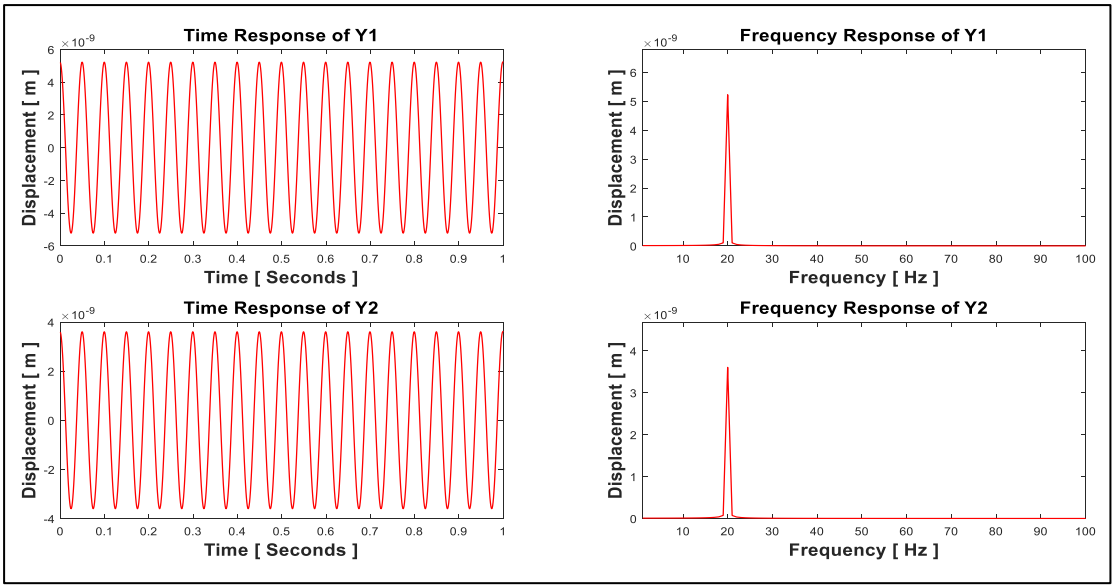

Figure 62: Time and frequency domains response of the unbalanced system in the y-direction.

It was found that the displacement response in time and frequency domains for radial direction at node 1 is almost constant which means that the displacement response of X_1 and Y_1 directions are similar. And same applies for the displacement response at node 2. This was expected as the coupling, bearings and shafts stiffness and damping in the model were independent of the rotational angle and the values in the vertical and horizontal directions were found to be very close to each other as per section 3.3 and 3.4. The displacement time response in X- direction was found to represent a sine wave while the response in Y- direction represented a cosine wave. The displacement time response amplitudes in X_1 and Y_1 directions were found be 5.214 × 10^{-3} (µm) and 5.265× 10^{-3} (µm), respectively. Likewise, displacement time response amplitudes in X_2 and Y_2 directions were found to be 3.597× 10^{-3} (µm) and 3.633× 10^{-3} (µm), respectively. Moreover, the displacement spectrum in the radial direction was found to be synchronized with 1X RPM amplitude as expected. The displacement spectrum amplitudes in X_1 and Y_1 directions were found to be 5.218× 10^{-3} (µm) and 5.223× 10^{-3}

(µm), respectively. Likewise, displacement spectrum amplitudes in X_2 *and* Y_2 directions were found to be 3.600× 10^{-3} (µm) and 3.604× 10^{-3} (µm), respectively. It can be noticed that the vibrations at node 1 is higher than node 2 which is expected as the subsystem 1 is of higher mass than subsystem 2 (as per unbalance force formula). There is a slight change between the amplitudes in the time and frequency domains. This is mainly due to the error associated in transforming the FFT built-in function results to the desired scale in Matlab.

4.2.2. The unbalanced response of the system in the angular direction

The unbalanced response of the system in an angular direction (θ_1, θ_2) was obtained with a rotating speed of 1200 RPM equivalent to 20 Hz at the 1X frequency. Eccentricity of 1 mm was introduced to the system. Figure 63 shows the time and frequency domains response of the unbalanced system in angular direction.

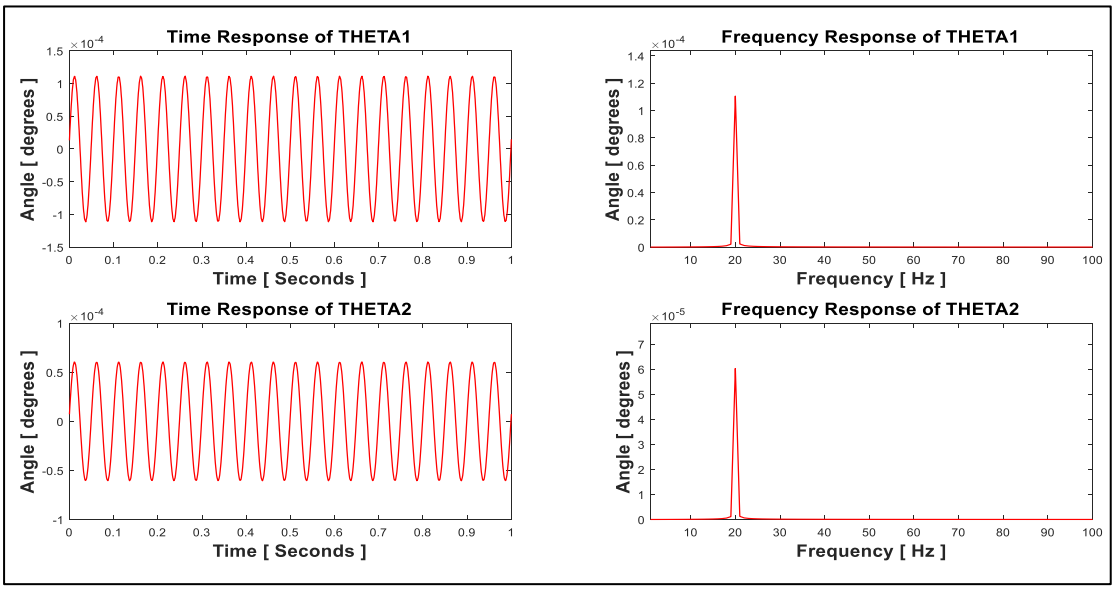

Figure 63: Time and frequency domains response of the unbalanced system in angular direction.

It was found that angle time response in angular direction was found to represent a sine wave as per the excitation force. The angle time response amplitudes in $\theta_1 \; and \; \theta_2$ directions were found to be 1.114× 10^{-4} (degrees) and 0.605× 10^{-4} (degrees), respectively. Moreover, the angle spectrum amplitudes in $\theta_1 \; and \; \theta_2$ directions were found be 1.1051× 10^{-4} (degrees) and 0.602× 10^{-4} (degrees), respectively. There is a slight change between the amplitudes in the time and frequency domains as explained in section 4.2.1.

4.3. Vibration response of unbalance and parallel misalignment faults in the rotor-coupling-bearing system in the radial direction

The response of the system in the radial direction (X_1, X_2, Y_1, Y_2) was obtained after adding a parallel misalignment to the unbalanced system with a rotating speed of 1200 RPM. Eccentricity of 1 mm was introduced to the system in both radial directions (vertical and horizontal) and parallel misalignment distance of 1mm. Figures 64 and 65 present the time and frequency domains response of the unbalance and parallel misalignment fault of the system in the radial direction.

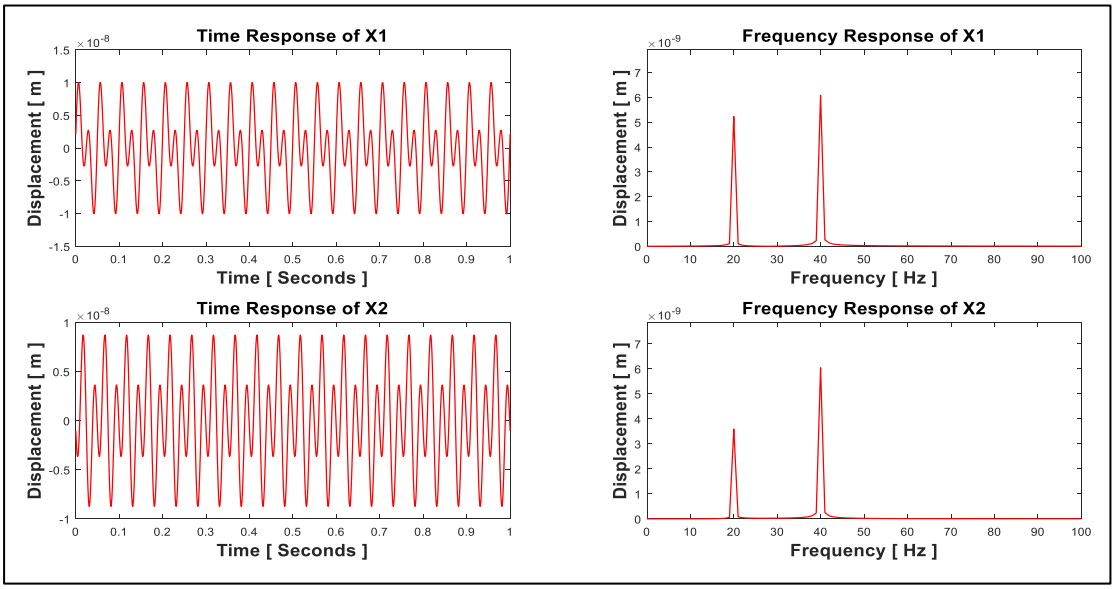

Figure 64: Time and frequency domains response of unbalance and parallel misalignment fault in x-direction.

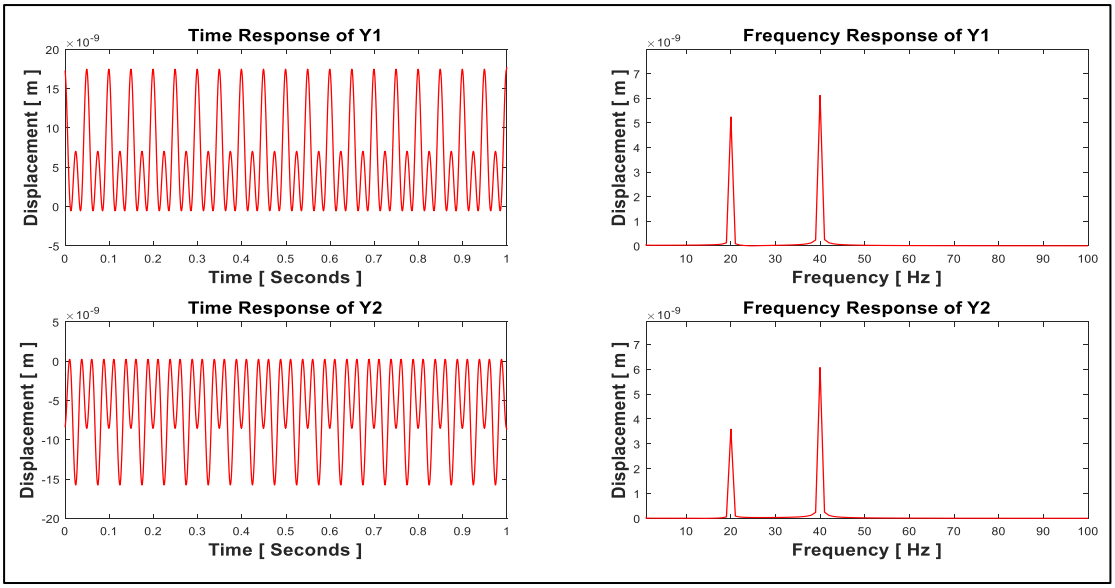

Figure 65: Time and frequency domains response of the unbalance and parallel misalignment fault in y-direction.

It was found that the displacement response in time and frequency domains for radial direction at node 1 is almost constant which means that the displacement response of X_1 and Y_1 directions are similar. And same applies for the displacement response at node 2. The same explanation as in section 4.2.1 applies here. The displacement time response in X and Y directions were found to be as a combination of sine and cosine waves. The displacement time response positive amplitudes in X_1 and X_2 directions were found be 10.027 × 10^{-3} (µm) and 8.724 × 10^{-3} (µm), respectively. Likewise, displacement time response positive amplitudes in Y_1 and Y_2 directions were found to be 17.721 × 10^{-3} (µm) and 0.248 × 10^{-3} (µm), respectively. As the figures imply, the time response is more complicated than the unbalanced system and need to be analyzed in the frequency domain. Moreover, the displacement spectrum in the radial direction was found to be synchronized with 1X and 2X RPM amplitudes. Table 8 shows the displacement spectrum of unbalance and parallel misalignment in the radial direction.

Table 8

Displacement spectrum of unbalance and parallel misalignment in radial direction

Amplitude	X_1	X_2	Y_1	Y_2
1X RPM (μm)	5.226×10^{-3}	3.592×10^{-3}	5.240×10^{-3}	3.587×10^{-3}
2XRPM (μm)	6.084×10^{-3}	6.041×10^{-3}	6.115×10^{-3}	6.066×10^{-3}

As it can be noticed that the 1X RPM values in the radial direction didn't change significantly due to the parallel misalignment. On the other hand, the parallel misalignment fault was clearly synchronized with the 2X RPM as it was generally accepted by many researchers in chapter 2. The amplitudes of 2X RPM are almost constant in all directions which could be due to the similar model properties in those directions.

4.4. Vibration response of unbalance and angular misalignment faults in the rotor-coupling-bearing system in the angular direction

The response of the system in the angular direction (θ_1, θ_2) was obtained after adding an angular misalignment to the unbalanced system with a rotating speed of 1200 RPM. Eccentricity of 1 mm was introduced to the system and angular misalignment of 1 degree. Figure 66 presents the time and frequency domains response of the unbalance and angular misalignment fault of the system in angular direction.

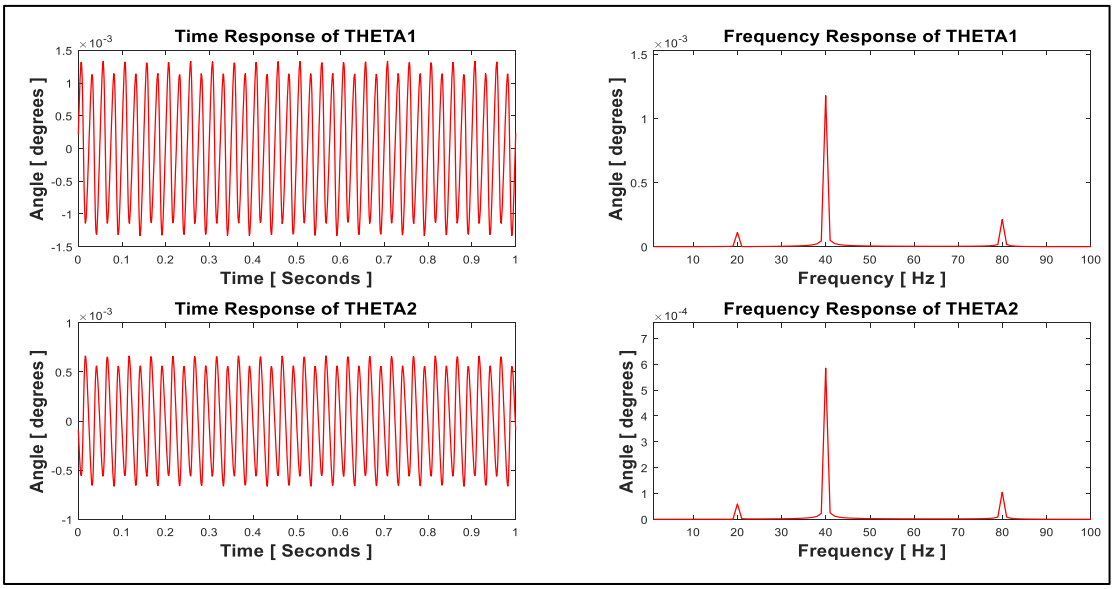

Figure 66: Time and frequency domains response of unbalance and angular misalignment fault.

The angular time response in θ_1 *and* θ_2 directions were found to be of the complicated signal. The angular time response positive amplitudes in θ_1 *and* θ_2 directions were found be 1.3×10^{-3} (degrees) and 0.664×10^{-4} (degrees), respectively. It is noticed that the time domain response in angular direction had increased due to misalignment compared to the unbalanced system. Moreover, the angular spectrum was found to be

synchronized with 1X, 2X and 4X RPM amplitudes. Table 9 shows the angular spectrum of the unbalance and misaligned system.

Table 9

Angular spectrum of unbalanced and misaligned system

Amplitude	$\boldsymbol{\theta_1}$	$\boldsymbol{\theta_2}$
1X RPM (degree)	0.1×10^{-3}	0.0595×10^{-3}
2XRPM (degree)	1.2×10^{-3}	0.5847×10^{-3}
4XRPM (degree)	0.2×10^{-3}	0.1051×10^{-3}

As it can be noticed that the 1X RPM values in the angular direction didn't change significantly due to the angular misalignment. In contrast, the angular misalignment fault was clearly synchronized with the 2X and 4X RPM as it was generally accepted by many researchers in chapter 2. Unlike parallel misalignment, the amplitudes of 2X and 4X RPM were higher in node 1 due to the higher moment of inertia as described earlier in section 4.2.1.

4.5. Effect of changing misalignment level on the rotor-coupling-bearing system

The effect of changing the misalignment level on the system was investigated on both parallel and angular misalignments.

4.5.1. Effect of changing parallel misalignment distance

The effect of changing parallel misalignment on the rotor-coupling-bearing system was visualized by changing the parallel misalignment distance from 0.2 mm to 1.2 mm with a step of 0.2 mm while the rotational speed was constant at 1200 RPM. Figure 67 illustrates the effect of changing parallel misalignment on the model.

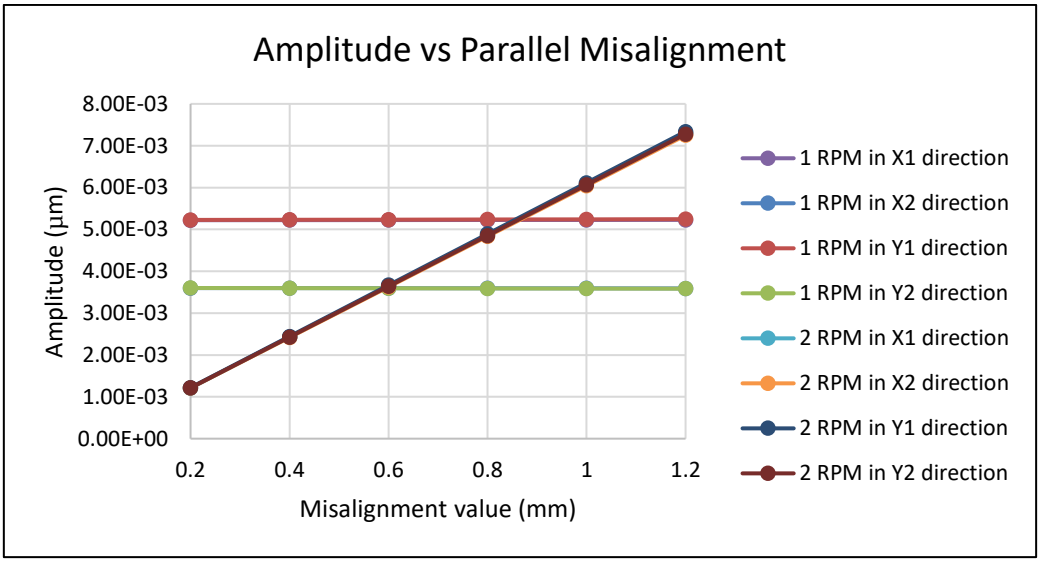

Figure 67: Effect of parallel misalignment level on vibration response.

It can be noticed that the 1 X RPM amplitudes were constant in the radial direction with higher amplitudes at node 1. Moreover, the 2X RPM amplitudes were increasing linearly with the increase of parallel misalignment distance. This is due to the linear parallel misalignment force introduced to the system. As noticed in section 4.3 that the 2 X parallel misalignment vibrations are the same in the radial direction for nodes 1 and

2.

4.5.2. Effect of changing angular misalignment degree

The effect of changing angular misalignment on the rotor-coupling-bearing system was visualized by changing the angular misalignment degree from 0.2 degrees to 1.2 degrees with a step of 0.2 degrees while the rotational speed was constant at 1200 RPM. Figure 68 illustrates the effect of changing parallel misalignment on the model.

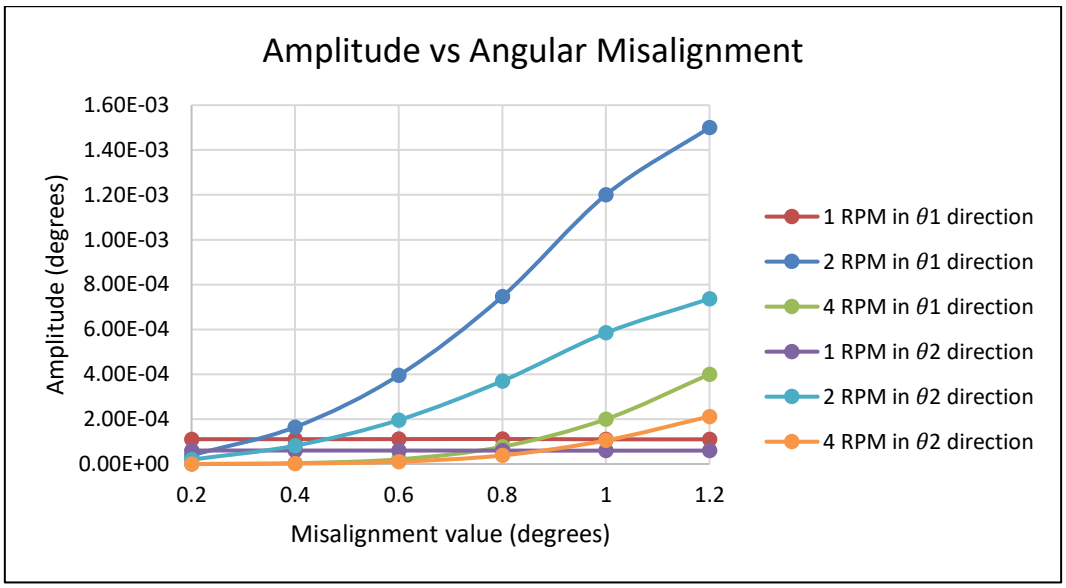

Figure 68: Effect of angular misalignment level on vibration response.

It can be noticed that the 1 X RPM amplitudes were constant in the angular direction. Moreover, the 2X and 4X RPM amplitudes were increasing with the increase of angular misalignment degree. This is due to the non-linear angular misalignment force introduced to the system. As noticed in section 4.4 that the 2X and 4X angular misalignment vibrations were higher in node 1 than node 2 which resulted from the higher moment of inertia of subsystem 1 as per equation 30. The 2X RPM showed a rapid increase in the amplitude compared to 4X RPM.

4.6. Effect of changing rotational speed on the rotor-coupling-bearing system

The effect of changing rotational speed on the system was investigated on both parallel and angular misalignments.

4.6.1. Effect of changing rotational speed on an unbalanced and parallelly misaligned system

The effect of changing rotational speed on the rotor-coupling-bearing system under parallel misalignment fault was visualized by changing the rotational speed from 1200 RPM to 2700 RPM with a step of 300 RPM while the parallel misalignment distance was constant at 1 mm. Figure 69 illustrates the effect of the rotational speed on the unbalanced and parallelly misaligned system.

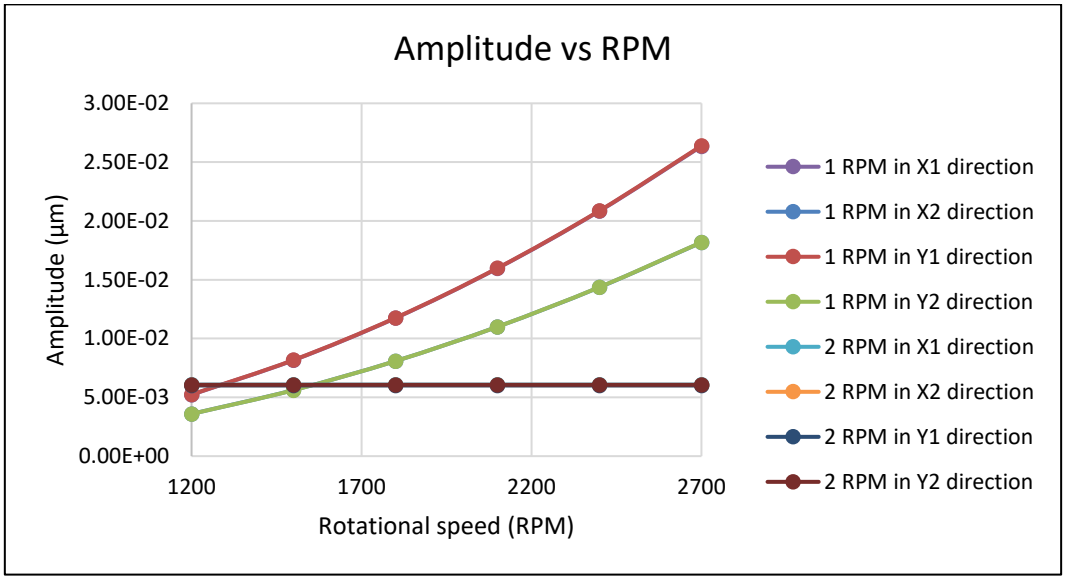

Figure 69: Effect of rotational speed on the vibration response of the unbalanced and parallelly misaligned system.

It can be noticed that the 1 RPM amplitudes in radial direction were increasing with the

increase in rotational speed. This is mainly due to the unbalanced force acting on the system as explained in section 4.3. Moreover, the increase of 1X response is more rapid at node 1 (X_1 and Y_1) than node 2. This can be justified, as the system in node 1 is more flexible than node 2. In addition, the 2X RPM amplitudes were constant with the change in RPM which was expected as the parallel misalignment force model depends on the stiffness of the system not the rotational speed.

4.6.2. Effect of changing rotational speed on unbalanced and angularly misaligned system

The effect of changing rotational speed on the rotor-coupling-bearing system under angular misalignment fault was visualized by changing the rotational speed from 1200 RPM to 2700 RPM with a step of 300 RPM while the angular misalignment was constant at 1 degree. Figure 70 illustrates the effect of the rotational speed on the unbalanced and angularly misaligned system.

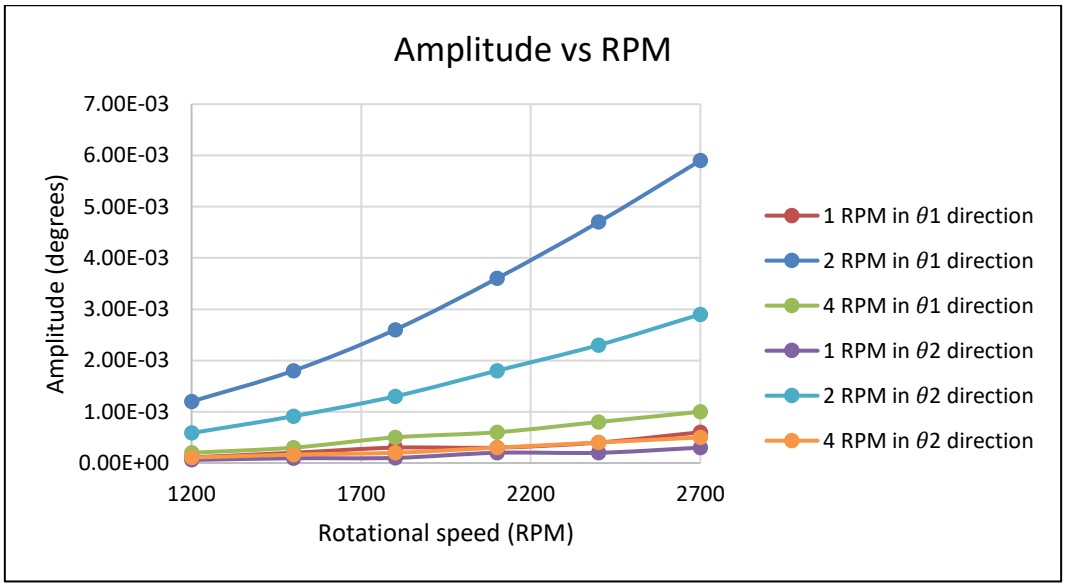

Figure 70: Effect of rotational speed on the vibration response of the unbalanced and angularly misaligned system.

It can be noticed that the 1 RPM amplitudes in angular direction were increasing with the increase in rotational speed. This is mainly due to the unbalanced force acting on the system as explained in section 4.4. In addition, the 2X and 4X RPM amplitudes were also increasing when RPM was increased which was expected as the angular misalignment force model depends on the rotational speed. Moreover, the 2X and 4X RPM amplitudes are more rapid at node 1 (θ_1) than node 2 (θ_2) which can be justified, as the system in node 1 is more flexible than node 2. The 2X RPM showed a rapid increase in the amplitude compared to 4X RPM.

4.7. Effect of changing flexible coupling type on vibration response

The effect of changing flexible coupling type on the system was investigated on both parallel and angular misalignments.

4.7.1. Effect of changing flexible coupling type on unbalanced and parallelly misaligned system

The effect of changing flexible coupling type on the model under unbalance and parallel misalignment faults was examined at a rotational speed of 1200 RPM parallel misalignment distance of 1 mm. Figures 71 and 72 show the effect of coupling type on the unbalanced and parallelly misaligned system.

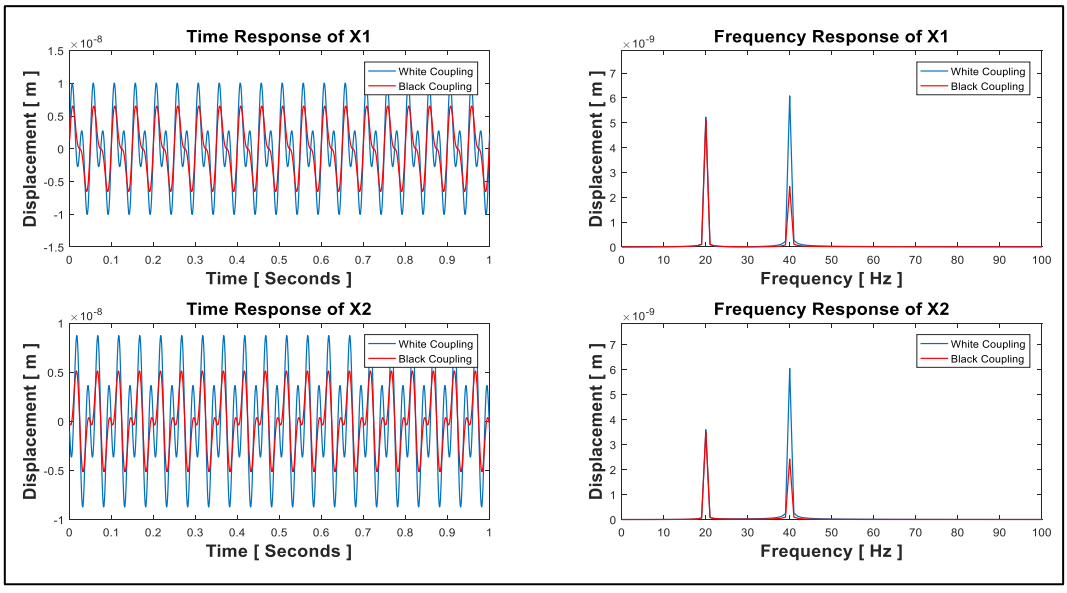

Figure 71: Effect of changing coupling type on unbalanced and parallelly misaligned system in the x-direction.

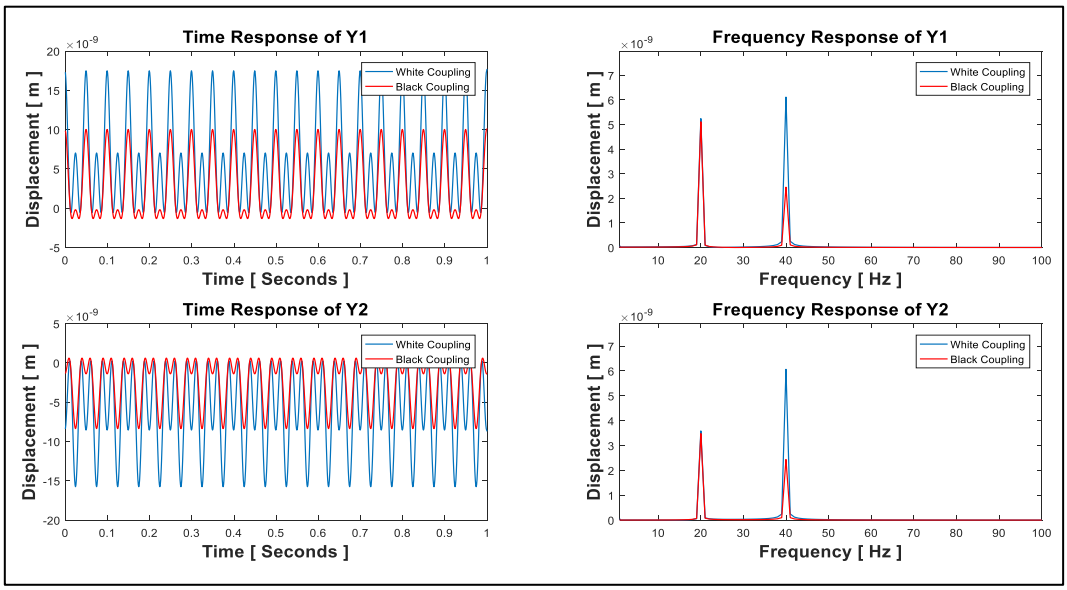

Figure 72: Effect of changing coupling type on the unbalanced and parallelly misaligned system in the y-direction.

In time response graphs, it was found that the amplitudes are higher for the white coupling (stiffer) which is due to the ability of the black coupling (more flexible) to absorb vibrations in the radial direction. Table 10 shows the displacement spectrum of unbalance and parallel misalignment in the radial direction for the two couplings.

Table 10

Amplitudes of vibration spectrum for white and black couplings

Coupling	**Amplitude**	X_1	X_2	Y_1	Y_2
White	1X RPM (µm)	5.226×10^{-3}	3.592×10^{-3}	5.240×10^{-3}	3.587×10^{-3}
	2X RPM (µm)	6.084×10^{-3}	6.041×10^{-3}	6.115×10^{-3}	6.066×10^{-3}
Black	1X RPM (µm)	5.102×10^{-3}	3.478×10^{-3}	5.110×10^{-3}	3.478×10^{-3}
	2X RPM (µm)	2.428×10^{-3}	2.418×10^{-3}	2.453×10^{-3}	2.437×10^{-3}

It can be noticed that the 1X RPM amplitudes were higher in white coupling by around 2.4% only which is due to the difference in the system's masses in the unbalance force formulas. On the other hand, the 2X RPM amplitudes were higher in white coupling by around 60% which can be justified as the difference in the two couplings stiffness.

4.7.2. Effect of changing flexible coupling type on unbalanced and angularly misaligned system

The effect of changing flexible coupling type on the model under unbalance and angular misalignment faults was examined at a rotational speed of 1200 RPM angular misalignment of 1 degree. Figure73 shows the effect of coupling type on the unbalanced and angularly misaligned system.

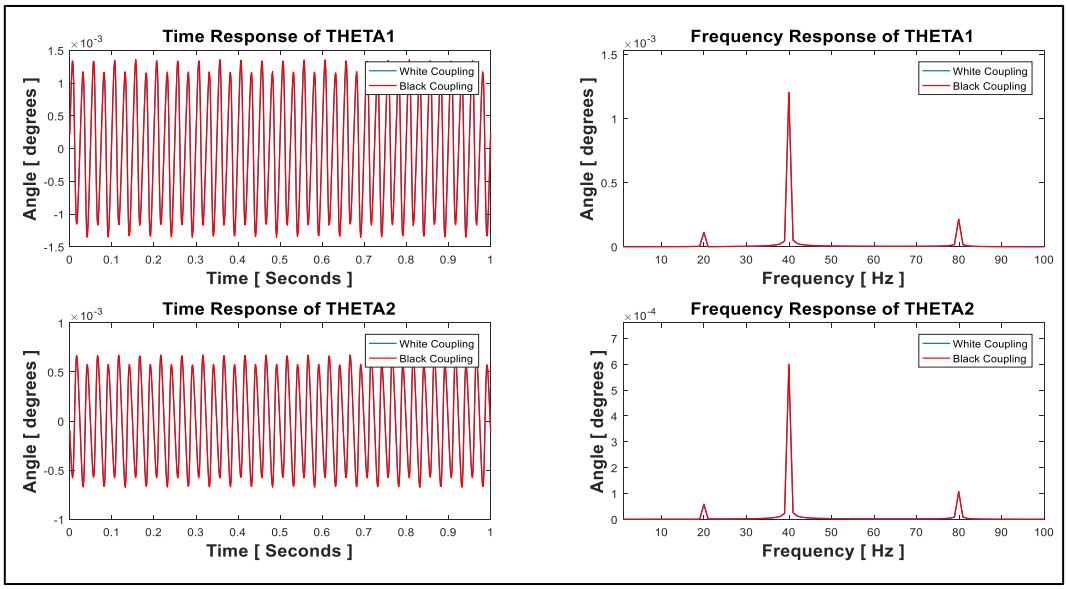

Figure 73: Effect of changing coupling type on unbalanced and angularly misaligned system in the y-direction.

It can be noticed that changing the coupling type didn't affect the vibration spectrum significantly. It was expected that the black coupling will absorb more vibrations and

result in fewer vibration amplitudes. However, the small values of the moment of inertia of the two couplings and the minor difference between them had led to not visualizing the effect of coupling change. In other words, the chosen two coupling types don't have large enough angular stiffness variances to examine the amplitudes variations.

4.8. Validation of numerical modeling method

In order to verify the current modeling method, the current model was compared to a recent study - Wang and Gong numerical simulation model under parallel misalignment fault. This model was chosen as the authors provided sufficient data to compare the displacement responses at the coupling location in both directions (vertically and horizontally). However, the parameters which were not provided by the authors were assumed to have reasonable values. The numerical simulation solver was used to be 12 DOF with 2 nodes. Figure 74 illustrates the simulated model of Wang and Gong.

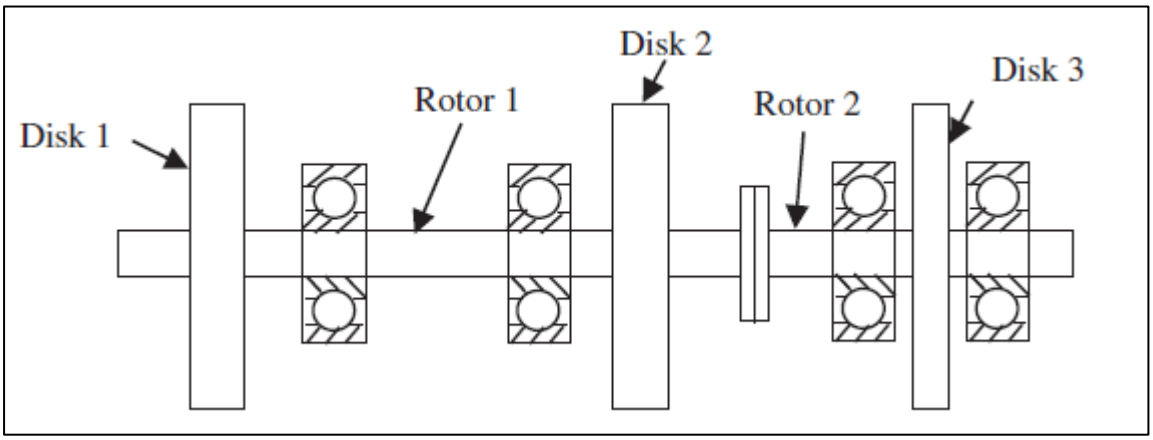

Figure 74: Physical model of Wang and Gong.

Prior to comparing the two models, necessary assumptions were made to allow the implementation of the model with the provided data.

- The system was divided into two subsystems of mass, stiffness, and damping with 12 DOF.
- Coupling mass was neglected as it wasn't mentioned by the author.
- Coupling stiffness in axial direction was assumed to be 10 times higher than

bending stiffness and coupling angular stiffness was assumed to be 1/1000 of the radial stiffness. These are the same ratios obtained in the current study for a flexible coupling.

- Coupling damping was set to zero as the authors didn't introduce it.
- The disks masses were added to the rotor mass at the center of gravity of each node and assumed to cause unbalance of 0.001 mm.
- Bearings equivalent stiffness in x and y directions at each node were added for a given direction (x and y).

The provided data by Wang and Gong are given in table 11.

Table 11

Numerical model data of Wang and Gong

Rotor 1		
Diameter (m)	Length (m)	M_1 (kg)
0.03	0.88	24.8
Rotor 2		
Diameter (m)	Length (m)	M_2 (kg)
0.04	0.4	5.92
Disks		
I_{z1} (Kg/m^2)	I_{x1} (Kg/m^2)	I_{y1} (Kg/m^2)
0.5	0.025	0.025
Bearings		
$KB1_x$, $KB2_x$ (N/m)	$KB1_y, KB2_y$ (N/m)	$CB1_{x-y}, CB2_{x-y}$ (N.m/s)
7.50×10^6	5.00×10^7	2000
Rotor and disks material properties		
Youngs Modulus (N/m^2)	Poisson ratio	Density (Kg/m^3)
2.1E+11	0.3	7800
Coupling bending stiffness (N/m)		
1×10^5		

It should be noted that authors considered that the bearings were assumed to be string elements connected to ground in the vertical direction. Therefore, the stiffness of the bearing in the vertical direction was higher than its stiffness in the horizontal direction. Based on the given data, the radial stiffness of the two shafts was estimated to be 3.67×10^{4} N/m and 1.24×10^{6} N/m for shafts 1 and 2, respectively. The axial stiffness of the two shafts was estimated to be 1.69×10^{8} N/m and 6.59×10^{8} N/m for shafts 1 and 2, respectively. The angular stiffness of the two shafts was estimated to be 7.30×10^{3} N.m and 5.07×10^{4} N.m for shafts 1 and 2, respectively. Table 12 summarizes the numerical model input data of Wang and Gong system.

Table 12

Summary of the numerical model input data for Wang and Gong system

Parameter	Value	unit	Parameter	Value	unit
m_1	24.8	Kg	$KS2_z$	6.59×10^8	N/m
m_2	5.92	Kg	$KS1T_z$	7.30×10^3	N.m/rad
I_{x1}	0.05	Kg.m^2	$KS2T_z$	5.07×10^4	N.m/rad
I_{x2}	0.025	Kg.m^2	KC_x	1×10^5	N/m
I_{y1}	0.05	Kg.m^2	KC_y	1×10^5	N/m
I_{y2}	0.025	Kg.m^2	KC_z	1×10^6	N/m
I_{z1}	0.1	Kg.m^2	KCT_x	1×10^2	N.m/rad
I_{z2}	0.05	Kg.m^2	KCT_y	1×10^2	N.m/rad
$KB1_x$	15×10^6	N/m	KCT_z	1×10^3	N.m/rad
$KB1_y$	10×10^7	N/m	$CB1_x$	4000	N.s/m
$KB2_x$	15×10^6	N/m	$CB1_y$	4000	N.s/m
$KB2_y$	10×10^7	N/m	$CB2_x$	4000	N.s/m
$KS1_x$	3.67×10^4	N/m	$CB2_y$	4000	N.s/m
$KS1_y$	3.67×10^4	N/m	CC_x	0	N.s/m
$KS1_z$	1.69×10^8	N/m	CC_y	0	N.s/m
$KS2_x$	1.24×10^6	N/m	CC_z	0	N.s/m
$KS2_y$	1.24×10^6	N/m			

As the mentioned paper presented the radial vibrations of the rotating system at coupling node 1 in vertical and horizontal directions, the response of the system in the radial direction was obtained with parallel misalignment and unbalance faults at the

same rotating speed of 3800 RPM. Eccentricity of 0.001 mm and parallel misalignment of 1 mm was introduced to the system in both radial directions (vertical and horizontal). Figure 75 presents the time and frequency domains response of the unbalance and parallel misalignment faults of the system in the radial direction.

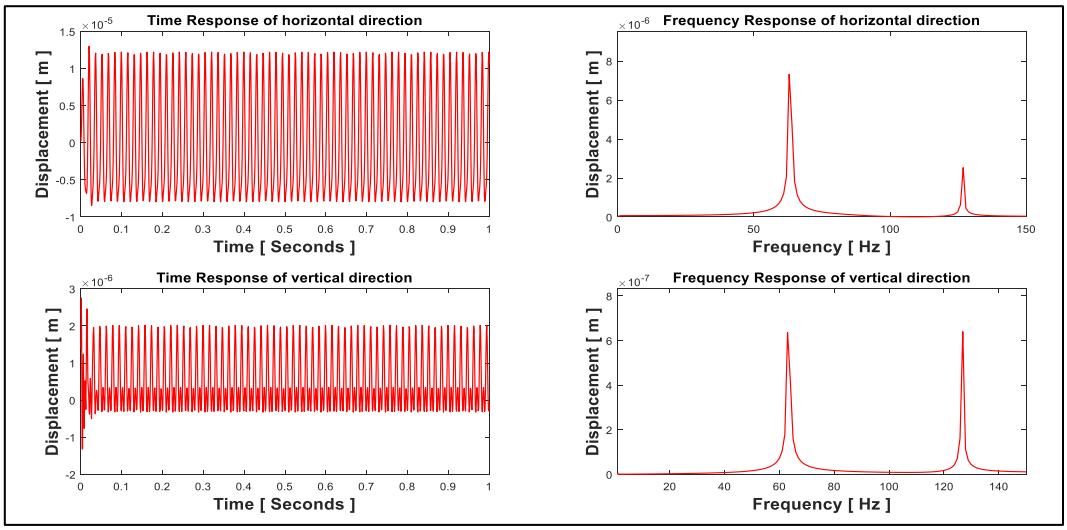

Figure 75: Response of unbalance and parallel misalignment faults in Wang and Gong system.

It can be noticed that both models had similar behavior as the vibrations at 1X and 2X amplitudes were present with horizontal vibrations higher than vertical vibrations which was expected as the bearings were supported to the ground in the vertical direction. As it was illustrated in previous sections that the parallel misalignment fault was synchronized with the 2X amplitudes of the vibration spectrum. Table 13 presents the 2X amplitudes of the current model and Wang and Gong's model.

Table 13

Comparison of the current model with Wang and Gong's model

Model	**Amplitude**	**Horizontal Direction**	**Vertical Direction**
Current Model	2X RPM (μm)	2.53	0.63
Wang and Gong	2X RPM (μm)	2	0.4

As the vibration amplitudes depend on the models' stiffness, the current model 2X amplitudes were matching with the 2X amplitudes in Wang and Gong model to a certain degree. The variation of the 2X amplitudes between the two models can be justified by the assumptions highlighted in table 11 for the coupling mass, damping and stiffness in some directions as those data were not provided by Wang and Gong paper.

CHAPTER 5: CONCLUSIONS AND FUTURE WORK

Numerical modeling of the rotor-coupling-bearing system under unbalance and misalignment faults was developed in this investigation, using the Lagrange method. Unbalance, parallel and angular misalignment forces were used as the excitation forces in the model. The geometrical model was developed using Solidworks and then was imported to Abaqus to estimate the stiffness of the chosen flexible coupling in this study (spiral coupling). The damping coefficients of the spiral coupling were experimentally derived using Logarithmic decrement method (impact test). The numerical simulation solver was built using Matlab to evaluate the time and frequency vibration responses of the model. It was found that the natural frequencies of the model were high enough to avoid any resonance during the analysis on a rotational speed of 1200-2700 RPM.

For parallel misalignment, it was found to be synchronized with the 2X RPM rotational speed. The vibrations in the radial direction were found to be constant in x and y directions as the model were independent of the rotational angle and the parameters in the vertical and horizontal directions were found to be very close to each other. Moreover, the vibrations of the two subsystems (node 1 and 2) were found to be similar due to the similar stiffnesses of the two subsystems. By changing the misalignment level on the model while keeping all other parameters constant, the 2X RPM was found to be increasing linearly as it was expected beforehand from the linear model and the linear parallel misalignment force equation. In addition, it was found that the parallel misalignment vibrations (2X RPM) were independent of the system's rotational speed. Finally, the effect of changing the coupling type by changing the used coupling (white spiral coupling) to a slightly more flexible one (black spiral coupling) was found to rapidly decrease the vibrations on the system.

For angular misalignment, it was found to be synchronized with the 2X and 4X RPM rotational speeds. The amplitudes of 2XRPM and 4X RPM were higher in node 1 than node 2 due to the higher moment of inertia in subsystem 1. By changing the misalignment level on the model while keeping all other parameters constant, the 2X and 4X RPM were found to be increasing non-linearly as per the nonlinear angular misalignment force equation. The 2X RPM showed a rapid increase in the amplitude compared to 4X RPM. In addition, it was found that the rotational speed affects the angular misalignment spectrum 2X and 4X RPM and make their amplitudes increase in a non-linear way. Finally, the effect of changing the coupling type to a slightly different coupling (more flexible coupling) was not visible in the angular direction due to the negligible variance in the moment of inertia for the two couplings.

The future work for this study is to update the parallel and angular misalignment forces to visualize the 3X and 5X RPM in the vibration spectrum. The unbalance response was evident in the 1X RPM spectrum, but some researcher has shown that the 1X RPM is originating from misalignment as well which will require more research. Moreover, the stiffness matrix was assumed to be constant (independent of rotational angle) which might not be applicable for all flexible couplings. Therefore, the development of the variable parameter stiffness matrix is helpful to visualize the vibration spectrum around 360 degrees. In addition, updating of the Matlab program will be required in case the type of coupling will contain resilient member such as rubber. It is also necessary to examine a different type of flexible couplings to predict the coupling types effect on the angular misalignment spectrum.

REFERENCES

Büchholdt, hans A. (2012). Structural Dynamics for Engineers. In *Structural Dynamics for Engineers*. https://doi.org/10.1680/sdfe.25592

Chandra Sekhar Reddy, M., & Sekhar, A. S. (2015). Detection and monitoring of coupling misalignment in rotors using torque measurements. *Measurement: Journal of the International Measurement Confederation*, *61*, 111–122. https://doi.org/10.1016/j.measurement.2014.10.031

Chatelet, E., D'Ambrosio, F., & Jacquet-Richardet, G. (2005). Toward global modelling approaches for dynamic analyses of rotating assemblies of turbomachines. *Journal of Sound and Vibration*, *282*(1–2), 163–178. https://doi.org/10.1016/j.jsv.2004.02.035

Elbhbah, K., & Sinha, J. K. (2013). Vibration-based condition monitoring of rotating machines using a machine composite spectrum. *Journal of Sound and Vibration*. https://doi.org/10.1016/j.jsv.2012.12.024

Engineer, P., Division, F. P., Corporation, T. B., Misalignment, M., & Misalignment, F. (n.d.). *COUPLING MISALIGNMENT FORCES by C.* 111–116.

FESSLER, H. (2013). Design of Machine Elements. *Engineering Design*, pp. 203–207. https://doi.org/10.1016/b978-0-08-011192-6.50016-5

Forsthoffer, M. S. (2017). Gears and Couplings. In *Forsthoffer's More Best Practices for Rotating Equipment*. https://doi.org/10.1016/b978-0-12-809277-4.00004-8

Hariharan, V., & Srinivasan, P. S. S. (2009). Vibration analysis of misaligned shaft - ball bearing system. *Indian Journal of Science and Technology*, *2*(9), 45–50. https://doi.org/10.17485/ijst/2009/v2i9/2952144

Hujare, D. P., & Karnik, M. G. (2018). Vibration responses of parallel misalignment in

Al shaft rotor bearing system with rigid coupling. *Materials Today: Proceedings*, *5*(11), 23863–23871. https://doi.org/10.1016/j.matpr.2018.10.178

Krämer, E. (2013). Dynamics of Rotors and Foundations. In *Dynamics of Rotors and Foundations*. https://doi.org/10.1007/978-3-662-02798-1

Lalanné, F. (1991). Rotordynamics Prediction in Engineering. In *Journal of Sound and Vibration*. https://doi.org/10.1016/0022-460X(91)90506-F

Lees.A.W. (2007). Misalignment in rigidly coupled rotors. *Journal of Sound and Vibration*, *305*(1–2), 261–271. https://doi.org/10.1016/j.jsv.2007.04.008

Mancuso, J. R., Zilberman, J., Corcoran, J. P., & D'Ercole, S. (1994). Flexible-element couplings: how safe is safe? *Hydrocarbon Processing*.

Ming Xu, & Marangoni, R. D. (2007). FEATURE ARTICLE items of special interest, tutorials, and surveys: Flexible Couplings: Study and Application. *The Shock and Vibration Digest*. https://doi.org/10.1177/058310249002200903

Sawalhi, N., Ganeriwala, S., & Tóth, M. (2019). Parallel misalignment modeling and coupling bending stiffness measurement of a rotor-bearing system. *Applied Acoustics*, *144*, 124–141. https://doi.org/10.1016/j.apacoust.2017.07.022

Sekhar, A. S., & Prabhu, B. S. (1995). Effects of coupling misalignment on vibrations of rotating machinery. *Journal of Sound and Vibration*, *185*(4), 655–671. https://doi.org/10.1006/jsvi.1995.0407

Shaft Alignment Handbook by John Piotrowski [Books and Reports]. (2005). *IEEE Power Engineering Review*. https://doi.org/10.1109/mper.1995.469603

Tadeo, A. T., & Cavalca, K. L. (2005). A comparison of flexible coupling models for updating in rotating machinery response. *Journal of the Brazilian Society of Mechanical Sciences and Engineering*, *25*(3), 235–246. https://doi.org/10.1590/s1678-58782003000300004

Tadeo, A. T., Cavalca, K. L., & Brennan, M. J. (2011). Dynamic characterization of a mechanical coupling for a rotating shaft. *Proceedings of the Institution of Mechanical Engineers, Part C: Journal of Mechanical Engineering Science*, *225*(3), 604–616. https://doi.org/10.1243/09544062JMES2214

Tuckmantel, F. W. da S., & Cavalca, K. L. (2019). Vibration signatures of a rotor-coupling-bearing system under angular misalignment. *Mechanism and Machine Theory*, *133*, 559–583. https://doi.org/10.1016/j.mechmachtheory.2018.12.014

Vermolen, F. (2005). Introduction into Finite Elements. In *Analysis*.

Walden, W. (2000). How coupling types affect bearing forces.

Wang, H., & Gong, J. (2019). Dynamic analysis of coupling misalignment and unbalance coupled faults. *Journal of Low Frequency Noise Vibration and Active Control*, (196), 1–14. https://doi.org/10.1177/1461348418821582

Wang, N., & Jiang, D. (2018). Vibration response characteristics of a dual-rotor with unbalance-misalignment coupling faults: Theoretical analysis and experimental study. *Mechanism and Machine Theory*, *125*, 207–219. https://doi.org/10.1016/j.mechmachtheory.2018.03.009

Xu, M., & Marangoni, R. D. (1994). Vibration analysis of a motor-flexible coupling-rotor system subject to misalignment and unbalance, Part I: Theoretical model and analysis. *Journal of Sound and Vibration*, Vol. 176, pp. 663–679. https://doi.org/10.1006/jsvi.1994.1405

Zhao, G., Liu, Z., & Chen, F. (2008). Meshing Force of Misaligned Spline Coupling and the Influence on Rotor System. *International Journal of Rotating Machinery*, *2008*, 1–8. https://doi.org/10.1155/2008/321308

APPENDIX 1: MASS, DAMPING, GYROSCOPIC AND STIFFNESS MATRICES FOR KRAMER'S MODEL

$$[M_c] = \begin{bmatrix} m_i & 0 & 0 & 0 & 0 & 0 & 0 & 0 \\ 0 & m_i & 0 & 0 & 0 & 0 & 0 & 0 \\ 0 & 0 & I_{mi} & 0 & 0 & 0 & 0 & 0 \\ 0 & 0 & 0 & I_{mi} & 0 & 0 & 0 & 0 \\ 0 & 0 & 0 & 0 & m_j & 0 & 0 & 0 \\ 0 & 0 & 0 & 0 & 0 & m_j & 0 & 0 \\ 0 & 0 & 0 & 0 & 0 & 0 & I_{mj} & 0 \\ 0 & 0 & 0 & 0 & 0 & 0 & 0 & I_{mj} \end{bmatrix}$$

$$[K_c] = \begin{bmatrix} 0 & 0 & 0 & 0 & 0 & 0 & 0 & 0 \\ 0 & 0 & 0 & 0 & 0 & 0 & 0 & 0 \\ 0 & 0 & k_R & \Omega_{C_R} & 0 & 0 & -k_R & -\Omega_{C_R} \\ 0 & 0 & -\Omega_{C_R} & k_R & 0 & 0 & \Omega_{C_R} & -k_R \\ 0 & 0 & 0 & 0 & 0 & 0 & 0 & 0 \\ 0 & 0 & 0 & 0 & 0 & 0 & 0 & 0 \\ 0 & 0 & -k_R & -\Omega_{C_R} & 0 & 0 & k_R & \Omega_{C_R} \\ 0 & 0 & \Omega_{C_R} & -k_R & 0 & 0 & -\Omega_{C_R} & k_R \end{bmatrix}$$

$$[C_c] = \begin{bmatrix} 0 & 0 & 0 & 0 & 0 & 0 & 0 & 0 \\ 0 & 0 & 0 & 0 & 0 & 0 & 0 & 0 \\ 0 & 0 & C_R & 0 & 0 & 0 & -C_R & 0 \\ 0 & 0 & 0 & C_R & 0 & 0 & 0 & -C_R \\ 0 & 0 & 0 & 0 & 0 & 0 & 0 & 0 \\ 0 & 0 & 0 & 0 & 0 & 0 & 0 & 0 \\ 0 & 0 & -C_R & 0 & 0 & 0 & C_R & 0 \\ 0 & 0 & 0 & -C_R & 0 & 0 & 0 & C_R \end{bmatrix}$$

$$[G_c] = \begin{bmatrix} 0 & 0 & 0 & 0 & 0 & 0 & 0 & 0 \\ 0 & 0 & 0 & 0 & 0 & 0 & 0 & 0 \\ 0 & 0 & 0 & -I_{pmi} & 0 & 0 & 0 & 0 \\ 0 & 0 & I_{pmi} & 0 & 0 & 0 & 0 & 0 \\ 0 & 0 & 0 & 0 & 0 & 0 & 0 & 0 \\ 0 & 0 & 0 & 0 & 0 & 0 & 0 & 0 \\ 0 & 0 & 0 & 0 & 0 & 0 & 0 & -I_{pmj} \\ 0 & 0 & 0 & 0 & 0 & 0 & I_{pmj} & 0 \end{bmatrix}$$

Where I_m and I_{pm} are the mass moments of inertia and polar moment of inertia, respectively.

APPENDIX 2: DAMPING AND STIFFNESS MATRICES FOR NELSON AND CRANDALL'S FLEXIBLE COUPLING MODELS

$$[\,K_c\,] = \begin{bmatrix} K_T & 0 & 0 & 0 & -K_T & 0 & 0 & 0 \\ 0 & K_T & 0 & 0 & 0 & -K_T & 0 & 0 \\ 0 & 0 & K_R & 0 & 0 & 0 & -K_R & 0 \\ 0 & 0 & 0 & K_R & 0 & 0 & 0 & -K_R \\ -K_T & 0 & 0 & 0 & K_T & 0 & 0 & 0 \\ 0 & -K_T & 0 & 0 & 0 & K_T & 0 & 0 \\ 0 & 0 & -K_R & 0 & 0 & 0 & K_R & 0 \\ 0 & 0 & 0 & -K_R & 0 & 0 & 0 & K_R \end{bmatrix}$$

$$[\,C_c\,] = \begin{bmatrix} C_T & 0 & 0 & 0 & -C_T & 0 & 0 & 0 \\ 0 & C_T & 0 & 0 & 0 & -C_T & 0 & 0 \\ 0 & 0 & C_R & 0 & 0 & 0 & -C_R & 0 \\ 0 & 0 & 0 & C_R & 0 & 0 & 0 & -C_R \\ -C_T & 0 & 0 & 0 & C_T & 0 & 0 & 0 \\ 0 & -C_T & 0 & 0 & 0 & C_T & 0 & 0 \\ 0 & 0 & -C_R & 0 & 0 & 0 & C_R & 0 \\ 0 & 0 & 0 & -C_R & 0 & 0 & 0 & C_R \end{bmatrix}$$

APPENDIX 3: DERIVATION OF PARALLEL AND ANGULAR MISALIGNMENT FORCES AS PER WANG AND JIANG

Misalignment in the dual-rotor system and its misalignment fault schematic is shown below.

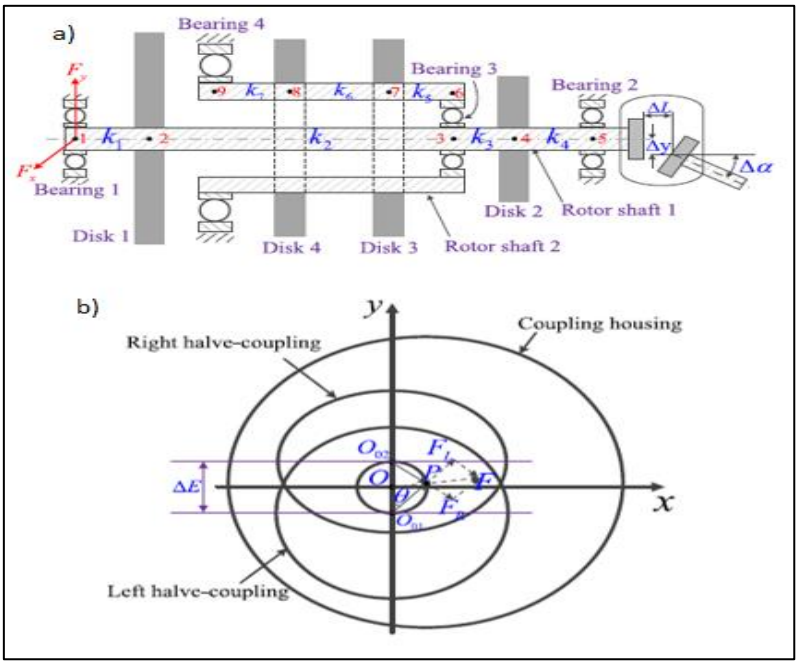

The rotating shafts had a geometric center O and dynamic center P due to the relative motion of the shafts. The dynamic center coordinates can be given by.

$$x = \Delta E \sin\theta \cos\theta = \frac{1}{2}(\Delta y + \Delta L \tan(\frac{\Delta\alpha}{2}))\sin 2\theta$$

$$y = \Delta E \cos\theta \cos\theta - \frac{1}{2}\Delta E = \frac{1}{2}(\Delta y + \Delta L \tan(\frac{\Delta\alpha}{2}))\cos 2\theta$$

Then, the linear velocity of P can be expressed as below.

$$v_P = \sqrt[2]{\left(\frac{dx}{dt}\right)^2 + \left(\frac{dy}{dt}\right)^2} = \omega_1 . \left(\Delta y + \Delta L . \tan\left(\frac{\Delta\alpha}{2}\right)\right)$$

Noting that $\omega_P = \frac{v_P}{\Delta E/2} = 2\omega_1$

Now the acceleration of point P can be given as.

$$a_P = \sqrt[2]{\left(\frac{d^2x}{dt^2}\right)^2 + \left(\frac{d^2y}{dt^2}\right)^2} = -2\omega_1^2 . \left(\Delta y + \Delta L . \tan\left(\frac{\Delta\alpha}{2}\right)\right)$$

The parallel and angular misalignment forces can be obtained using newtons second law of motion.

$$F_x = m_o\, \omega^2(\Delta y + \Delta L \tan(\frac{\Delta\alpha}{2}))\sin 2\omega t$$

$$F_y = m_o\, \omega^2(\Delta y + \Delta L\, tan(\tfrac{\Delta\alpha}{2}))cos2\omega t$$

Where ΔE is the combined misalignment amount, Δy is the parallel misalignment distance, α is the angular misalignment angle. m_o is the mass of the coupling. ω is the rotational speed.

APPENDIX 4: DERIVATION OF ANGULAR MISALIGNMENT FORCES BY XU AND MARANGONI

The angular misalignment torque vector can be decomposed as below.

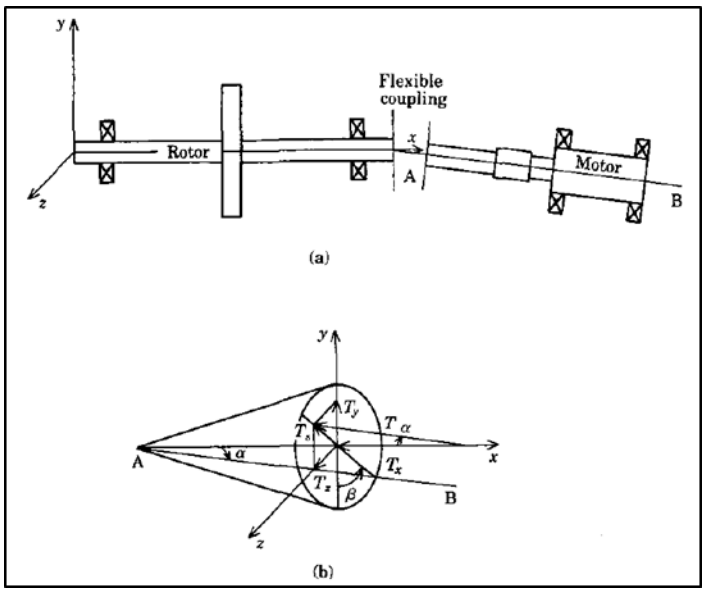

$T_x = T\cos\alpha$ and $T_s = T\sin\alpha$

The torque in the YZ plane can be further decomposed as.

$T_y = T\sin\alpha\cos\beta$ and $T_z = T\sin\alpha\sin\beta$

Euler's equation of motion can then be applied in the x, y, and z-direction as follows.

$$T_x = I_x\ \dot{\omega}_x + \omega_y\,\omega_z\,(I_z - I_y)$$

$$T_y = I_y\ \dot{\omega}_y + \omega_z\,\omega_x\,(I_x - I_z)$$

$$T_z = I_z\ \dot{\omega}_z + \omega_x\,\omega_y\,(I_y - I_x)$$

Euler's equation of motion can be further reduced as the angular motion is only in x-direction.

$$T\cos\alpha = I_R\,\epsilon_R$$

Given that the acceleration of angularly misaligned shafts.

$$\epsilon_R/\omega_M^2 = B_2\sin 2\theta_M - B_4\sin 4\theta_M + \ldots\ldots + (-1)^{n+1}B_{2n}\sin 2n\theta_M + \ldots\ldots$$

Substituting it into Euler's equation result in the following.

$$T = (I_R \Omega^2 / \cos\alpha)(\sum_{n=1}^{\infty}(-1)^{n+1} B_{2n} \sin 2n\Omega t)$$

Where $T_y = \sum_{n=1}^{\infty} E_{2n} \sin 2n\Omega t$, $T_z = \sum_{n=1}^{\infty} G_{2n} \sin 2n\Omega t$

And $E_{2n} = (-1)^{n+1} I_R \ \Omega^2 B_{2n} \tan\alpha \cos\beta$, $G_{2n} = (-1)^{n+1} I_R \ \Omega^2 B_{2n} \tan\alpha \sin\beta$

Where K_b is the bending stiffness, J_R is the polar moment of inertia, Ω is the rotational speed, α is the misalignment angle with the axial direction, β is the misalignment angle with the radial direction and B_{2n} is an even multiple of the rotational speed, ϵ_R is the angular acceleration.

APPENDIX 5: MODELING OF ROTOR-COUPLING-BEARING SYSTEM USING LAGRANGE ENERGY METHOD

The system under observation is modeled of two half's coupling masses and a set of stiffness and damping as illustrated in the figure:

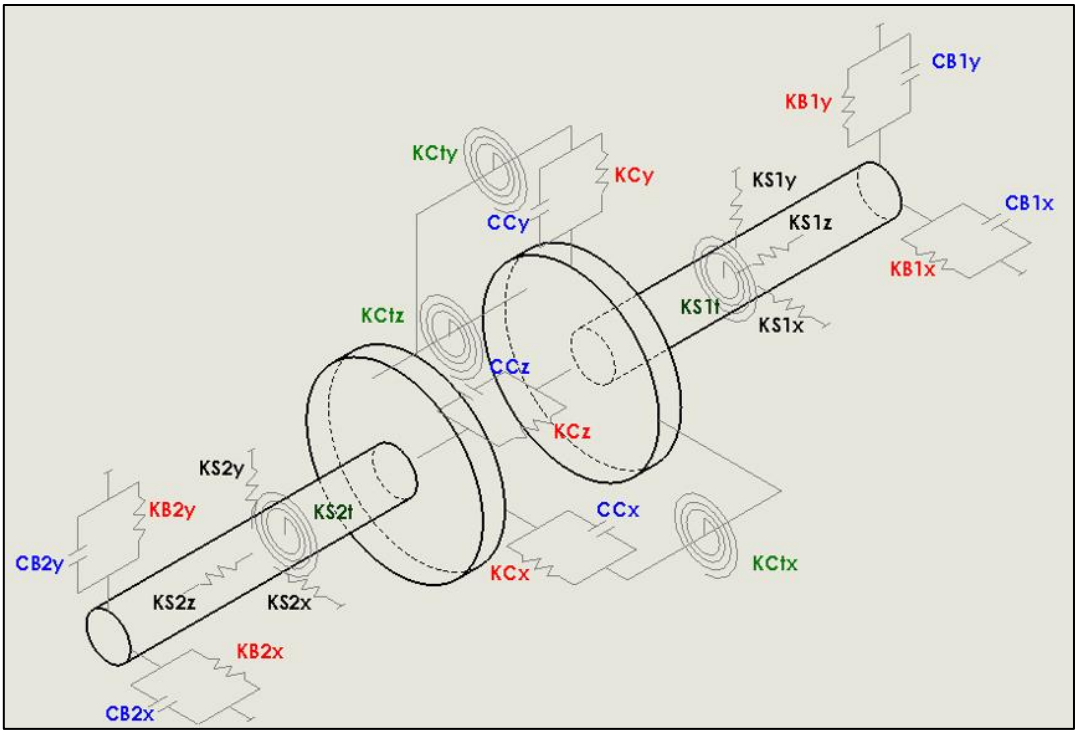

The system is of 12 degrees of freedom (DOF) with six DOF for each mass as below:

$$\{x\} = \begin{Bmatrix} X_1 \\ X_2 \\ Y_1 \\ Y_2 \\ Z_1 \\ Z_2 \\ \theta_1 \\ \theta_2 \\ \beta_1 \\ \beta_2 \\ \alpha_1 \\ \alpha_2 \end{Bmatrix}$$; Where

X_1 *is a displacement in radial direction for mass* 1
X_2 *is a displacement in radial direction for mass* 2
Y_1 *is a displacement in radial direction for mass* 1
Y_2 *is a displacement in radial direction for mass* 2
Z_1 *is the displacement in axial direction for mass* 1
Z_2 *is the displacement in axial direction for mass* 2
θ_1 *is the rotation about* $Z-$ *axes for mass* 1
θ_2 *is the rotation about* $Z-$ *axes for mass* 2
β_1 *is the rotation about* $X-$ *axes for mass* 1
β_2 *is the rotation about* $X-$ *axes for mass* 2
α_1 *is the rotation about* $Y-$ *axes for mass* 1
α_2 *is the rotation about* $Y-$ *axes for mass* 2

Using Lagrange energy method

$$\frac{\partial}{\partial t}\frac{\partial T}{\partial \dot{q}_i} + \frac{\partial V}{\partial q_i} + \frac{\partial D}{\partial \dot{q}_i} = F_i$$

Where

T is the kinetic energy of the system
V is the potential energy of the system
D is the damping energy of the system
F is the external forces acting on the system
q is the independent generalized displacement
t is the time

The kinetic energy equation is:

$$T = \frac{1}{2}m_1\dot{X_1}^2 + \frac{1}{2}m_2\dot{X_2}^2 + \frac{1}{2}m_1\dot{Y_1}^2 + \frac{1}{2}m_2\dot{Y_2}^2 + \frac{1}{2}I_{z1}\dot{\theta_1}^2 + \frac{1}{2}I_{z2}\dot{\theta_2}^2 + \frac{1}{2}I_{x1}\dot{\beta_1}^2 + \frac{1}{2}I_{x2}\dot{\beta_2}^2 + \frac{1}{2}I_{y1}\dot{\alpha_1}^2 + \frac{1}{2}I_{y2}\dot{\alpha_2}^2$$

The potential energy equation is:

$$V = \frac{1}{2}(KB1_x \,//\, KS1_x)X_1^2 + \frac{1}{2}(KB1_y \,//\, KS1_y)Y_1^2 + \frac{1}{2}(KB2_x \,//\, KS2_x)X_2^2 + \frac{1}{2}(KB2_y \,//\, KS2_y)Y_2^2 + \frac{1}{2}KC_x(X_1 - X_2)^2 + \frac{1}{2}KC_y(Y_1 - Y_2)^2 + \frac{1}{2}KC_z(Z_1 - Z_2)^2 + \frac{1}{2}KCT_x(\beta_1 - \beta_2)^2 + \frac{1}{2}KCT_y(\alpha_1 - \alpha_2)^2 + \frac{1}{2}KCT_z(\theta_1 - \theta_2)^2 + \frac{1}{2}KS1_zZ_1^2 + \frac{1}{2}KS2_zZ_2^2 + \frac{1}{2}KS1T_z\theta_1^2 + \frac{1}{2}KS2T_z\theta_2^2$$

The dissipation energy equation is:

$$D = \frac{1}{2}CB1_x\dot{X_1}^2 + \frac{1}{2}CB1_y\dot{Y_1}^2 + \frac{1}{2}CB2_x\dot{X_2}^2 + \frac{1}{2}CB2_y\dot{Y_2}^2 + \frac{1}{2}CC_x(\dot{X_1} - \dot{X_2})^2 + \frac{1}{2}CC_y(\dot{Y_1} - \dot{Y_2})^2 + \frac{1}{2}CC_z(\dot{Z_1} - \dot{Z_2})^2$$

Differentiating kinetic energy equation with respect to $\dot{X}_1$ and then with respect to t:

$$\frac{\partial T}{\partial \dot{X}_1} = m_1 \dot{X}_1 \quad and\ then\ differentiate\ \frac{\partial}{\partial t}\frac{\partial T}{\partial \dot{X}_1} = m_1 \ddot{X}_1$$

Differentiating kinetic energy equation with respect to $\dot{X}_2$ and then with respect to t:

$$\frac{\partial T}{\partial \dot{X}_2} = m_2 \dot{X}_2 \quad and\ then\ differentiate\ \frac{\partial}{\partial t}\frac{\partial T}{\partial \dot{X}_2} = m_2 \ddot{X}_2$$

Differentiating kinetic energy equation with respect to $\dot{Y}_1$ and then with respect to t:

$$\frac{\partial T}{\partial \dot{Y}_1} = m_1 \dot{Y}_1 \quad and\ then\ differentiate\ \frac{\partial}{\partial t}\frac{\partial T}{\partial \dot{Y}_1} = m_1 \ddot{Y}_1$$

Differentiating kinetic energy equation with respect to $\dot{Y}_2$ and then with respect to t:

$$\frac{\partial T}{\partial \dot{Y}_2} = m_2 \dot{Y}_2 \quad and\ then\ differentiate\ \frac{\partial}{\partial t}\frac{\partial T}{\partial \dot{Y}_2} = m_2 \ddot{Y}_2$$

Differentiating kinetic energy equation with respect to $\dot{Z}_1$ and then with respect to t:

$$\frac{\partial T}{\partial \dot{Z}_1} = m_1 \dot{Z}_1 \quad and\ then\ differentiate\ \frac{\partial}{\partial t}\frac{\partial T}{\partial \dot{Z}_1} = m_1 \ddot{Z}_1$$

Differentiating kinetic energy equation with respect to $\dot{Z}_2$ and then with respect to t:

$$\frac{\partial T}{\partial \dot{Z}_2} = m_2 \dot{Z}_2 \quad and\ then\ differentiate\ \frac{\partial}{\partial t}\frac{\partial T}{\partial \dot{Z}_2} = m_2 \ddot{Z}_2$$

Differentiating kinetic energy equation with respect to $\dot{\theta}_1$ and then with respect to t:

$$\frac{\partial T}{\partial \dot{\theta}_1} = I_{z1} \dot{\theta}_1 \quad and\ then\ differentiate\ \frac{\partial}{\partial t}\frac{\partial T}{\partial \dot{\theta}_1} = I_{z1} \ddot{\theta}_1$$

Differentiating kinetic energy equation with respect to $\dot{\theta}_2$ and then with respect to t:

$$\frac{\partial T}{\partial \dot{\theta}_2} = I_{z2} \dot{\theta}_2\ and\ then\ differentiate\ \frac{\partial}{\partial t}\frac{\partial T}{\partial \dot{\theta}_2} = I_{z2} \ddot{\theta}_2$$

Differentiating kinetic energy equation with respect to $\dot{\beta}_1$ and then with respect to t:

$$\frac{\partial T}{\partial \dot{\beta}_1} = I_{x1}\,\dot{\beta}_1 \quad and\ then\ differentiate\ \frac{\partial}{\partial t}\frac{\partial T}{\partial \dot{\beta}_1} = I_{x1}\,\ddot{\beta}_1$$

Differentiating kinetic energy equation with respect to $\dot{\beta}_2$ and then with respect to t:

$$\frac{\partial T}{\partial \dot{\beta}_2} = I_{x2}\,\dot{\beta}_2 \quad and\ then\ differentiate\ \frac{\partial}{\partial t}\frac{\partial T}{\partial \dot{\beta}_2} = I_{x2}\,\ddot{\beta}_2$$

Differentiating kinetic energy equation with respect to $\dot{\alpha}_1$ and then with respect to t:

$$\frac{\partial T}{\partial \dot{\alpha}_1} = I_{y1}\,\dot{\alpha}_1 \quad and\ then\ differentiate\ \frac{\partial}{\partial t}\frac{\partial T}{\partial \dot{\alpha}_1} = I_{y1}\,\ddot{\alpha}_1$$

Differentiating kinetic energy equation with respect to $\dot{\alpha}_2$ and then with respect to t:

$$\frac{\partial T}{\partial \dot{\alpha}_2} = I_{y2}\,\dot{\alpha}_2 \quad and\ then\ differentiate\ \frac{\partial}{\partial t}\frac{\partial T}{\partial \dot{\alpha}_2} = I_{y2}\,\ddot{\alpha}_1$$

Differentiating the potential energy equation with respect to X_1:

$$\frac{\partial V}{\partial X_1} = KBS1_x X_1 + KC_x(X_1 - X_2)$$

And then,

$$K_{11} = \frac{\partial}{\partial X_1}\frac{\partial V}{\partial X_1} = KBS1_x + KC_x = (KB1_x \,//\, KS1_x) + KC_x$$

$$K_{21} = K_{12} = \frac{\partial}{\partial X_2}\frac{\partial V}{\partial X_1} = -KC_x$$

$$K_{31} = K_{13} = \frac{\partial}{\partial Y_1}\frac{\partial V}{\partial X_1} = 0$$

$$K_{41} = K_{14} = \frac{\partial}{\partial Y_2}\frac{\partial V}{\partial X_1} = 0$$

$$K_{51} = K_{15} = \frac{\partial}{\partial Z_1}\frac{\partial V}{\partial X_1} = 0$$

$$K_{61} = K_{16} = \frac{\partial}{\partial Z_2}\frac{\partial V}{\partial X_1} = 0$$

$$K_{71} = K_{17} = \frac{\partial}{\partial \theta_1}\frac{\partial V}{\partial X_1} = 0$$

$$K_{81} = K_{18} = \frac{\partial}{\partial \theta_2}\frac{\partial V}{\partial X_1} = 0$$

$$K_{91} = K_{19} = \frac{\partial}{\partial \beta_1}\frac{\partial V}{\partial X_1} = 0$$

$$K_{10-1} = K_{1-10} = \frac{\partial}{\partial \beta_2}\frac{\partial V}{\partial X_1} = 0$$

$$K_{11-1} = K_{1-11} = \frac{\partial}{\partial \alpha_1}\frac{\partial V}{\partial X_1} = 0$$

$$K_{12-1} = K_{1-12} = \frac{\partial}{\partial \alpha_2}\frac{\partial V}{\partial X_1} = 0$$

Differentiating the potential energy equation with respect to X_2:

$$\frac{\partial V}{\partial X_2} = KBS2_x X_2 - KC_x(X_1 - X_2)$$

And then,

$$K_{12} = K_{21} = \frac{\partial}{\partial X_1}\frac{\partial V}{\partial X_2} = -KC_x$$

$$K_{22} = \frac{\partial}{\partial X_2}\frac{\partial V}{\partial X_2} = KBS2_x + KC_x = (KB2_x \,//\, KS2_x) + KC_x$$

$$K_{32} = K_{23} = \frac{\partial}{Y_1}\frac{\partial}{\partial X_2} = 0$$

$$K_{42} = K_{24} = \frac{\partial}{\partial Y_2}\frac{\partial V}{\partial X_2} = 0$$

$$K_{52} = K_{25} = \frac{\partial}{\partial Z_1}\frac{\partial V}{\partial X_2} = 0$$

$$K_{62} = K_{26} = \frac{\partial}{\partial Z_2}\frac{\partial V}{\partial X_2} = 0$$

$$K_{72} = K_{27} = \frac{\partial}{\partial \theta_1}\frac{\partial V}{\partial X_2} = 0$$

$$K_{82} = K_{28} = \frac{\partial}{\partial \theta_2}\frac{\partial V}{\partial X_2} = 0$$

$$K_{92} = K_{29} = \frac{\partial}{\partial \beta_1}\frac{\partial V}{\partial X_2} = 0$$

$$K_{10-2} = K_{2-10} = \frac{\partial}{\partial \beta_2}\frac{\partial V}{\partial X_2} = 0$$

$$K_{11-2} = K_{2-11} = \frac{\partial}{\partial \alpha_1}\frac{\partial V}{\partial X_2} = 0$$

$$K_{12-2} = K_{2-12} = \frac{\partial}{\partial \alpha_2}\frac{\partial V}{\partial X_2} = 0$$

Differentiating the potential energy equation with respect to Y_1:

$$\frac{\partial V}{\partial Y_1} = KBS1_y Y_1 + KC_y(Y_1 - Y_2)$$

And then,

$$K_{13} = K_{31} = \frac{\partial}{\partial X_1}\frac{\partial V}{\partial Y_1} = 0$$

$$K_{23} = K_{32} = \frac{\partial}{\partial X_2}\frac{\partial V}{\partial Y_1} = 0$$

$$K_{33} = \frac{\partial}{\partial Y_1}\frac{\partial V}{\partial Y_1} = KBS1_y + KC_y = \left(KB1_y \,//\, KS1_y\right) + KC_y$$

$$K_{43} = K_{34} = \frac{\partial}{\partial Y_2}\frac{\partial V}{\partial Y_1} = -KC_y$$

$$K_{53} = K_{35} = \frac{\partial}{\partial Z_1}\frac{\partial V}{\partial Y_1} = 0$$

$$K_{63} = K_{36} = \frac{\partial}{\partial Z_2}\frac{\partial V}{\partial Y_1} = 0$$

$$K_{73} = K_{37} = \frac{\partial}{\partial \theta_1}\frac{\partial V}{\partial Y_1} = 0$$

$$K_{83} = K_{38} = \frac{\partial}{\partial \theta_2}\frac{\partial V}{\partial Y_1} = 0$$

$$K_{93} = K_{39} = \frac{\partial}{\partial \beta_1}\frac{\partial V}{\partial Y_1} = 0$$

$$K_{10-3} = K_{3-10} = \frac{\partial}{\partial \beta_2}\frac{\partial V}{\partial Y_1} = 0$$

$$K_{11-3} = K_{3-11} = \frac{\partial}{\partial \alpha_1}\frac{\partial V}{\partial Y_1} = 0$$

$$K_{12-3} = K_{3-12} = \frac{\partial}{\partial \alpha_2}\frac{\partial V}{\partial Y_1} = 0$$

Differentiating the potential energy equation with respect to Y_2:

$$\frac{\partial V}{\partial Y_2} = KBS2_y Y_2 - KC_y(Y_1 - Y_2)$$

And then,

$$K_{14} = K_{41} = \frac{\partial}{\partial X_1}\frac{\partial V}{\partial Y_2} = 0$$

$$K_{24} = K_{42} = \frac{\partial}{\partial X_2}\frac{\partial V}{\partial Y_2} = 0$$

$$K_{34} = K_{43} = \frac{\partial}{\partial Y_1}\frac{\partial V}{\partial Y_2} = -KC_y$$

$$K_{44} = \frac{\partial}{\partial Y_2}\frac{\partial V}{\partial Y_2} = KBS2_y + KC_y = \left(KB2_y \,//\, KS2_y\right) + KC_y$$

$$K_{54} = K_{45} = \frac{\partial}{\partial Z_1}\frac{\partial V}{\partial Y_2} = 0$$

$$K_{64} = K_{46} = \frac{\partial}{\partial Z_2}\frac{\partial V}{\partial Y_2} = 0$$

$$K_{74} = K_{47} = \frac{\partial}{\partial \theta_1}\frac{\partial V}{\partial Y_2} = 0$$

$$K_{84} = K_{48} = \frac{\partial}{\partial \theta_2}\frac{\partial V}{\partial Y_2} = 0$$

$$K_{94} = K_{49} = \frac{\partial}{\partial \beta_1}\frac{\partial V}{\partial Y_2} = 0$$

$$K_{10-4} = K_{4-10} = \frac{\partial}{\partial \beta_2}\frac{\partial V}{\partial Y_2} = 0$$

$$K_{11-4} = K_{4-11} = \frac{\partial}{\partial \alpha_1}\frac{\partial V}{\partial Y_2} = 0$$

$$K_{12-4} = K_{4-12} = \frac{\partial}{\partial \alpha_2}\frac{\partial V}{\partial Y_2} = 0$$

Differentiating the potential energy equation with respect to Z_1:

$$\frac{\partial V}{\partial Z_1} = KC_z(Z_1 - Z_2) + KS1_z Z_1$$

And then,

$$K_{15} = K_{51} = \frac{\partial}{\partial x_1}\frac{\partial V}{\partial Z_1} = 0$$

$$K_{25} = K_{52} = \frac{\partial}{\partial X_2}\frac{\partial V}{\partial Z_1} = 0$$

$$K_{35} = K_{53} = \frac{\partial}{\partial Y_1}\frac{\partial V}{\partial Z_1} = 0$$

$$K_{45} = K_{54} = \frac{\partial}{\partial Y_2}\frac{\partial V}{\partial Z_1} = 0$$

$$K_{55} = \frac{\partial}{\partial Z_1}\frac{\partial V}{\partial Z_1} = KC_z + KS1_z$$

$$K_{65} = K_{56} = \frac{\partial}{\partial Z_2}\frac{\partial V}{\partial Z_1} = -KC_z$$

$$K_{75} = K_{57} = \frac{\partial}{\partial \theta_1}\frac{\partial V}{\partial Z_1} = 0$$

$$K_{85} = K_{58} = \frac{\partial}{\partial \theta_2}\frac{\partial V}{\partial Z_1} = 0$$

$$K_{95} = K_{59} = \frac{\partial}{\partial \beta_1}\frac{\partial V}{\partial Z_1} = 0$$

$$K_{10-5} = K_{5-10} = \frac{\partial}{\partial \beta_2}\frac{\partial V}{\partial Z_1} = 0$$

$$K_{11-5} = K_{5-11} = \frac{\partial}{\partial \alpha_1}\frac{\partial V}{\partial Z_1} = 0$$

$$K_{12-5} = K_{5-12} = \frac{\partial}{\partial \alpha_2}\frac{\partial V}{\partial Z_1} = 0$$

Differentiating the potential energy equation with respect to Z_2:

$$\frac{\partial V}{\partial Z_2} = -KC_z(Z_1 - Z_2) + KS2_z Z_2$$

And then,

$$K_{16} = K_{61} = \frac{\partial}{\partial x_1}\frac{\partial V}{\partial Z_2} = 0$$

$$K_{26} = K_{62} = \frac{\partial}{\partial X_2}\frac{\partial V}{\partial Z_2} = 0$$

$$K_{36} = K_{63} = \frac{\partial}{\partial Y_1}\frac{\partial V}{\partial Z_2} = 0$$

$$K_{46} = K_{64} = \frac{\partial}{\partial Y_2}\frac{\partial V}{\partial Z_2} = 0$$

$$K_{56} = K_{65} = \frac{\partial}{\partial Z_1}\frac{\partial V}{\partial Z_2} = -KC_z$$

$$K_{66} = \frac{\partial}{\partial Z_2}\frac{\partial V}{\partial Z_2} = KC_z + KS2_z$$

$$K_{76} = K_{67} = \frac{\partial}{\partial \theta_1}\frac{\partial V}{\partial Z_2} = 0$$

$$K_{86} = K_{68} = \frac{\partial}{\partial \theta_2}\frac{\partial V}{\partial Z_2} = 0$$

$$K_{96} = K_{69} = \frac{\partial}{\partial \beta_1}\frac{\partial V}{\partial Z_2} = 0$$

$$K_{10-6} = K_{6-10} = \frac{\partial}{\partial \beta_2}\frac{\partial V}{\partial Z_2} = 0$$

$$K_{11-6} = K_{6-11} = \frac{\partial}{\partial \alpha_1}\frac{\partial V}{\partial Z_2} = 0$$

$$K_{12-6} = K_{6-12} = \frac{\partial}{\partial \alpha_2}\frac{\partial V}{\partial Z_2} = 0$$

Differentiating the potential energy equation with respect to θ_1:

$$\frac{\partial V}{\partial \theta_1} = KCT_z(\theta_1 - \theta_2) + KS1T_z\theta_1$$

And then,

$$K_{17} = K_{71} = \frac{\partial}{\partial X_1}\frac{\partial V}{\partial \theta_1} = 0$$

$$K_{27} = K_{72} = \frac{\partial}{\partial X_2}\frac{\partial V}{\partial \theta_1} = 0$$

$$K_{37} = K_{73} = \frac{\partial}{\partial Y_1}\frac{\partial V}{\partial \theta_1} = 0$$

$$K_{47} = K_{74} = \frac{\partial}{\partial Y_2}\frac{\partial V}{\partial \theta_1} = 0$$

$$K_{57} = K_{75} = \frac{\partial}{\partial Z_1}\frac{\partial V}{\partial \theta_1} = 0$$

$$K_{67} = K_{76} = \frac{\partial}{\partial Z_2}\frac{\partial V}{\partial \theta_1} = 0$$

$$K_{77} = \frac{\partial}{\partial \theta_1}\frac{\partial V}{\partial \theta_1} = KCT_z + KS1T_z$$

$$K_{87} = K_{78} = \frac{\partial}{\partial \theta_2}\frac{\partial V}{\partial \theta_1} = -KCT_z$$

$$K_{97} = K_{79} = \frac{\partial}{\partial \beta_1}\frac{\partial V}{\partial \theta_1} = 0$$

$$K_{10-7} = K_{7-10} = \frac{\partial}{\partial \beta_2}\frac{\partial V}{\partial \theta_1} = 0$$

$$K_{11-7} = K_{7-11} = \frac{\partial}{\partial \alpha_1}\frac{\partial V}{\partial \theta_1} = 0$$

$$K_{12-7} = K_{7-12} = \frac{\partial}{\partial \alpha_2}\frac{\partial V}{\partial \theta_1} = 0$$

Differentiating the potential energy equation with respect to θ_2:

$$\frac{\partial V}{\partial \theta_2} = -KCT_z(\theta_1 - \theta_2) + KS2T_z\theta_2$$

And then,

$$K_{18} = K_{81} = \frac{\partial}{\partial X_1}\frac{\partial V}{\partial \theta_2} = 0$$

$$K_{28} = K_{82} = \frac{\partial}{\partial X_2}\frac{\partial V}{\partial \theta_2} = 0$$

$$K_{38} = K_{83} = \frac{\partial}{\partial Y_1}\frac{\partial V}{\partial \theta_2} = 0$$

$$K_{48} = K_{84} = \frac{\partial}{\partial Y_2}\frac{\partial V}{\partial \theta_2} = 0$$

$$K_{58} = K_{85} = \frac{\partial}{\partial Z_1}\frac{\partial V}{\partial \theta_2} = 0$$

$$K_{68} = K_{86} = \frac{\partial}{\partial Z_2}\frac{\partial V}{\partial \theta_2} = 0$$

$$K_{78} = K_{87} = \frac{\partial}{\partial \theta_1}\frac{\partial V}{\partial \theta_2} = -KCT_z$$

$$K_{88} = \frac{\partial}{\partial \theta_2}\frac{\partial V}{\partial \theta_2} = KCT_z + KS2T_z$$

$$K_{98} = K_{89} = \frac{\partial}{\partial \beta_1}\frac{\partial V}{\partial \theta_2} = 0$$

$$K_{10-8} = K_{8-10} = \frac{\partial}{\partial \beta_2}\frac{\partial V}{\partial \theta_2} = 0$$

$$K_{11-8} = K_{8-11} = \frac{\partial}{\partial \alpha_1}\frac{\partial V}{\partial \theta_2} = 0$$

$$K_{12-8} = K_{8-12} = \frac{\partial}{\partial \alpha_2}\frac{\partial V}{\partial \theta_2} = 0$$

Differentiating the potential energy equation with respect to β_1:

$$\frac{\partial V}{\partial \beta_1} = KCT_x(\beta_1 - \beta_2)$$

And then,

$$K_{19} = K_{91} = \frac{\partial}{\partial X_1}\frac{\partial V}{\partial \beta_1} = 0$$

$$K_{29} = K_{92} = \frac{\partial}{\partial X_2}\frac{\partial V}{\partial \beta_1} = 0$$

$$K_{39} = K_{93} = \frac{\partial}{\partial Y_1}\frac{\partial V}{\partial \beta_1} = 0$$

$$K_{49} = K_{94} = \frac{\partial}{\partial Y_2}\frac{\partial V}{\partial \beta_1} = 0$$

$$K_{59} = K_{95} = \frac{\partial}{\partial Z_1}\frac{\partial V}{\partial \beta_1} = 0$$

$$K_{69} = K_{96} = \frac{\partial}{\partial Z_2}\frac{\partial V}{\partial \beta_1} = 0$$

$$K_{79} = K_{97} = \frac{\partial}{\partial \theta_1}\frac{\partial V}{\partial \beta_1} = 0$$

$$K_{89} = K_{98} = \frac{\partial}{\partial \theta_2}\frac{\partial V}{\partial \beta_1} = 0$$

$$K_{99} = \frac{\partial}{\partial \beta_1}\frac{\partial V}{\partial \beta_1} = KCT_x$$

$$K_{10-9} = K_{9-10} = \frac{\partial}{\partial \beta_2}\frac{\partial V}{\partial \beta_1} = -KCT_x$$

$$K_{11-9} = K_{9-11} = \frac{\partial}{\partial \alpha_1}\frac{\partial V}{\partial \beta_1} = 0$$

$$K_{12-9} = K_{9-12} = \frac{\partial}{\partial \alpha_2}\frac{\partial V}{\partial \beta_1} = 0$$

Differentiating the potential energy equation with respect to β_2:

$$\frac{\partial V}{\partial \beta_2} = -KCT_x(\beta_1 - \beta_2)$$

And then,

$$K_{1-10} = K_{10-1} = \frac{\partial}{\partial X_1}\frac{\partial V}{\partial \beta_2} = 0$$

$$K_{2-10} = K_{10-2} = \frac{\partial}{\partial X_2}\frac{\partial V}{\partial \beta_2} = 0$$

$$K_{3-10} = K_{10-3} = \frac{\partial}{\partial Y_1}\frac{\partial V}{\partial \beta_2} = 0$$

$$K_{4-10} = K_{10-4} = \frac{\partial}{\partial Y_2}\frac{\partial V}{\partial \beta_2} = 0$$

$$K_{5-10} = K_{10-5} = \frac{\partial}{\partial Z_1}\frac{\partial V}{\partial \beta_2} = 0$$

$$K_{6-10} = K_{10-6} = \frac{\partial}{\partial Z_2}\frac{\partial V}{\partial \beta_2} = 0$$

$$K_{7-10} = K_{10-7} = \frac{\partial}{\partial \theta_1}\frac{\partial V}{\partial \beta_2} = 0$$

$$K_{8-10} = K_{10-8} = \frac{\partial}{\partial \theta_2}\frac{\partial V}{\partial \beta_2} = 0$$

$$K_{9-10} = K_{10-9} = \frac{\partial}{\partial \beta_1}\frac{\partial V}{\partial \beta_2} = -KCT_x$$

$$K_{10-10} = K_{10-10} = \frac{\partial}{\partial \beta_2}\frac{\partial V}{\partial \beta_2} = KCT_x$$

$$K_{11-10} = K_{10-11} = \frac{\partial}{\partial \alpha_1}\frac{\partial V}{\partial \beta_2} = 0$$

$$K_{12-10} = K_{10-12} = \frac{\partial}{\partial \alpha_2}\frac{\partial V}{\partial \beta_2} = 0$$

Differentiating the potential energy equation with respect to α_1:

$$\frac{\partial V}{\partial \alpha_1} = KCT_y(\alpha_1 - \alpha_2)$$

And then,

$$K_{1-11} = K_{11-1} = \frac{\partial}{\partial X_1}\frac{\partial V}{\partial \alpha_1} = 0$$

$$K_{2-11} = K_{11-2} = \frac{\partial}{\partial X_2}\frac{\partial V}{\partial \alpha_1} = 0$$

$$K_{3-11} = K_{11-3} = \frac{\partial}{\partial Y_1}\frac{\partial V}{\partial \alpha_1} = 0$$

$$K_{4-11} = K_{11-4} = \frac{\partial}{\partial Y_2}\frac{\partial V}{\partial \alpha_1} = 0$$

$$K_{5-11} = K_{11-5} = \frac{\partial}{\partial Z_1}\frac{\partial V}{\partial \alpha_1} = 0$$

$$K_{6-11} = K_{11-6} = \frac{\partial}{\partial Z_2}\frac{\partial V}{\partial \alpha_1} = 0$$

$$K_{7-11} = K_{11-7} = \frac{\partial}{\partial \theta_1}\frac{\partial V}{\partial \alpha_1} = 0$$

$$K_{8-11} = K_{11-8} = \frac{\partial}{\partial \theta_2}\frac{\partial V}{\partial \alpha_1} = 0$$

$$K_{9-11} = K_{11-9} = \frac{\partial}{\partial \beta_1}\frac{\partial V}{\partial \alpha_1} = 0$$

$$K_{10-11} = K_{11-10} = \frac{\partial}{\partial \beta_2}\frac{\partial V}{\partial \alpha_1} = 0$$

$$K_{11-11} = \frac{\partial}{\partial \alpha_1}\frac{\partial V}{\partial \alpha_1} = KCT_y$$

$$K_{12-11} = K_{11-12} = \frac{\partial}{\partial \alpha_2}\frac{\partial V}{\partial \alpha_1} = -KCT_y$$

Differentiating the potential energy equation with respect to α_2:

$$\frac{\partial V}{\partial \alpha_2} = -KCT_y(\alpha_1 - \alpha_2)$$

And then,

$$K_{1-12} = K_{12-1} = \frac{\partial}{\partial X_1}\frac{\partial V}{\partial \alpha_2} = 0$$

$$K_{2-12} = K_{12-2} = \frac{\partial}{\partial X_2}\frac{\partial V}{\partial \alpha_2} = 0$$

$$K_{3-12} = K_{12-3} = \frac{\partial}{\partial Y_1}\frac{\partial V}{\partial \alpha_2} = 0$$

$$K_{4-12} = K_{12-4} = \frac{\partial}{\partial Y_2}\frac{\partial V}{\partial \alpha_2} = 0$$

$$K_{5-12} = K_{12-5} = \frac{\partial}{\partial Z_1}\frac{\partial V}{\partial \alpha_2} = 0$$

$$K_{6-12} = K_{12-6} = \frac{\partial}{\partial Z_2}\frac{\partial V}{\partial \alpha_2} = 0$$

$$K_{7-12} = K_{12-7} = \frac{\partial}{\partial \theta_1}\frac{\partial V}{\partial \alpha_2} = 0$$

$$K_{8-12} = K_{12-8} = \frac{\partial}{\partial \theta_2}\frac{\partial V}{\partial \alpha_2} = 0$$

$$K_{9-12} = K_{12-9} = \frac{\partial}{\partial \beta_1}\frac{\partial V}{\partial \alpha_2} = 0$$

$$K_{10-12} = K_{12-10} = \frac{\partial}{\partial \beta_2}\frac{\partial V}{\partial \alpha_2} = 0$$

$$K_{11-12} = K_{12-11} = \frac{\partial}{\partial \alpha_1}\frac{\partial V}{\partial \alpha_2} = -KCT_y$$

$$K_{12-12} = \frac{\partial}{\partial \alpha_2}\frac{\partial V}{\partial \alpha_2} = KCT_y$$

Differentiating the dissipation equation with respect to $\dot{X}_1$:

$$\frac{\partial D}{\partial \dot{X}_1} = CB1_x \dot{X}_1 + CC_x\left(\dot{X}_1 - \dot{X}_2\right)$$

And then,

$$C_{11} = \frac{\partial}{\partial \dot{X}_1}\frac{\partial D}{\partial \dot{X}_1} = CB1_x + CC_x$$

$$C_{21} = C_{12} = \frac{\partial}{\partial \dot{X}_2}\frac{\partial D}{\partial \dot{X}_1} = -CC_x$$

$$C_{31} = C_{13} = \frac{\partial}{\partial \dot{Y}_1}\frac{\partial D}{\partial \dot{X}_1} = 0$$

$$C_{41} = C_{14} = \frac{\partial}{\partial \dot{Y}_2}\frac{\partial D}{\partial \dot{X}_1} = 0$$

$$C_{51} = C_{15} = \frac{\partial}{\partial \dot{Z}_1}\frac{\partial D}{\partial \dot{X}_1} = 0$$

$$C_{61} = C_{16} = \frac{\partial}{\partial \dot{Z}_2}\frac{\partial D}{\partial \dot{X}_1} = 0$$

$$C_{71} = C_{17} = \frac{\partial}{\partial \dot{\theta}_1}\frac{\partial D}{\partial \dot{X}_1} = 0$$

$$C_{81} = C_{18} = \frac{\partial}{\partial \dot{\theta}_2}\frac{\partial D}{\partial \dot{X}_1} = 0$$

$$C_{91} = C_{19} = \frac{\partial}{\partial \dot{\beta}_1}\frac{\partial D}{\partial \dot{X}_1} = 0$$

$$C_{10-1} = C_{1-10} = \frac{\partial}{\partial \dot{\beta}_2}\frac{\partial D}{\partial \dot{X}_1} = 0$$

$$C_{11-1} = C_{1-11} = \frac{\partial}{\partial \dot{\alpha}_1}\frac{\partial D}{\partial \dot{X}_1} = 0$$

$$C_{12-1} = C_{1-12} = \frac{\partial}{\partial \dot{\alpha}_2}\frac{\partial D}{\partial \dot{X}_1} = 0$$

Differentiating the dissipation equation with respect to $\dot{X}_2$:

$$\frac{\partial D}{\partial \dot{X}_2} = CB2_x \dot{X}_2 - CC_x\left(\dot{X}_1 - \dot{X}_2\right)$$

And then,

$$C_{12} = C_{21} = \frac{\partial}{\partial \dot{X}_1}\frac{\partial D}{\partial \dot{X}_2} = -CC_x$$

$$C_{22} = \frac{\partial}{\partial \dot{X}_2}\frac{\partial D}{\partial \dot{X}_2} = CB2_x + CC_x$$

$$C_{32} = C_{23} = \frac{\partial}{\dot{Y}_1}\frac{\partial D}{\partial \dot{X}_2} = 0$$

$$C_{42} = C_{24} = \frac{\partial}{\partial \dot{Y}_2}\frac{\partial D}{\partial \dot{X}_2} = 0$$

$$C_{52} = C_{25} = \frac{\partial}{\partial \dot{Z}_1}\frac{\partial D}{\partial \dot{X}_2} = 0$$

$$C_{62} = C_{26} = \frac{\partial}{\partial \dot{Z}_2}\frac{\partial D}{\partial \dot{X}_2} = 0$$

$$C_{72} = C_{27} = \frac{\partial}{\partial \dot{\theta}_1}\frac{\partial D}{\partial \dot{X}_2} = 0$$

$$C_{82} = C_{28} = \frac{\partial}{\partial \dot{\theta}_2}\frac{\partial D}{\partial \dot{X}_2} = 0$$

$$C_{92} = C_{29} = \frac{\partial}{\partial \dot{\beta}_1}\frac{\partial D}{\partial \dot{X}_2} = 0$$

$$C_{10-2} = C_{2-10} = \frac{\partial}{\partial \dot{\beta}_2}\frac{\partial D}{\partial \dot{X}_2} = 0$$

$$C_{11-2} = C_{2-11} = \frac{\partial}{\partial \dot{\alpha}_1}\frac{\partial D}{\partial \dot{X}_2} = 0$$

$$C_{12-2} = C_{2-12} = \frac{\partial}{\partial \dot{\alpha}_2}\frac{\partial D}{\partial \dot{X}_2} = 0$$

Differentiating the dissipation equation with respect to $\dot{Y}_1$:

$$\frac{\partial D}{\partial Y_1} = CB1_y\dot{Y}_1 + CC_y\left(\dot{Y}_1 - \dot{Y}_2\right)$$

And then,

$$C_{13} = C_{31} = \frac{\partial}{\partial \dot{X}_1}\frac{\partial D}{\partial \dot{Y}_1} = 0$$

$$C_{23} = C_{32} = \frac{\partial}{\partial \dot{X}_2}\frac{\partial D}{\partial \dot{Y}_1} = 0$$

$$C_{33} = \frac{\partial}{\partial \dot{Y}_1}\frac{\partial D}{\partial \dot{Y}_1} = CB1_y + CC_y$$

$$C_{43} = C_{34} = \frac{\partial}{\partial \dot{Y}_2}\frac{\partial D}{\partial \dot{Y}_1} = -CC_y$$

$$C_{53} = C_{35} = \frac{\partial}{\partial \dot{Z}_1}\frac{\partial D}{\partial \dot{Y}_1} = 0$$

$$C_{63} = C_{36} = \frac{\partial}{\partial \dot{Z}_2}\frac{\partial D}{\partial \dot{Y}_1} = 0$$

$$C_{73} = C_{37} = \frac{\partial}{\partial \dot{\theta}_1}\frac{\partial D}{\partial \dot{Y}_1} = 0$$

$$C_{83} = C_{38} = \frac{\partial}{\partial \dot{\theta}_2}\frac{\partial D}{\partial \dot{Y}_1} = 0$$

$$C_{93} = C_{39} = \frac{\partial}{\partial \dot{\beta}_1}\frac{\partial D}{\partial \dot{Y}_1} = 0$$

$$C_{10-3} = C_{3-10} = \frac{\partial}{\partial \dot{\beta}_2}\frac{\partial D}{\partial \dot{Y}_1} = 0$$

$$C_{11-3} = C_{3-11} = \frac{\partial}{\partial \dot{\alpha}_1}\frac{\partial D}{\partial \dot{Y}_1} = 0$$

$$C_{12-3} = C_{3-12} = \frac{\partial}{\partial \dot{\alpha}_2}\frac{\partial D}{\partial \dot{Y}_1} = 0$$

Differentiating the dissipation equation with respect to $\dot{Y}_2$:

$$\frac{\partial V}{\partial Y_2} = CB2_y\dot{Y}_2 - CC_y\left(\dot{Y}_1 - \dot{Y}_2\right)$$

And then,

$$C_{14} = C_{41} = \frac{\partial}{\partial \dot{X}_1}\frac{\partial D}{\partial \dot{Y}_2} = 0$$

$$C_{24} = C_{42} = \frac{\partial}{\partial \dot{X}_2}\frac{\partial D}{\partial \dot{Y}_2} = 0$$

$$C_{34} = C_{43} = \frac{\partial}{\partial \dot{Y}_1}\frac{\partial D}{\partial \dot{Y}_2} = -CC_y$$

$$C_{44} = \frac{\partial}{\partial \dot{Y}_2}\frac{\partial D}{\partial \dot{Y}_2} = CB2_y + CC_y$$

$$C_{54} = C_{45} = \frac{\partial}{\partial \dot{Z}_1}\frac{\partial D}{\partial \dot{Y}_2} = 0$$

$$C_{64} = C_{46} = \frac{\partial}{\partial \dot{Z}_2}\frac{\partial D}{\partial \dot{Y}_2} = 0$$

$$C_{74} = C_{47} = \frac{\partial}{\partial \dot{\theta}_1}\frac{\partial D}{\partial \dot{Y}_2} = 0$$

$$C_{84} = C_{48} = \frac{\partial}{\partial \dot{\theta}_2}\frac{\partial D}{\partial \dot{Y}_2} = 0$$

$$C_{94} = C_{49} = \frac{\partial}{\partial \dot{\beta}_1}\frac{\partial D}{\partial \dot{Y}_2} = 0$$

$$C_{10-4} = C_{4-10} = \frac{\partial}{\partial \dot{\beta}_2}\frac{\partial D}{\partial \dot{Y}_2} = 0$$

$$C_{11-4} = C_{4-11} = \frac{\partial}{\partial \dot{\alpha}_1}\frac{\partial D}{\partial \dot{Y}_2} = 0$$

$$C_{12-4} = C_{4-12} = \frac{\partial}{\partial \dot{\alpha}_2}\frac{\partial D}{\partial \dot{Y}_2} = 0$$

Differentiating the dissipation equation with respect to $\dot{Z}_1$:

$$\frac{\partial D}{\partial \dot{Z}_1} = CC_z\left(\dot{Z}_1 - \dot{Z}_2\right)$$

And then,

$$C_{15} = C_{51} = \frac{\partial}{\partial \dot{X}_1}\frac{\partial D}{\partial \dot{Z}_1} = 0$$

$$C_{25} = C_{52} = \frac{\partial}{\partial \dot{X}_2}\frac{\partial D}{\partial \dot{Z}_1} = 0$$

$$C_{35} = C_{53} = \frac{\partial}{\partial \dot{Y}_1}\frac{\partial D}{\partial \dot{Z}_1} = 0$$

$$C_{45} = C_{54} = \frac{\partial}{\partial \dot{Y}_2}\frac{\partial D}{\partial \dot{Z}_1} = 0$$

$$C_{55} = \frac{\partial}{\partial \dot{Z}_1}\frac{\partial D}{\partial \dot{Z}_1} = CC_z$$

$$C_{65} = C_{56} = \frac{\partial}{\partial \dot{Z}_2}\frac{\partial D}{\partial \dot{Z}_1} = -CC_z$$

$$C_{75} = C_{57} = \frac{\partial}{\partial \dot{\theta}_1}\frac{\partial D}{\partial \dot{Z}_1} = 0$$

$$C_{85} = C_{58} = \frac{\partial}{\partial \dot{\theta}_2}\frac{\partial D}{\partial \dot{Z}_1} = 0$$

$$C_{95} = C_{59} = \frac{\partial}{\partial \dot{\beta}_1}\frac{\partial D}{\partial \dot{Z}_1} = 0$$

$$C_{10-5} = C_{5-10} = \frac{\partial}{\partial \dot{\beta}_2}\frac{\partial D}{\partial \dot{Z}_1} = 0$$

$$C_{11-5} = C_{5-11} = \frac{\partial}{\partial \dot{\alpha}_1}\frac{\partial D}{\partial \dot{Z}_1} = 0$$

$$C_{12-5} = C_{5-12} = \frac{\partial}{\partial \dot{\alpha}_2}\frac{\partial D}{\partial \dot{Z}_1} = 0$$

Differentiating the dissipation equation with respect to $\dot{Z}_2$:

$$\frac{\partial D}{\partial \dot{Z}_2} = -CC_z\left(\dot{Z}_1 - \dot{Z}_2\right)$$

And then,

$$C_{16} = C_{61} = \frac{\partial}{\partial \dot{X}_1}\frac{\partial D}{\partial \dot{Z}_2} = 0$$

$$C_{26} = C_{62} = \frac{\partial}{\partial \dot{X}_2}\frac{\partial D}{\partial \dot{Z}_2} = 0$$

$$C_{36} = C_{63} = \frac{\partial}{\partial \dot{Y}_1}\frac{\partial D}{\partial \dot{Z}_2} = 0$$

$$C_{46} = C_{64} = \frac{\partial}{\partial \dot{Y}_2}\frac{\partial D}{\partial \dot{Z}_2} = 0$$

$$C_{56} = C_{65} = \frac{\partial}{\partial \dot{Z}_1}\frac{\partial D}{\partial \dot{Z}_2} = -CC_z$$

$$C_{66} = \frac{\partial}{\partial \dot{Z}_2}\frac{\partial D}{\partial \dot{Z}_2} = CC_z$$

$$C_{76} = C_{67} = \frac{\partial}{\partial \dot{\theta}_1}\frac{\partial D}{\partial \dot{Z}_2} = 0$$

$$C_{86} = C_{68} = \frac{\partial}{\partial \dot{\theta}_2}\frac{\partial D}{\partial \dot{Z}_2} = 0$$

$$C_{96} = C_{69} = \frac{\partial}{\partial \dot{\beta}_1}\frac{\partial D}{\partial \dot{Z}_2} = 0$$

$$C_{10-6} = C_{6-10} = \frac{\partial}{\partial \dot{\beta}_2}\frac{\partial D}{\partial \dot{Z}_2} = 0$$

$$C_{11-6} = C_{6-11} = \frac{\partial}{\partial \dot{\alpha}_1}\frac{\partial D}{\partial \dot{Z}_2} = 0$$

$$C_{12-6} = C_{6-12} = \frac{\partial}{\partial \dot{\alpha}_2}\frac{\partial D}{\partial \dot{Z}_2} = 0$$

Differentiating the dissipation equation with respect to $\dot{\theta}_1$:

$$\frac{\partial D}{\partial \dot{\theta}_1} = 0$$

Differentiating the dissipation equation with respect to $\dot{\theta}_2$:

$$\frac{\partial D}{\partial \dot{\theta}_2} = 0$$

Differentiating the dissipation equation with respect to $\dot{\beta}_1$:

$$\frac{\partial D}{\partial \dot{\beta}_1} = 0$$

Differentiating the dissipation equation with respect to $\dot{\beta}_2$:

$$\frac{\partial D}{\partial \dot{\beta}_2} = 0$$

Differentiating the dissipation equation with respect to $\dot{\alpha}_1$:

$$\frac{\partial D}{\partial \dot{\alpha}_1} = 0$$

Differentiating the dissipation equation with respect to $\dot{\alpha}_2$:

$$\frac{\partial D}{\partial \dot{\alpha}_2} = 0$$

The mass matrix [M] is:

m_1	0	0	0	0	0	0	0	0	0	0	0
0	m_2	0	0	0	0	0	0	0	0	0	0
0	0	m_1	0	0	0	0	0	0	0	0	0
0	0	0	m_2	0	0	0	0	0	0	0	0
0	0	0	0	m_1	0	0	0	0	0	0	0
0	0	0	0	0	m_2	0	0	0	0	0	0
0	0	0	0	0	0	I_{z1}	0	0	0	0	0
0	0	0	0	0	0	0	I_{z2}	0	0	0	0
0	0	0	0	0	0	0	0	I_{x1}	0	0	0
0	0	0	0	0	0	0	0	0	I_{x2}	0	0
0	0	0	0	0	0	0	0	0	0	I_{y1}	0

0	0	0	0	0	0	0	0	0	0	0	I_{y2}

The stiffness matrix [K] is:

$KBS1_x + KC_x$	$-KC_x$	0	0	0	0	0	0	0	0	0	0
$-KC_x$	$KBS2_x + KC_x$	0	0	0	0	0	0	0	0	0	0
0	0	$KBS1_y + KC_y$	$-KC_y$	0	0	0	0	0	0	0	0
0	0	$-KC_y$	$KBS2_y + KC_y$	0	0	0	0	0	0	0	0
0	0	0	0	$KC_z + KS1_z$	$-KC_z$	0	0	0	0	0	0
0	0	0	0	$-KC_z$	$KC_z + KS2_z$	0	0	0	0	0	0
0	0	0	0	0	0	$KCT_z + KS1T_z$	$-KCT_z$	0	0	0	0
0	0	0	0	0	0	$-KCT_z$	$KCT_z + KS2T_z$	0	0	0	0
0	0	0	0	0	0	0	0	KCT_x	$-KCT_x$	0	0
0	0	0	0	0	0	0	0	$-KCT_x$	KCT_x	0	0
0	0	0	0	0	0	0	0	0	0	KCT_y	$-KCT_y$
0	0	0	0	0	0	0	0	0	0	$-KCT_y$	KCT_y

The damping matrix [D] is:

$CB1_x + CC_x$	$-CC_x$	0	0	0	0	0	0	0	0	0	0
$-CC_x$	$CB2_x + CC_x$	0	0	0	0	0	0	0	0	0	0
0	0	$CB1_y + CC_y$	$-CC_y$	0	0	0	0	0	0	0	0
0	0	$-CC_y$	$CB2_y + CC_y$	0	0	0	0	0	0	0	0
0	0	0	0	CC_z	$-CC_z$	0	0	0	0	0	0
0	0	0	0	$-CC_z$	CC_z	0	0	0	0	0	0
0	0	0	0	0	0	0	0	0	0	0	0
0	0	0	0	0	0	0	0	0	0	0	0
0	0	0	0	0	0	0	0	0	0	0	0
0	0	0	0	0	0	0	0	0	0	0	0
0	0	0	0	0	0	0	0	0	0	0	0
0	0	0	0	0	0	0	0	0	0	0	0

APPENDIX 6: NUMERICAL SOLVING CODE USING MATALB

Main program

```
%%%%%%%%%%%%%%%%%%%%%%%%%%%%%%%%%%%%%%%%%%%%%%%%%%%%%%%%%%%%%%%%%%%%%%
%%%                   Bism Allah Alrahman Alrahim                  %%%
%%%                                                                %%%
%%%                                                                %%%
%%%                                                                %%%
%%%           NUMERICAL  SIMULATION  OF  DYNAMIC  RESPONSE         %%%
%%%                                                                %%%
%%%              OF  A  Rotor-Coupling-Bearing System              %%%
%%%                                                                %%%
%%%                                                                %%%
%%%                                                                %%%
%%%                          Doha, June,2019                       %%%
%%%                                                                %%%
%%%%%%%%%%%%%%%%%%%%%%%%%%%%%%%%%%%%%%%%%%%%%%%%%%%%%%%%%%%%%%%%%%%%%%

close all
clear all
clc

disp(' ')
disp(' ')
disp('================================================================
====')
disp('======        NUMERICAL SIMULATION OF DYNAMIC RESPONSE
======')
disp('======           OF  A ROTOR-COUPLING-BEARING SYSTEM
======')
disp('================================================================
====')
disp('================================================================
====')
disp(' ')
disp(' ')
disp(' ')
disp('  >>     Execution of the Main Program')

Program_1_Data

Program_2_SimulationData

Program_3_Forces

Program_4_GoSimulation

Program_5_FastFourierTransform

Program_6_NaturalFrequency
```

Program_7_PlotGraphs

Program_1_Data

```
%% ======================================================================= %%
disp(' ')
disp('  >>     Execution of Program_1 : Data')


%% ======================================================================= %%
global KB1X KB1Y KB2X KB2Y KS1X KS1Y KS1Z KS2X KS2Y KS2Z KS1T KS2T
global KCX KCY KCZ KCTX KCTY KCTZ
global CB1X CB1Y CB2X CB2Y
global CCX CCY CCZ
global e1 e2 w RPM FREQ
global m1 m2 Ix1 Iy1 Iz1 Ix2 Iy2 Iz2

%% ======================================================================= %%
%%=======     Rotor-Coupling-Bearing System GENERAL DATA ==================
%%=============================================================================

e1   = 0.001;           %Eccentricity of Shaft 1 in (m)
e2   = 0.001;           %Eccentricity of Shaft 2 in (m)
FREQ = 20;              %Frequency of the system in (Hz)
RPM  = FREQ * 60;       %Rotational speed of the system in (RPM)
w    = 2*pi*FREQ;       %Rotational speed of the system in (rad/s)
delL = 0.0301;          %Flexible distance in the coupling in(m)
dely = 0.001;           %parallel misalignment distance in(m)
dela = 1;               %Angular misalignment in (Degrees)
radius = 0.0381;        %radius of coupling in (m)

m1   = 0.21745;         %Mass of the Subsystem 1 in (Kg)
m2   = 0.15138;         %Mass of the Subsystem 2 in (Kg)
Iz1  = 1.8350E-5;       %Moment of inertia of Subsystem 1 around Z-axis
(Axial direction)  in (Kg.m2)
Iz2  = 1.6463E-5;       %Moment of inertia of Subsystem 2 around Z-axis
(Axial direction)  in (Kg.m2)
Ix1  = 2.3309E-4;       %Moment of inertia of Subsystem 1 around x-axis
(Radial direction) in (Kg.m2)
Ix2  = 4.9009E-5;       %Moment of inertia of Subsystem 2 around x-axis
(Radial direction) in (Kg.m2)
Iy1  = 2.3284E-4;       %Moment of inertia of Subsystem 1 around y-axis
(Radial direction) in (Kg.m2)
Iy2  = 4.8755E-5;       %Moment of inertia of Subsystem 2 around y-axis
(Radial direction) in (Kg.m2)

KB1X = 6.56E8;          %Stiffness coefficient of bearing 1 in x-axis
direction in (N/m)
KB1Y = 6.56E8;          %Stiffness coefficient of bearing 1 in y-axis
direction in (N/m)
KB2X = 6.56E8;          %Stiffness coefficient of bearing 2 in x-axis
direction in (N/m)
KB2Y = 6.56E8;          %Stiffness coefficient of bearing 2 in y-axis
direction in (N/m)
KS1X = 1.28115E6;       %Stiffness coefficient of shaft 1 in x-axis
direction in (N/m)
KS1Y = 1.28115E6;       %Stiffness coefficient of shaft 1 in y-axis
direction in (N/m)
KS1Z = 3.4309458E8;     %Stiffness coefficient of shaft 1 in z-axis
direction in (N/m)
KS2X = 7.26606E6;       %Stiffness coefficient of shaft 2 in x-axis
direction in (N/m)
```

```
KS2Y = 7.26606E6;       %Stiffness coefficient of shaft 2 in y-axis
direction in (N/m)
KS2Z = 6.11852E8;       %Stiffness coefficient of shaft 2 in z-axis
direction in (N/m)
KS1T = 3790.15;         %Angular stiffness of shaft 1 in torsional direction
in (N.m/rad)
KS2T = 6759.10;         %Angular stiffness of shaft 2 in torsional direction
in (N.m/rad)
KCX  = 16066;           %Stiffness coefficient of coupling in x-direction in
(N/m)
KCY  = 16122;           %Stiffness coefficient of coupling in y-direction in
(N/m)
KCZ  = 171920;          %Stiffness coefficient of coupling in z-direction in
(N/m)
KCTX = 13.999;          %Angular stiffness of coupling about x-direction in
(N.m/rad)
KCTY = 13.928;          %Angular stiffness of coupling about y-direction in
(N.m/rad)
KCTZ = 328.711;         %Angular stiffness of coupling about z-direction in
(N.m/rad)

CB1X = 1.8E3;           %Damping coefficient of bearing 1 in x-direction in
(N.s/m)
CB1Y = 1.8E3;           %Damping coefficient of bearing 1 in y-direction in
(N.s/m)
CB2X = 1.8E3;           %Damping coefficient of bearing 2 in x-direction in
(N.s/m)
CB2Y = 1.8E3;           %Damping coefficient of bearing 2 in y-direction in
(N.s/m)
CCX  = 3.42;            %Damping coefficient of coupling  in x-direction in
(N.s/m)
CCY  = 3.27;            %Damping coefficient of coupling  in y-direction in
(N.s/m)
CCZ  = 5.65;            %Damping coefficient of coupling  in z-direction in
(N.s/m)
```

Program_2_SimulationData

```
%% ====================================================================== %%
disp(' ')
disp('  >>     Execution of Program_2 : Simulation Data'  )

%% ====================================================================== %%

global MaxSimTime  DeltaSimTime  SimTime  NSimTimeSteps


%% ====================================================================== %%
%==                          Simulation Parameters                       ==%
%=========================================================================%

MaxSimTime    = 1;                            % Maximum Simulation Time in
(s)
DeltaSimTime  = 0.001;                       % Increment of Simlation Time
in (s)
SimTime       = 0:DeltaSimTime:MaxSimTime;    % Simulation Time Vector in
(s)
NSimTimeSteps = length(SimTime);              % Number of Simulation Steps
(Units)
```

Program_3_Forces

```
 %% ======================================================================== %%
disp(' ')
disp('  >>     Execution of the program_3 : Forces' )


%% ======================================================================== %%

global F1  F2  F3  F4  F5  F6  F7  F8  F9 F10  F11  F12

%% ======================================================================== %%
   F1  = zeros(1,NSimTimeSteps);            %Create empty array for force -
X1     - in (N)
   F2  = zeros(1,NSimTimeSteps);            %Create empty array for force -
X2     - in (N)
   F3  = zeros(1,NSimTimeSteps);            %Create empty array for force -
Y1     - in (N)
   F4  = zeros(1,NSimTimeSteps);            %Create empty array for force -
Y2     - in (N)
   F5  = zeros(1,NSimTimeSteps);            %Create empty array for force -
Z1     - in (N)
   F6  = zeros(1,NSimTimeSteps);            %Create empty array for force -
Z2     - in (N)
   F7  = zeros(1,NSimTimeSteps);            %Create empty array for force -
THETA1 - in (N.m)
   F8  = zeros(1,NSimTimeSteps);            %Create empty array for force -
THETA2 - in (N.m)
   F9  = zeros(1,NSimTimeSteps);            %Create empty array for force -
BETA1  - in (N.m)
   F10 = zeros(1,NSimTimeSteps);            %Create empty array for force -
BETA2  - in (N.m)
   F11 = zeros(1,NSimTimeSteps);            %Create empty array for force -
ALPHA1 - in (N.m)
   F12 = zeros(1,NSimTimeSteps);            %Create empty array for force -
ALPHA2 - in (N.m)

 %================================================%
 %==              Force Vector                  ==%
 %================================================%

 for i = 1:NSimTimeSteps,
     F1(i) = m1*e1*w^2*sin(w*SimTime(i))+ KCX * (dely/4)*sin(2*w*SimTime(i))
;      %Force array - X1 - in (N)
     F2(i) = m2*e2*w^2*sin(w*SimTime(i))- KCX * (dely/4)*sin(2*w*SimTime(i))
;      %Force array - X2 - in (N)
     F3(i) = m1*e1*w^2*cos(w*SimTime(i))+ KCY *
(dely/4)*(1+cos(2*w*SimTime(i)));   %Force array - Y1 - in (N)
     F4(i) = m2*e2*w^2*cos(w*SimTime(i))- KCY *
(dely/4)*(1+cos(2*w*SimTime(i)));   %Force array - Y2 - in (N)
     F7(i) = Iz1*e1/radius*w^2*sin(w*SimTime(i))+Iz1*-
((8*w^2*sin(2*SimTime(i)*w)*cos(dela)*(cos(dela) -
1))/(((cos(2*SimTime(i)*w)*(cos(dela) - 1))/(2*cos(dela)^2 + 2) -
1)^2*(2*cos(dela)^2 + 2)^2));
     F8(i) = Iz2*e2/radius*w^2*sin(w*SimTime(i))-Iz2*-
((8*w^2*sin(2*SimTime(i)*w)*cos(dela)*(cos(dela) -
1))/(((cos(2*SimTime(i)*w)*(cos(dela) - 1))/(2*cos(dela)^2 + 2) -
1)^2*(2*cos(dela)^2 + 2)^2));
end
```

Program_4_GoSimulation

```
 %% ======================================================================== %%
disp(' ')
disp('  >>     Execution of program_4 : Go Simulation ')

%% ======================================================================== %%

global Time
global X1 X2 Y1 Y2 Z1 Z2 THETA1 BETA1 ALPHA1 THETA2 BETA2 ALPHA2
global X1_dot X2_dot Y1_dot Y2_dot Z1_dot Z2_dot THETA1_dot BETA1_dot
ALPHA1_dot THETA2_dot BETA2_dot ALPHA2_dot
global X1_Ddot X2_Ddot Y1_Ddot Y2_Ddot Z1_Ddot Z2_Ddot THETA1_Ddot
BETA1_Ddot ALPHA1_Ddot THETA2_Ddot BETA2_Ddot ALPHA2_Ddot

global Displ_X1          Veloc_X1         Accel_X1
global Displ_X2          Veloc_X2         Accel_X2
global Displ_Y1          Veloc_Y1         Accel_Y1
global Displ_Y2          Veloc_Y2         Accel_Y2
global Displ_Z1          Veloc_Z1         Accel_Z1
global Displ_Z2          Veloc_Z2         Accel_Z2
global Displ_THETA1      Veloc_THETA1     Accel_THETA1
global Displ_THETA2      Veloc_THETA2     Accel_THETA2
global Displ_BETA1       Veloc_BETA1      Accel_BETA1
global Displ_BETA2       Veloc_BETA2      Accel_BETA2
global Displ_ALPHA1      Veloc_ALPHA1     Accel_ALPHA1
global Displ_ALPHA2      Veloc_ALPHA2     Accel_ALPHA2

%% ======================================================================== %%
%==                          Initial Conditions                           ==%
%==========================================================================%
X1_0          = 0;       %Create zero intial condition for displacement - X1
- in (m)
X2_0          = 0;       %Create zero intial condition for displacement - X2
- in (m)
Y1_0          = 0;       %Create zero intial condition for displacement - Y1
- in (m)
Y2_0          = 0;       %Create zero intial condition for displacement - Y2
- in (m)
Z1_0          = 0;       %Create zero intial condition for displacement - Z1
- in (m)
Z2_0          = 0;       %Create zero intial condition for displacement - Z2
- in (m)
THETA1_0      = 0;       %Create zero intial condition for angle - THETA1  -
in (rad)
THETA2_0      = 0;       %Create zero intial condition for angle - THETA2  -
in (rad)
BETA1_0       = 0;       %Create zero intial condition for angle - BETA1   -
in (rad)
BETA2_0       = 0;       %Create zero intial condition for angle - BETA2   -
in (rad)
ALPHA1_0      = 0;       %Create zero intial condition for angle - ALPHA1  -
in (rad)
ALPHA2_0      = 0;       %Create zero intial condition for angle - ALPHA2  -
in (rad)
X1_dot_0      = 0;       %Create zero intial condition for velocity - X1   -
in (m/s)
X2_dot_0      = 0;       %Create zero intial condition for velocity - X1   -
in (m/s)
```

```
Y1_dot_0     = 0;       %Create zero intial condition for velocity - X1   -
in (m/s)
Y2_dot_0     = 0;       %Create zero intial condition for velocity - X1   -
in (m/s)
Z1_dot_0     = 0;       %Create zero intial condition for velocity - X1   -
in (m/s)
Z2_dot_0     = 0;       %Create zero intial condition for velocity - X1   -
in (m/s)
THETA1_dot_0 = 0;       %Create zero intial condition for angular velocity -
THETA1 - in (rad/s)
THETA2_dot_0 = 0;       %Create zero intial condition for angular velocity -
THETA2 - in (rad/s)
BETA1_dot_0  = 0;       %Create zero intial condition for angular velocity -
BETA1  - in (rad/s)
BETA2_dot_0  = 0;       %Create zero intial condition for angular velocity -
BETA2  - in (rad/s)
ALPHA1_dot_0 = 0;       %Create zero intial condition for angular velocity -
ALPHA1 - in (rad/s)
ALPHA2_dot_0 = 0;       %Create zero intial condition for angular velocity -
ALPHA2 - in (rad/s)

%% ===================================================================== %%
%==               Starting of the For-Loop Calculation                  ==%
%=========================================================================%

h1 = waitbar(0,'Please wait...Calculation in Progress !');
for i = 1:NSimTimeSteps,

waitbar(i/NSimTimeSteps,h1)
%% ===================================================================== %%
%==                            Mass Matrix                              ==%
%=========================================================================%


          Mass(1,1)  = m1;
          Mass(1,2)  = 0;
          Mass(1,3)  = 0;
          Mass(1,4)  = 0;
          Mass(1,5)  = 0;
          Mass(1,6)  = 0;
          Mass(1,7)  = 0;
          Mass(1,8)  = 0;
          Mass(1,9)  = 0;
          Mass(1,10) = 0;
          Mass(1,11) = 0;
          Mass(1,12) = 0;

          Mass(2,1)  = 0;
          Mass(2,2)  = m2;
          Mass(2,3)  = 0;
          Mass(2,4)  = 0;
          Mass(2,5)  = 0;
          Mass(2,6)  = 0;
          Mass(2,7)  = 0;
          Mass(2,8)  = 0;
          Mass(2,9)  = 0;
          Mass(2,10) = 0;
          Mass(2,11) = 0;
          Mass(2,12) = 0;

          Mass(3,1)  = 0;
          Mass(3,2)  = 0;
          Mass(3,3)  = m1;
          Mass(3,4)  = 0;
          Mass(3,5)  = 0;
          Mass(3,6)  = 0;
```

```
Mass(3,7)  = 0;
Mass(3,8)  = 0;
Mass(3,9)  = 0;
Mass(3,10) = 0;
Mass(3,11) = 0;
Mass(3,12) = 0;

Mass(4,1)  = 0;
Mass(4,2)  = 0;
Mass(4,3)  = 0;
Mass(4,4)  = m2;
Mass(4,5)  = 0;
Mass(4,6)  = 0;
Mass(4,7)  = 0;
Mass(4,8)  = 0;
Mass(4,9)  = 0;
Mass(4,10) = 0;
Mass(4,11) = 0;
Mass(4,12) = 0;

Mass(5,1)  = 0;
Mass(5,2)  = 0;
Mass(5,3)  = 0;
Mass(5,4)  = 0;
Mass(5,5)  = m1;
Mass(5,6)  = 0;
Mass(5,7)  = 0;
Mass(5,8)  = 0;
Mass(5,9)  = 0;
Mass(5,10) = 0;
Mass(5,11) = 0;
Mass(5,12) = 0;

Mass(6,1)  = 0;
Mass(6,2)  = 0;
Mass(6,3)  = 0;
Mass(6,4)  = 0;
Mass(6,5)  = 0;
Mass(6,6)  = m2;
Mass(6,7)  = 0;
Mass(6,8)  = 0;
Mass(6,9)  = 0;
Mass(6,10) = 0;
Mass(6,11) = 0;
Mass(6,12) = 0;

Mass(7,1)  = 0;
Mass(7,2)  = 0;
Mass(7,3)  = 0;
Mass(7,4)  = 0;
Mass(7,5)  = 0;
Mass(7,6)  = 0;
Mass(7,7)  = Iz1;
Mass(7,8)  = 0;
Mass(7,9)  = 0;
Mass(7,10) = 0;
Mass(7,11) = 0;
Mass(7,12) = 0;

Mass(8,1)  = 0;
Mass(8,2)  = 0;
Mass(8,3)  = 0;
Mass(8,4)  = 0;
Mass(8,5)  = 0;
Mass(8,6)  = 0;
Mass(8,7)  = 0;
Mass(8,8)  = Iz2;
```

```
          Mass(8,9)  = 0;
          Mass(8,10) = 0;
          Mass(8,11) = 0;
          Mass(8,12) = 0;

          Mass(9,1)  = 0;
          Mass(9,2)  = 0;
          Mass(9,3)  = 0;
          Mass(9,4)  = 0;
          Mass(9,5)  = 0;
          Mass(9,6)  = 0;
          Mass(9,7)  = 0;
          Mass(9,8)  = 0;
          Mass(9,9)  = Ix1;
          Mass(9,10) = 0;
          Mass(9,11) = 0;
          Mass(9,12) = 0;

          Mass(10,1)  = 0;
          Mass(10,2)  = 0;
          Mass(10,3)  = 0;
          Mass(10,4)  = 0;
          Mass(10,5)  = 0;
          Mass(10,6)  = 0;
          Mass(10,7)  = 0;
          Mass(10,8)  = 0;
          Mass(10,9)  = 0;
          Mass(10,10) = Ix2;
          Mass(10,11) = 0;
          Mass(10,12) = 0;

          Mass(11,1)  = 0;
          Mass(11,2)  = 0;
          Mass(11,3)  = 0;
          Mass(11,4)  = 0;
          Mass(11,5)  = 0;
          Mass(11,6)  = 0;
          Mass(11,7)  = 0;
          Mass(11,8)  = 0;
          Mass(11,9)  = 0;
          Mass(11,10) = 0;
          Mass(11,11) = Iy1;
          Mass(11,12) = 0;

          Mass(12,1)  = 0;
          Mass(12,2)  = 0;
          Mass(12,3)  = 0;
          Mass(12,4)  = 0;
          Mass(12,5)  = 0;
          Mass(12,6)  = 0;
          Mass(12,7)  = 0;
          Mass(12,8)  = 0;
          Mass(12,9)  = 0;
          Mass(12,10) = 0;
          Mass(12,11) = 0;
          Mass(12,12) = Iy2;

     INVMM = inv(Mass);                                   %Creating mass
inverse matrix

%% ====================================================================== %%
%==                          Stiffness Matrix                            ==%
%=========================================================================%

          Stiff(1,1)  = KB1X + KCX + KS1X;
          Stiff(1,2)  = -KCX;
```

```
Stiff(1,3)  = 0;
Stiff(1,4)  = 0;
Stiff(1,5)  = 0;
Stiff(1,6)  = 0;
Stiff(1,7)  = 0;
Stiff(1,8)  = 0;
Stiff(1,9)  = 0;
Stiff(1,10) = 0;
Stiff(1,11) = 0;
Stiff(1,12) = 0;

Stiff(2,1)  = -KCX;
Stiff(2,2)  = KB2X + KCX + KS2X;
Stiff(2,3)  = 0;
Stiff(2,4)  = 0;
Stiff(2,5)  = 0;
Stiff(2,6)  = 0;
Stiff(2,7)  = 0;
Stiff(2,8)  = 0;
Stiff(2,9)  = 0;
Stiff(2,10) = 0;
Stiff(2,11) = 0;
Stiff(2,12) = 0;

Stiff(3,1)  = 0;
Stiff(3,2)  = 0;
Stiff(3,3)  = KB1Y + KCY + KS1Y;
Stiff(3,4)  = -KCY;
Stiff(3,5)  = 0;
Stiff(3,6)  = 0;
Stiff(3,7)  = 0;
Stiff(3,8)  = 0;
Stiff(3,9)  = 0;
Stiff(3,10) = 0;
Stiff(3,11) = 0;
Stiff(3,12) = 0;

Stiff(4,1)  = 0;
Stiff(4,2)  = 0;
Stiff(4,3)  = -KCY;
Stiff(4,4)  = KB2Y + KCY + KS2Y;
Stiff(4,5)  = 0;
Stiff(4,6)  = 0;
Stiff(4,7)  = 0;
Stiff(4,8)  = 0;
Stiff(4,9)  = 0;
Stiff(4,10) = 0;
Stiff(4,11) = 0;
Stiff(4,12) = 0;

Stiff(5,1)  = 0;
Stiff(5,2)  = 0;
Stiff(5,3)  = 0;
Stiff(5,4)  = 0;
Stiff(5,5)  = KCZ + KS1Z;
Stiff(5,6)  = -KCZ;
Stiff(5,7)  = 0;
Stiff(5,8)  = 0;
Stiff(5,9)  = 0;
Stiff(5,10) = 0;
Stiff(5,11) = 0;
Stiff(5,12) = 0;

Stiff(6,1)  = 0;
Stiff(6,2)  = 0;
Stiff(6,3)  = 0;
Stiff(6,4)  = 0;
```

```
Stiff(6,5)  = -KCZ;
Stiff(6,6)  = KCZ + KS2Z;
Stiff(6,7)  = 0;
Stiff(6,8)  = 0;
Stiff(6,9)  = 0;
Stiff(6,10) = 0;
Stiff(6,11) = 0;
Stiff(6,12) = 0;

Stiff(7,1)  = 0;
Stiff(7,2)  = 0;
Stiff(7,3)  = 0;
Stiff(7,4)  = 0;
Stiff(7,5)  = 0;
Stiff(7,6)  = 0;
Stiff(7,7)  = KCTZ + KS1T;
Stiff(7,8)  = -KCTZ;
Stiff(7,9)  = 0;
Stiff(7,10) = 0;
Stiff(7,11) = 0;
Stiff(7,12) = 0;

Stiff(8,1)  = 0;
Stiff(8,2)  = 0;
Stiff(8,3)  = 0;
Stiff(8,4)  = 0;
Stiff(8,5)  = 0;
Stiff(8,6)  = 0;
Stiff(8,7)  = -KCTZ;
Stiff(8,8)  = KCTZ + KS2T;
Stiff(8,9)  = 0;
Stiff(8,10) = 0;
Stiff(8,11) = 0;
Stiff(8,12) = 0;

Stiff(9,1)  = 0;
Stiff(9,2)  = 0;
Stiff(9,3)  = 0;
Stiff(9,4)  = 0;
Stiff(9,5)  = 0;
Stiff(9,6)  = 0;
Stiff(9,7)  = 0;
Stiff(9,8)  = 0;
Stiff(9,9)  = KCTX;
Stiff(9,10) = -KCTX;
Stiff(9,11) = 0;
Stiff(9,12) = 0;

Stiff(10,1)  = 0;
Stiff(10,2)  = 0;
Stiff(10,3)  = 0;
Stiff(10,4)  = 0;
Stiff(10,5)  = 0;
Stiff(10,6)  = 0;
Stiff(10,7)  = 0;
Stiff(10,8)  = 0;
Stiff(10,9)  = -KCTX;
Stiff(10,10) = KCTX;
Stiff(10,11) = 0;
Stiff(10,12) = 0;

Stiff(11,1)  = 0;
Stiff(11,2)  = 0;
Stiff(11,3)  = 0;
Stiff(11,4)  = 0;
Stiff(11,5)  = 0;
Stiff(11,6)  = 0;
```

```
            Stiff(11,7)  = 0;
            Stiff(11,8)  = 0;
            Stiff(11,9)  = 0;
            Stiff(11,10) = 0;
            Stiff(11,11) = KCTY;
            Stiff(11,12) = -KCTY;

            Stiff(12,1)  = 0;
            Stiff(12,2)  = 0;
            Stiff(12,3)  = 0;
            Stiff(12,4)  = 0;
            Stiff(12,5)  = 0;
            Stiff(12,6)  = 0;
            Stiff(12,7)  = 0;
            Stiff(12,8)  = 0;
            Stiff(12,9)  = 0;
            Stiff(12,10) = 0;
            Stiff(12,11) = -KCTY;
            Stiff(12,12) = KCTY;
%% ====================================================================== %%
%==                              Damping Matrix                          ==%
%=========================================================================%

            Damp(1,1)  = CB1X + CCX;
            Damp(1,2)  = -CCX;
            Damp(1,3)  = 0;
            Damp(1,4)  = 0;
            Damp(1,5)  = 0;
            Damp(1,6)  = 0;
            Damp(1,7)  = 0;
            Damp(1,8)  = 0;
            Damp(1,9)  = 0;
            Damp(1,10) = 0;
            Damp(1,11) = 0;
            Damp(1,12) = 0;

            Damp(2,1)  = -CCX;
            Damp(2,2)  = CB2X + CCX;
            Damp(2,3)  = 0;
            Damp(2,4)  = 0;
            Damp(2,5)  = 0;
            Damp(2,6)  = 0;
            Damp(2,7)  = 0;
            Damp(2,8)  = 0;
            Damp(2,9)  = 0;
            Damp(2,10) = 0;
            Damp(2,11) = 0;
            Damp(2,12) = 0;

            Damp(3,1)  = 0;
            Damp(3,2)  = 0;
            Damp(3,3)  = CB1Y + CCY;
            Damp(3,4)  = -CCY;
            Damp(3,5)  = 0;
            Damp(3,6)  = 0;
            Damp(3,7)  = 0;
            Damp(3,8)  = 0;
            Damp(3,9)  = 0;
            Damp(3,10) = 0;
            Damp(3,11) = 0;
            Damp(3,12) = 0;

            Damp(4,1)  = 0;
            Damp(4,2)  = 0;
            Damp(4,3)  = -CCY;
            Damp(4,4)  = CB2Y + CCY;
            Damp(4,5)  = 0;
```

```
Damp(4,6)  = 0;
Damp(4,7)  = 0;
Damp(4,8)  = 0;
Damp(4,9)  = 0;
Damp(4,10) = 0;
Damp(4,11) = 0;
Damp(4,12) = 0;

Damp(5,1)  = 0;
Damp(5,2)  = 0;
Damp(5,3)  = 0;
Damp(5,4)  = 0;
Damp(5,5)  = CCZ;
Damp(5,6)  = -CCZ;
Damp(5,7)  = 0;
Damp(5,8)  = 0;
Damp(5,9)  = 0;
Damp(5,10) = 0;
Damp(5,11) = 0;
Damp(5,12) = 0;

Damp(6,1)  = 0;
Damp(6,2)  = 0;
Damp(6,3)  = 0;
Damp(6,4)  = 0;
Damp(6,5)  = -CCZ;
Damp(6,6)  = CCZ;
Damp(6,7)  = 0;
Damp(6,8)  = 0;
Damp(6,9)  = 0;
Damp(6,10) = 0;
Damp(6,11) = 0;
Damp(6,12) = 0;

Damp(7,1)  = 0;
Damp(7,2)  = 0;
Damp(7,3)  = 0;
Damp(7,4)  = 0;
Damp(7,5)  = 0;
Damp(7,6)  = 0;
Damp(7,7)  = 0;
Damp(7,8)  = 0;
Damp(7,9)  = 0;
Damp(7,10) = 0;
Damp(7,11) = 0;
Damp(7,12) = 0;

Damp(8,1)  = 0;
Damp(8,2)  = 0;
Damp(8,3)  = 0;
Damp(8,4)  = 0;
Damp(8,5)  = 0;
Damp(8,6)  = 0;
Damp(8,7)  = 0;
Damp(8,8)  = 0;
Damp(8,9)  = 0;
Damp(8,10) = 0;
Damp(8,11) = 0;
Damp(8,12) = 0;

Damp(9,1)  = 0;
Damp(9,2)  = 0;
Damp(9,3)  = 0;
Damp(9,4)  = 0;
Damp(9,5)  = 0;
Damp(9,6)  = 0;
Damp(9,7)  = 0;
```

```
            Damp(9,8)  = 0;
            Damp(9,9)  = 0;
            Damp(9,10) = 0;
            Damp(9,11) = 0;
            Damp(9,12) = 0;

            Damp(10,1)  = 0;
            Damp(10,2)  = 0;
            Damp(10,3)  = 0;
            Damp(10,4)  = 0;
            Damp(10,5)  = 0;
            Damp(10,6)  = 0;
            Damp(10,7)  = 0;
            Damp(10,8)  = 0;
            Damp(10,9)  = 0;
            Damp(10,10) = 0;
            Damp(10,11) = 0;
            Damp(10,12) = 0;

            Damp(11,1)  = 0;
            Damp(11,2)  = 0;
            Damp(11,3)  = 0;
            Damp(11,4)  = 0;
            Damp(11,5)  = 0;
            Damp(11,6)  = 0;
            Damp(11,7)  = 0;
            Damp(11,8)  = 0;
            Damp(11,9)  = 0;
            Damp(11,10) = 0;
            Damp(11,11) = 0;
            Damp(11,12) = 0;

            Damp(12,1)  = 0;
            Damp(12,2)  = 0;
            Damp(12,3)  = 0;
            Damp(12,4)  = 0;
            Damp(12,5)  = 0;
            Damp(12,6)  = 0;
            Damp(12,7)  = 0;
            Damp(12,8)  = 0;
            Damp(12,9)  = 0;
            Damp(12,10) = 0;
            Damp(12,11) = 0;
            Damp(12,12) = 0;

%% ======================================================================== %%
%==                      Launching  SIMULATION                            ==%
%==========================================================================%


   %options = simset('MaxStep',DeltaSimTime/5);
   options = simset('MaxStep',1e-5);

 %================================================%
 %==              Force Matrix                  ==%
 %================================================%

   ST  = SimTime';                  %Transpose of time array to create
vector

   FF1  = F1';                      %Transpose of force in X1     array to
create vector in (N)
   FF2  = F2';                      %Transpose of force in X2     array to
create vector in (N)
   FF3  = F3';                      %Transpose of force in Y1     array to
create vector in (N)
```

```
   FF4  = F4';                        %Transpose of force in Y2     array to
create vector in (N)
   FF5  = F5';                        %Transpose of force in Z1     array to
create vector in (N)
   FF6  = F6';                        %Transpose of force in Z2     array to
create vector in (N)
   FF7  = F7';                        %Transpose of force in THETA1 array to
create vector in (N.m)
   FF8  = F8';                        %Transpose of force in THETA2 array to
create vector in (N.m)
   FF9  = F9';                        %Transpose of force in BETA1  array to
create vector in (N.m)
   FF10  = F10';                      %Transpose of force in BETA2  array to
create vector in (N.m)
   FF11  = F11';                      %Transpose of force in ALPHA1 array to
create vector in (N.m)
   FF12  = F12';                      %Transpose of force in ALPHA2 array to
create vector in (N.m)


TStartSim = SimTime(i);                %Setting simulation starting time
TFinalSim = TStartSim + DeltaSimTime;  %Setting simulation final    time


sim('Rotor_Coupling_Bearing_System_12DOF',[TStartSim TFinalSim],options);
%Starting simulation in Simulink

    %================== LOADING OF THE RESULTS  ==========================%

     load X_File.mat                                                 %Saving
displacement results in X.mat file
     load V_File.mat                                                 %Saving
Velocity     results in V.mat file
     load A_File.mat                                                 %Saving
Acceleration results in A.mat file

     Vect01 = X_Variable';
     Vect02 = V_Variable';
     Vect03 = A_Variable';

     Time  = Vect01(:,1);  %-------------------------% Time Vector
     Nmax  = length(Time); %-------------------------% length of the vector


     X1       = Vect01(:, 2); %--------> Displacements and Angles <-------%
     X2       = Vect01(:, 3);
     Y1       = Vect01(:, 4);
     Y2       = Vect01(:, 5);
     Z1       = Vect01(:, 6);
     Z2       = Vect01(:, 7);
     THETA1   = Vect01(:, 8);
     THETA2   = Vect01(:, 9);
     BETA1    = Vect01(:,10);
     BETA2    = Vect01(:,11);
     ALPHA1   = Vect01(:,12);
     ALPHA2   = Vect01(:,13);


     X1_dot      = Vect02(:, 2);  %-------------> Velocities <------------%
     X2_dot      = Vect02(:, 3);
     Y1_dot      = Vect02(:, 4);
     Y2_dot      = Vect02(:, 5);
     Z1_dot      = Vect02(:, 6);
     Z2_dot      = Vect02(:, 7);
     THETA1_dot  = Vect02(:, 8);
```

```
THETA2_dot  = Vect02(:, 9);
BETA1_dot   = Vect02(:,10);
BETA2_dot   = Vect02(:,11);
ALPHA1_dot  = Vect02(:,12);
ALPHA2_dot  = Vect02(:,13);


X1_Ddot       = Vect03(:, 2);   %----------> Accelerations <---------%
X2_Ddot       = Vect03(:, 3);
Y1_Ddot       = Vect03(:, 4);
Y2_Ddot       = Vect03(:, 5);
Z1_Ddot       = Vect03(:, 6);
Z2_Ddot       = Vect03(:, 7);
THETA1_Ddot   = Vect03(:, 8);
THETA2_Ddot   = Vect03(:, 9);
BETA1_Ddot    = Vect03(:,10);
BETA2_Ddot    = Vect03(:,11);
ALPHA1_Ddot   = Vect03(:,12);
ALPHA2_Ddot   = Vect03(:,13);

%======== Up-Dating of the initial conditions for next step =========%



X1_0            = X1(length(X1));
X1_dot_0        = X1_dot(length(X1_dot));

X2_0            = X2(length(X2));
X2_dot_0        = X2_dot(length(X2_dot));

Y1_0            = Y1(length(Y1));
Y1_dot_0        = Y1_dot(length(Y1_dot));

Y2_0            = Y2(length(Y2));
Y2_dot_0        = Y2_dot(length(Y2_dot));

Z1_0            = Z1(length(Z1));
Z1_dot_0        = Z1_dot(length(Z1_dot));

Z2_0            = Z2(length(Z2));
Z2_dot_0        = Z2_dot(length(Z2_dot));

THETA1_0        = THETA1(length(THETA1));
THETA1_dot_0    = THETA1_dot(length(THETA1_dot));

THETA2_0        = THETA2(length(THETA2));
THETA2_dot_0    = THETA2_dot(length(THETA2_dot));

BETA1_0         = BETA1(length(BETA1));
BETA1_dot_0     = BETA1_dot(length(BETA1_dot));

BETA2_0         = BETA2(length(BETA2));
BETA2_dot_0     = BETA2_dot(length(BETA2_dot));

ALPHA1_0        = ALPHA1(length(ALPHA1));
ALPHA1_dot_0    = ALPHA1_dot(length(ALPHA1_dot));

ALPHA2_0        = ALPHA2(length(ALPHA2));
ALPHA2_dot_0    = ALPHA2_dot(length(ALPHA2_dot));

%======== Building of the Data Output Arrays =========%

Displ_X1(i)     = X1(length(X1));
Veloc_X1(i)     = X1_dot(length(X1_Ddot));
```

```
    Accel_X1(i)     = X1_Ddot(length(X1_Ddot));

    Displ_X2(i)     = X2(length(X2));
    Veloc_X2(i)     = X2_dot(length(X2_dot));
    Accel_X2(i)     = X2_Ddot(length(X2_Ddot));

    Displ_Y1(i)     = Y1(length(Y1));
    Veloc_Y1(i)     = Y1_dot(length(Y1_dot));
    Accel_Y1(i)     = Y1_Ddot(length(Y1_Ddot));

    Displ_Y2(i)     = Y2(length(Y2));
    Veloc_Y2(i)     = Y2_dot(length(Y2_dot));
    Accel_Y2(i)     = Y2_Ddot(length(Y2_Ddot));

    Displ_Z1(i)     = Z1(length(Z1));
    Veloc_Z1(i)     = Z1_dot(length(Z1_dot));
    Accel_Z1(i)     = Z1_Ddot(length(Z1_Ddot));

    Displ_Z2(i)     = Z2(length(Z2));
    Veloc_Z2(i)     = Z2_dot(length(Z2_dot));
    Accel_Z2(i)     = Z2_Ddot(length(Z2_Ddot));

    Displ_THETA1(i)    = THETA1(length(THETA1));
    Veloc_THETA1(i)    = THETA1_dot(length(THETA1_dot));
    Accel_THETA1(i)    = THETA1_Ddot(length(THETA1_Ddot));

    Displ_THETA2(i)    = THETA2(length(THETA2));
    Veloc_THETA2(i)    = THETA2_dot(length(THETA2_dot));
    Accel_THETA2(i)    = THETA2_Ddot(length(THETA2_Ddot));

    Displ_BETA1(i)    = BETA1(length(BETA1));
    Veloc_BETA1(i)    = BETA1_dot(length(BETA1_dot));
    Accel_BETA1(i)    = BETA1_Ddot(length(BETA1_Ddot));

    Displ_BETA2(i)    = BETA2(length(BETA2));
    Veloc_BETA2(i)    = BETA2_dot(length(BETA2_dot));
    Accel_BETA2(i)    = BETA2_Ddot(length(BETA2_Ddot));

    Displ_ALPHA1(i)    = ALPHA1(length(ALPHA1));
    Veloc_ALPHA1(i)    = ALPHA1_dot(length(ALPHA1_dot));
    Accel_ALPHA1(i)    = ALPHA1_Ddot(length(ALPHA1_Ddot));

    Displ_ALPHA2(i)    = ALPHA2(length(ALPHA2));
    Veloc_ALPHA2(i)    = ALPHA2_dot(length(ALPHA2_dot));
    Accel_ALPHA2(i)    = ALPHA2_Ddot(length(ALPHA2_Ddot));

 end
close(h1)
```

Program_5_FastFourierTransform

```
%% ====================================================================== %%
disp(' ')
disp('  >>     Execution of program_5 : Fast Fourier Transform')

%% ====================================================================== %%
global f
global P1X1 P1X2 P1Y1 P1Y2 P1Z1 P1Z2 P1THETA1 P1BETA1 P1ALPHA1 P1THETA2
P1BETA2 P1ALPHA2
global P1X1_dot P1X2_dot P1Y1_dot P1Y2_dot P1Z1_dot P1Z2_dot P1THETA1_dot
P1BETA1_dot P1ALPHA1_dot P1THETA2_dot P1BETA2_dot P1ALPHA2_dot
global P1X1_Ddot P1X2_Ddot P1Y1_Ddot P1Y2_Ddot P1Z1_Ddot P1Z2_Ddot
P1THETA1_Ddot P1BETA1_Ddot P1ALPHA1_Ddot P1THETA2_Ddot P1BETA2_Ddot
P1ALPHA2_Ddot

%% ====================================================================== %%

Fs = 1/DeltaSimTime;        % Sampling frequency in (Hz)
t = SimTime;                % Time vector        in ( s)
L = length(t);              % Signal length
f = Fs*(0:(L/2))/L;         % Frequency rang    (x-axis)

%FFT for Displacement

FX1 = fft(Displ_X1);                                %FFT for Displacement
in X1 direction
P2X1 = abs(FX1/L);                                  %Taking absolute value
of the FFT /length
P1X1 = P2X1(1:L/2+1);                               %Considering half  the
frequency spectrum
P1X1(2:end-1) = 2*P1X1(2:end-1);                    %Magnifying   amplitude
to original value in (m)

FX2 = fft(Displ_X2);                                %FFT for Displacement
in X2 direction
P2X2 = abs(FX2/L);                                  %Taking absolute value
of the FFT /length
P1X2 = P2X2(1:L/2+1);                               %Considering half  the
frequency spectrum
P1X2(2:end-1) = 2*P1X2(2:end-1);                    %Magnifying   amplitude
to original value in (m)

FY1 = fft(Displ_Y1);                                %FFT for Displacement
in Y1 direction
P2Y1 = abs(FY1/L);                                  %Taking absolute value
of the FFT /length
P1Y1 = P2Y1(1:L/2+1);                               %Considering half  the
frequency spectrum
P1Y1(2:end-1) = 2*P1Y1(2:end-1);                    %Magnifying   amplitude
to original value in (m)

FY2 = fft(Displ_Y2);                                %FFT for Displacement
in Y2 direction
P2Y2 = abs(FY2/L);                                  %Taking absolute value
of the FFT /length
P1Y2 = P2Y2(1:L/2+1);                               %Considering half  the
frequency spectrum
P1Y2(2:end-1) = 2*P1Y2(2:end-1);                    %Magnifying   amplitude
to original value in (m)
```

```
FZ1 = fft(Displ_Z1);                                %FFT for Displacement
in Z1 direction
P2Z1 = abs(FZ1/L);                                  %Taking absolute value
of the FFT /length
P1Z1 = P2Z1(1:L/2+1);                               %Considering half  the
frequency spectrum
P1Z1(2:end-1) = 2*P1Z1(2:end-1);                    %Magnifying   amplitude
to original value in (m)

FZ2 = fft(Displ_Z2);                                %FFT for Displacement
in Z2 direction
P2Z2 = abs(FZ2/L);                                  %Taking absolute value
of the FFT /length
P1Z2 = P2Z2(1:L/2+1);                               %Considering half  the
frequency spectrum
P1Z2(2:end-1) = 2*P1Z2(2:end-1);                    %Magnifying   amplitude
to original value in (m)

FTHETA1 = fft(Displ_THETA1*180/pi);                 %FFT for Displacement in
THETA1 direction
P2THETA1 = abs(FTHETA1/L);                          %Taking absolute value
of the FFT /length
P1THETA1 = P2THETA1(1:L/2+1);                       %Considering half  the
frequency spectrum
P1THETA1(2:end-1) = 2*P1THETA1(2:end-1);            %Magnifying   amplitude
to original value in (degrees)

FTHETA2 = fft(Displ_THETA2*180/pi);                 %FFT for Displacement in
THETA2 direction
P2THETA2 = abs(FTHETA2/L);                          %Taking absolute value
of the FFT /length
P1THETA2 = P2THETA2(1:L/2+1);                       %Considering half  the
frequency spectrum
P1THETA2(2:end-1) = 2*P1THETA2(2:end-1);            %Magnifying   amplitude
to original value in (degrees)

FBETA1 = fft(Displ_BETA1*180/pi);                   %FFT for Displacement in
BETA1  direction
P2BETA1 = abs(FBETA1/L);                            %Taking absolute value
of the FFT /length
P1BETA1 = P2BETA1(1:L/2+1);                         %Considering half  the
frequency spectrum
P1BETA1(2:end-1) = 2*P1BETA1(2:end-1);              %Magnifying   amplitude
to original value in (degrees)

FBETA2 = fft(Displ_BETA2*180/pi);                   %FFT for Displacement in
BETA2  direction
P2BETA2 = abs(FBETA2/L);                            %Taking absolute value
of the FFT /length
P1BETA2 = P2BETA2(1:L/2+1);                         %Considering half  the
frequency spectrum
P1BETA2(2:end-1) = 2*P1BETA2(2:end-1);              %Magnifying   amplitude
to original value in (degrees)

FALPHA1 = fft(Displ_ALPHA1*180/pi);                 %FFT for Displacement in
ALPHA1 direction
P2ALPHA1 = abs(FALPHA1/L);                          %Taking absolute value
of the FFT /length
P1ALPHA1 = P2ALPHA1(1:L/2+1);                       %Considering half  the
frequency spectrum
P1ALPHA1(2:end-1) = 2*P1ALPHA1(2:end-1);            %Magnifying   amplitude
to original value in (degrees)

FALPHA2 = fft(Displ_ALPHA2*180/pi);                 %FFT for Displacement in
ALPHA2 direction
```

```
P2ALPHA2 = abs(FALPHA2/L);                          %Taking absolute value
of the FFT /length
P1ALPHA2 = P2ALPHA2(1:L/2+1);                       %Considering half  the
frequency spectrum
P1ALPHA2(2:end-1) = 2*P1ALPHA2(2:end-1);            %Magnifying   amplitude
to original value in (degrees)

% FFT for Velocity

FX1_dot = fft(Veloc_X1);                            %FFT for Velocity
in X1 direction
P2X1_dot = abs(FX1_dot/L);                          %Taking absolute value
of the FFT /length
P1X1_dot = P2X1_dot(1:L/2+1);                       %Considering half  the
frequency spectrum
P1X1_dot(2:end-1) = 2*P1X1_dot(2:end-1);            %Magnifying   amplitude
to original value in (m/s)

FX2_dot = fft(Veloc_X2);                            %FFT for Velocity
in X2 direction
P2X2_dot = abs(FX2_dot/L);                          %Taking absolute value
of the FFT /length
P1X2_dot = P2X2_dot(1:L/2+1);                       %Considering half  the
frequency spectrum
P1X2_dot(2:end-1) = 2*P1X2_dot(2:end-1);            %Magnifying   amplitude
to original value in (m/s)

FY1_dot = fft(Veloc_Y1);                            %FFT for Velocity
in Y1 direction
P2Y1_dot = abs(FY1_dot/L);                          %Taking absolute value
of the FFT /length
P1Y1_dot = P2Y1_dot(1:L/2+1);                       %Considering half  the
frequency spectrum
P1Y1_dot(2:end-1) = 2*P1Y1_dot(2:end-1);            %Magnifying   amplitude
to original value in (m/s)

FY2_dot = fft(Veloc_Y2);                            %FFT for Velocity
in Y2 direction
P2Y2_dot = abs(FY2_dot/L);                          %Taking absolute value
of the FFT /length
P1Y2_dot = P2Y2_dot(1:L/2+1);                       %Considering half  the
frequency spectrum
P1Y2_dot(2:end-1) = 2*P1Y2_dot(2:end-1);            %Magnifying   amplitude
to original value in (m/s)

FZ1_dot = fft(Veloc_Z1);                            %FFT for Velocity
in Z1 direction
P2Z1_dot = abs(FZ1_dot/L);                          %Taking absolute value
of the FFT /length
P1Z1_dot = P2Z1_dot(1:L/2+1);                       %Considering half  the
frequency spectrum
P1Z1_dot(2:end-1) = 2*P1Z1_dot(2:end-1);            %Magnifying   amplitude
to original value in (m/s)

FZ2_dot = fft(Veloc_Z2);                            %FFT for Velocity
in Z2 direction
P2Z2_dot = abs(FZ2_dot/L);                          %Taking absolute value
of the FFT /length
P1Z2_dot = P2Z2_dot(1:L/2+1);                       %Considering half  the
frequency spectrum
P1Z2_dot(2:end-1) = 2*P1Z2_dot(2:end-1);            %Magnifying   amplitude
to original value in (m/s)

FTHETA1_dot = fft(Veloc_THETA1*180/pi);             %FFT for Velocity     in
THETA1 direction
```

```
P2THETA1_dot = abs(FTHETA1_dot/L);                  %Taking absolute value
of the FFT /length
P1THETA1_dot = P2THETA1_dot(1:L/2+1);               %Considering half  the
frequency spectrum
P1THETA1_dot(2:end-1) = 2*P1THETA1_dot(2:end-1);    %Magnifying   amplitude
to original value in (degree/s)

FTHETA2_dot = fft(Veloc_THETA2*180/pi);             %FFT for Velocity     in
THETA2 direction
P2THETA2_dot = abs(FTHETA2_dot/L);                  %Taking absolute value
of the FFT /length
P1THETA2_dot = P2THETA2_dot(1:L/2+1);               %Considering half  the
frequency spectrum
P1THETA2_dot(2:end-1) = 2*P1THETA2_dot(2:end-1);    %Magnifying   amplitude
to original value in (degree/s)

FBETA1_dot = fft(Veloc_BETA1*180/pi);               %FFT for Velocity     in
BETA1  direction
P2BETA1_dot = abs(FBETA1_dot/L);                    %Taking absolute value
of the FFT /length
P1BETA1_dot = P2BETA1_dot(1:L/2+1);                 %Considering half  the
frequency spectrum
P1BETA1_dot(2:end-1) = 2*P1BETA1_dot(2:end-1);      %Magnifying   amplitude
to original value in (degree/s)

FBETA2_dot = fft(Veloc_BETA2*180/pi);               %FFT for Velocity     in
BETA2  direction
P2BETA2_dot = abs(FBETA2_dot/L);                    %Taking absolute value
of the FFT /length
P1BETA2_dot = P2BETA2_dot(1:L/2+1);                 %Considering half  the
frequency spectrum
P1BETA2_dot(2:end-1) = 2*P1BETA2_dot(2:end-1);      %Magnifying   amplitude
to original value in (degree/s)

FALPHA1_dot = fft(Veloc_ALPHA1*180/pi);             %FFT for Velocity     in
ALPHA1 direction
P2ALPHA1_dot = abs(FALPHA1_dot/L);                  %Taking absolute value
of the FFT /length
P1ALPHA1_dot = P2ALPHA1_dot(1:L/2+1);               %Considering half  the
frequency spectrum
P1ALPHA1_dot(2:end-1) = 2*P1ALPHA1_dot(2:end-1);    %Magnifying   amplitude
to original value in (degree/s)

FALPHA2_dot = fft(Veloc_ALPHA2*180/pi);              %FFT for Velocity
in ALPHA2 direction
P2ALPHA2_dot = abs(FALPHA2_dot/L);                  %Taking absolute value
of the FFT /length
P1ALPHA2_dot = P2ALPHA2_dot(1:L/2+1);               %Considering half  the
frequency spectrum
P1ALPHA2_dot(2:end-1) = 2*P1ALPHA2_dot(2:end-1);    %Magnifying   amplitude
to original value in (degree/s)


%FFT for Acceleration

FX1_Ddot = fft(Accel_X1);                           %FFT for Acceleration
in X1 direction
P2X1_Ddot = abs(FX1_Ddot/L);                        %Taking absolute value
of the FFT /length
P1X1_Ddot = P2X1_Ddot(1:L/2+1);                     %Considering half  the
frequency spectrum
P1X1_Ddot(2:end-1) = 2*P1X1_Ddot(2:end-1);          %Magnifying   amplitude
to original value in (m/s2)

FX2_Ddot = fft(Accel_X2);                           %FFT for Acceleration
in X2 direction
```

```
P2X2_Ddot = abs(FX2_Ddot/L);                          %Taking absolute value
of the FFT /length
P1X2_Ddot = P2X2_Ddot(1:L/2+1);                       %Considering half  the
frequency spectrum
P1X2_Ddot(2:end-1) = 2*P1X2_Ddot(2:end-1);            %Magnifying   amplitude
to original value in (m/s2)

FY1_Ddot = fft(Accel_Y1);                             %FFT for Acceleration
in Y1 direction
P2Y1_Ddot = abs(FY1_Ddot/L);                          %Taking absolute value
of the FFT /length
P1Y1_Ddot = P2Y1_Ddot(1:L/2+1);                       %Considering half  the
frequency spectrum in (m/s2)
P1Y1_Ddot(2:end-1) = 2*P1Y1_Ddot(2:end-1);            %Magnifying   amplitude
to original value

FY2_Ddot = fft(Accel_Y2);                             %FFT for Acceleration
in Y2 direction
P2Y2_Ddot = abs(FY2_Ddot/L);                          %Taking absolute value
of the FFT /length
P1Y2_Ddot = P2Y2_Ddot(1:L/2+1);                       %Considering half  the
frequency spectrum
P1Y2_Ddot(2:end-1) = 2*P1Y2_Ddot(2:end-1);            %Magnifying   amplitude
to original value in (m/s2)

FZ1_Ddot = fft(Accel_Z1);                             %FFT for Acceleration
in Z1 direction
P2Z1_Ddot = abs(FZ1_Ddot/L);                          %Taking absolute value
of the FFT /length
P1Z1_Ddot = P2Z1_Ddot(1:L/2+1);                       %Considering half  the
frequency spectrum
P1Z1_Ddot(2:end-1) = 2*P1Z1_Ddot(2:end-1);            %Magnifying   amplitude
to original value in (m/s2)

FZ2_Ddot = fft(Accel_Z2);                             %FFT for Acceleration
in Z2 direction
P2Z2_Ddot = abs(FZ2_Ddot/L);                          %Taking absolute value
of the FFT /length
P1Z2_Ddot = P2Z2_Ddot(1:L/2+1);                       %Considering half  the
frequency spectrum
P1Z2_Ddot(2:end-1) = 2*P1Z2_Ddot(2:end-1);            %Magnifying   amplitude
to original value in (m/s2)

FTHETA1_Ddot = fft(Accel_THETA1*180/pi);              %FFT for Acceleration in
THETA1 direction
P2THETA1_Ddot = abs(FTHETA1_Ddot/L);                  %Taking absolute value
of the FFT /length
P1THETA1_Ddot = P2THETA1_Ddot(1:L/2+1);               %Considering half  the
frequency spectrum
P1THETA1_Ddot(2:end-1) = 2*P1THETA1_Ddot(2:end-1);    %Magnifying   amplitude
to original value in (degree/s2)

FTHETA2_Ddot = fft(Accel_THETA2*180/pi);              %FFT for Acceleration in
THETA2 direction
P2THETA2_Ddot = abs(FTHETA2_Ddot/L);                  %Taking absolute value
of the FFT /length
P1THETA2_Ddot = P2THETA2_Ddot(1:L/2+1);               %Considering half  the
frequency spectrum
P1THETA2_Ddot(2:end-1) = 2*P1THETA2_Ddot(2:end-1);    %Magnifying   amplitude
to original value in (degree/s2)

FBETA1_Ddot = fft(Accel_BETA1*180/pi);                %FFT for Acceleration in
BETA1  direction
P2BETA1_Ddot = abs(FBETA1_Ddot/L);                    %Taking absolute value
of the FFT /length
```

```
P1BETA1_Ddot = P2BETA1_Ddot(1:L/2+1);                %Considering half  the
frequency spectrum
P1BETA1_Ddot(2:end-1) = 2*P1BETA1_Ddot(2:end-1);     %Magnifying   amplitude
to original value in (degree/s2)

FBETA2_Ddot = fft(Accel_BETA2*180/pi);               %FFT for Acceleration in
BETA2  direction
P2BETA2_Ddot = abs(FBETA2_Ddot/L);                   %Taking absolute value
of the FFT /length
P1BETA2_Ddot = P2BETA2_Ddot(1:L/2+1);                %Considering half  the
frequency spectrum
P1BETA2_Ddot(2:end-1) = 2*P1BETA2_Ddot(2:end-1);     %Magnifying   amplitude
to original value in (degree/s2)

FALPHA1_Ddot = fft(Accel_ALPHA1*180/pi);             %FFT for Acceleration in
ALPHA1 direction
P2ALPHA1_Ddot = abs(FALPHA1_Ddot/L);                 %Taking absolute value
of the FFT /length
P1ALPHA1_Ddot = P2ALPHA1_Ddot(1:L/2+1);              %Considering half  the
frequency spectrum
P1ALPHA1_Ddot(2:end-1) = 2*P1ALPHA1_Ddot(2:end-1);   %Magnifying   amplitude
to original value in (degree/s2)

FALPHA2_Ddot = fft(Accel_ALPHA2*180/pi);             %FFT for Acceleration in
ALPHA2 direction
P2ALPHA2_Ddot = abs(FALPHA2_Ddot/L);                 %Taking absolute value
of the FFT /length
P1ALPHA2_Ddot = P2ALPHA2_Ddot(1:L/2+1);              %Considering half  the
frequency spectrum
P1ALPHA2_Ddot(2:end-1) = 2*P1ALPHA2_Ddot(2:end-1);   %Magnifying   amplitude
to original value in (degree/s2)
```

Program_6_NaturalFrequency

```
%% ===================================================================== %%
disp(' ')
disp('  >>     Execution of program_6 : Go Simulation')

%% ===================================================================== %%
global FreqX1 FreqX2 FreqY1 FreqY2 FreqZ1 FreqZ2
global FreqTHETA1 FreqTHETA2 FreqBETA1 FreqBETA2 FreqALPHA1 FreqALPHA2

%% ===================================================================== %%

FreqX1          = 1/(2*pi)*sqrt(Stiff(1,1)/Mass(1,1));       %Natural
Frequency     of X1 in (Hz)
FreqX2          = 1/(2*pi)*sqrt(Stiff(2,2)/Mass(2,2));       %Natural
Frequency     of X2 in (Hz)
FreqY1          = 1/(2*pi)*sqrt(Stiff(3,3)/Mass(3,3));       %Natural
Frequency     of Y1 in (Hz)
FreqY2          = 1/(2*pi)*sqrt(Stiff(4,4)/Mass(4,4));       %Natural
Frequency     of Y2 in (Hz)
FreqZ1          = 1/(2*pi)*sqrt(Stiff(5,5)/Mass(5,5));       %Natural
Frequency     of Z1 in (Hz)
FreqZ2          = 1/(2*pi)*sqrt(Stiff(6,6)/Mass(6,6));       %Natural
Frequency     of Z2 in (Hz)
FreqTHETA1      = 1/(2*pi)*sqrt(Stiff(7,7)/Mass(7,7));       %Natural
Frequency of THETA1 in (Hz)
FreqTHETA2      = 1/(2*pi)*sqrt(Stiff(8,8)/Mass(8,8));       %Natural
Frequency of THETA2 in (Hz)
FreqBETA1       = 1/(2*pi)*sqrt(Stiff(9,9)/Mass(9,9));       %Natural
Frequency  of BETA1 in (Hz)
```

```
FreqBETA2  = 1/(2*pi)*sqrt(Stiff(10,10)/Mass(10,10));       %Natural
Frequency  of BETA2 in (Hz)
FreqALPHA1 = 1/(2*pi)*sqrt(Stiff(11,11)/Mass(11,11));       %Natural
Frequency of ALPHA1 in (Hz)
FreqALPHA2 = 1/(2*pi)*sqrt(Stiff(12,12)/Mass(12,12));       %Natural
Frequency of ALPHA2 in (Hz)
```

Program_7_PlotGraphs

```
%% ====================================================================
%%
disp(' ')
disp('  >>     Execution of program_ 7 : Plot Graphs')

%%
=====================================================================
%%
%==                          GRAPHICS  Printing
==%
%=====================================================================
=====%


     figure(1)
     subplot(6,2,1), plot(SimTime,Displ_X1,'r','LineWidth',1)
     xlabel('Time [ Seconds
]','FontName','Arial','Fontsize',10,'FontWeight','Bold')
     ylabel('Displacement [ m
]','FontName','Arial','Fontsize',5,'FontWeight','Bold')
     title('Displacement Time Response of X1')

     subplot(6,2,3), plot(SimTime,Displ_X2,'r','LineWidth',1)
     xlabel('Time [ Seconds
]','FontName','Arial','Fontsize',10,'FontWeight','Bold')
     ylabel('Displacement [ m
]','FontName','Arial','Fontsize',5,'FontWeight','Bold')
     title('Displacement Time Response of X2')

     subplot(6,2,5), plot(SimTime,Displ_Y1,'r','LineWidth',1)
     xlabel('Time [ Seconds
]','FontName','Arial','Fontsize',10,'FontWeight','Bold')
     ylabel('Displacement [ m
]','FontName','Arial','Fontsize',5,'FontWeight','Bold')
     title('Displacement Time Response of Y1')

     subplot(6,2,7),plot(SimTime,Displ_Y2,'r','LineWidth',1)
     xlabel('Time [ Seconds
]','FontName','Arial','Fontsize',10,'FontWeight','Bold')
     ylabel('Displacement [ m
]','FontName','Arial','Fontsize',5,'FontWeight','Bold')
     title('Displacement Time Response of Y2')

     subplot(6,2,9),plot(SimTime,Displ_Z1,'r','LineWidth',1)
     xlabel('Time [ Seconds
]','FontName','Arial','Fontsize',10,'FontWeight','Bold')
     ylabel('Displacement [ m
]','FontName','Arial','Fontsize',5,'FontWeight','Bold')
     title('Displacement Time Response of Z1')

     subplot(6,2,11),plot(SimTime,Displ_Z2,'r','LineWidth',1)
     xlabel('Time [ Seconds
]','FontName','Arial','Fontsize',10,'FontWeight','Bold')
     ylabel('Displacement [ m
]','FontName','Arial','Fontsize',5,'FontWeight','Bold')
     title('Displacement Time Response of Z2')
```

```
     subplot(6,2,2), plot(f,P1X1,'r','LineWidth',1)
     xlabel('Frequency [ Hz
]','FontName','Arial','Fontsize',10,'FontWeight','Bold')
     ylabel('Displacement [ m
]','FontName','Arial','Fontsize',5,'FontWeight','Bold')
     title('Frequency Response of X1')

     subplot(6,2,4), plot(f,P1X2,'r','LineWidth',1)
     xlabel('Frequency [ Hz
]','FontName','Arial','Fontsize',10,'FontWeight','Bold')
     ylabel('Displacement [ m
]','FontName','Arial','Fontsize',5,'FontWeight','Bold')
     title('Frequency Response of X2')

     subplot(6,2,6), plot(f,P1Y1,'r','LineWidth',1)
     xlabel('Frequency [ Hz
]','FontName','Arial','Fontsize',10,'FontWeight','Bold')
     ylabel('Displacement [ m
]','FontName','Arial','Fontsize',5,'FontWeight','Bold')
     title('Frequency Response of Y1')

     subplot(6,2,8), plot(f,P1Y2,'r','LineWidth',1)
     xlabel('Frequency [ Hz
]','FontName','Arial','Fontsize',10,'FontWeight','Bold')
     ylabel('Displacement [ m
]','FontName','Arial','Fontsize',5,'FontWeight','Bold')
     title('Frequency Response of Y2')


     subplot(6,2,10),plot(f,P1Z1,'r','LineWidth',1)
     xlabel('Frequency [ Hz
]','FontName','Arial','Fontsize',10,'FontWeight','Bold')
     ylabel('Displacement [ m
]','FontName','Arial','Fontsize',5,'FontWeight','Bold')
     title('Frequency Response of Z1')

     subplot(6,2,12),plot(f,P1Z2,'r','LineWidth',1)
     xlabel('Frequency [ Hz
]','FontName','Arial','Fontsize',10,'FontWeight','Bold')
     ylabel('Displacement [ m
]','FontName','Arial','Fontsize',5,'FontWeight','Bold')
     title('Frequency Response of Z2')



     figure(2)
     subplot(6,2,1),plot(SimTime,Displ_THETA1*180/pi,'r','LineWidth',1)
     xlabel('Time [ Seconds
]','FontName','Arial','Fontsize',10,'FontWeight','Bold')
     ylabel('Angle [ degrees
]','FontName','Arial','Fontsize',5,'FontWeight','Bold')
     title('Displacement Time Response of THETA1')

     subplot(6,2,3),plot(SimTime,Displ_THETA2*180/pi,'r','LineWidth',1)
     xlabel('Time [ Seconds
]','FontName','Arial','Fontsize',10,'FontWeight','Bold')
     ylabel('Angle [ degrees
]','FontName','Arial','Fontsize',5,'FontWeight','Bold')
     title('Displacement Time Response of THETA2')

     subplot(6,2,5),plot(SimTime,Displ_BETA1*180/pi,'r','LineWidth',1)
     xlabel('Time [ Seconds
]','FontName','Arial','Fontsize',10,'FontWeight','Bold')
```

```
     ylabel('Angle [ degrees
]','FontName','Arial','Fontsize',5,'FontWeight','Bold')
     title('Displacement Time Response of BETA1')

     subplot(6,2,7),plot(SimTime,Displ_BETA2*180/pi,'r','LineWidth',1)
     xlabel('Time [ Seconds
]','FontName','Arial','Fontsize',10,'FontWeight','Bold')
     ylabel('Angle [ degrees
]','FontName','Arial','Fontsize',5,'FontWeight','Bold')
     title('Displacement Time Response of BETA2')

     subplot(6,2,9),plot(SimTime,Displ_ALPHA1*180/pi,'r','LineWidth',1)
     xlabel('Time [ Seconds
]','FontName','Arial','Fontsize',10,'FontWeight','Bold')
     ylabel('Angle [ degrees
]','FontName','Arial','Fontsize',5,'FontWeight','Bold')
     title('Displacement Time Response of ALPHA1')

     subplot(6,2,11),plot(SimTime,Displ_ALPHA2*180/pi,'r','LineWidth',1)
     xlabel('Time [ Seconds
]','FontName','Arial','Fontsize',10,'FontWeight','Bold')
     ylabel('Angle [ degrees
]','FontName','Arial','Fontsize',5,'FontWeight','Bold')
     title('Displacement Time Response of ALPHA2')

     subplot(6,2,2),plot(f,P1THETA1,'r','LineWidth',1)
     xlabel('Frequency [ Hz
]','FontName','Arial','Fontsize',10,'FontWeight','Bold')
     ylabel('Angle [ degrees
]','FontName','Arial','Fontsize',5,'FontWeight','Bold')
     title('Frequency Response of THETA1')

     subplot(6,2,4),plot(f,P1THETA2,'r','LineWidth',1)
     xlabel('Frequency [ Hz
]','FontName','Arial','Fontsize',10,'FontWeight','Bold')
     ylabel('Angle [ degrees
]','FontName','Arial','Fontsize',5,'FontWeight','Bold')
     title('Frequency Response of THETA2')

     subplot(6,2,6),plot(f,P1BETA1,'r','LineWidth',1)
     xlabel('Frequency [ Hz
]','FontName','Arial','Fontsize',10,'FontWeight','Bold')
     ylabel('Angle [ degrees
]','FontName','Arial','Fontsize',5,'FontWeight','Bold')
     title('Frequency Response of BETA1')

     subplot(6,2,8),plot(f,P1BETA2,'r','LineWidth',1)
     xlabel('Frequency [ Hz
]','FontName','Arial','Fontsize',10,'FontWeight','Bold')
     ylabel('Angle [ degrees
]','FontName','Arial','Fontsize',5,'FontWeight','Bold')
     title('Frequency Response of BETA2')

     subplot(6,2,10),plot(f,P1ALPHA1,'r','LineWidth',1)
     xlabel('Frequency [ Hz
]','FontName','Arial','Fontsize',10,'FontWeight','Bold')
     ylabel('Angle [ degrees
]','FontName','Arial','Fontsize',5,'FontWeight','Bold')
     title('Frequency Response of ALPHA1')

     subplot(6,2,12),plot(f,P1ALPHA2,'r','LineWidth',1)
     xlabel('Frequency [ Hz
]','FontName','Arial','Fontsize',10,'FontWeight','Bold')
     ylabel('Angle [ degrees
]','FontName','Arial','Fontsize',5,'FontWeight','Bold')
     title('Frequency Response of ALPHA2')
```

```
     figure(3)
     subplot(6,2,1),plot(SimTime,Veloc_X1*180/pi,'r','LineWidth',1)
     xlabel('Time [ Seconds
]','FontName','Arial','Fontsize',10,'FontWeight','Bold')
     ylabel('Velocity [ m/s
]','FontName','Arial','Fontsize',5,'FontWeight','Bold')
     title('Velocity Time Response of X1')

     subplot(6,2,3), plot(SimTime,Veloc_X2,'r','LineWidth',1)
     xlabel('Time [ Seconds
]','FontName','Arial','Fontsize',10,'FontWeight','Bold')
     ylabel('Velocity [ m/s
]','FontName','Arial','Fontsize',5,'FontWeight','Bold')
     title('Velocity Time Response of X2')

     subplot(6,2,5), plot(SimTime,Veloc_Y1,'r','LineWidth',1)
     xlabel('Time [ Seconds
]','FontName','Arial','Fontsize',10,'FontWeight','Bold')
     ylabel('Velocity [ m/s
]','FontName','Arial','Fontsize',5,'FontWeight','Bold')
     title('Velocity Time Response of Y1')

     subplot(6,2,7), plot(SimTime,Veloc_Y2,'r','LineWidth',1)
     xlabel('Time [ Seconds
]','FontName','Arial','Fontsize',10,'FontWeight','Bold')
     ylabel('Velocity [ m/s
]','FontName','Arial','Fontsize',5,'FontWeight','Bold')
     title('Velocity Time Response of Y2')

     subplot(6,2,9),plot(SimTime,Veloc_Z1,'r','LineWidth',1)
     xlabel('Time [ Seconds
]','FontName','Arial','Fontsize',10,'FontWeight','Bold')
     ylabel('Velocity [ m/s
]','FontName','Arial','Fontsize',5,'FontWeight','Bold')
     title('Velocity Time Response of Z1')

     subplot(6,2,11),plot(SimTime,Veloc_Z2,'r','LineWidth',1)
     xlabel('Time [ Seconds
]','FontName','Arial','Fontsize',10,'FontWeight','Bold')
     ylabel('Velocity [ m/s
]','FontName','Arial','Fontsize',5,'FontWeight','Bold')
     title('Velocity Time Response of Z2')

     subplot(6,2,2),plot(f,P1X1_dot,'r','LineWidth',1)
     xlabel('Frequency [ Hz
]','FontName','Arial','Fontsize',10,'FontWeight','Bold')
     ylabel('Velocity [ m/s
]','FontName','Arial','Fontsize',5,'FontWeight','Bold')
     title('Frequency Response of X1')


     subplot(6,2,4),plot(f,P1X2_dot,'r','LineWidth',1)
     xlabel('Frequency [ Hz
]','FontName','Arial','Fontsize',10,'FontWeight','Bold')
     ylabel('Velocity [ m/s
]','FontName','Arial','Fontsize',5,'FontWeight','Bold')
     title('Frequency Response of X2')


     subplot(6,2,6), plot(f,P1Y1_dot,'r','LineWidth',1)
     xlabel('Frequency [ Hz
]','FontName','Arial','Fontsize',10,'FontWeight','Bold')
```

```
     ylabel('Velocity [ m/s
]','FontName','Arial','Fontsize',5,'FontWeight','Bold')
     title('Frequency Response of Y1')


     subplot(6,2,8), plot(f,P1Y2_dot,'r','LineWidth',1)
     xlabel('Frequency [ Hz
]','FontName','Arial','Fontsize',10,'FontWeight','Bold')
     ylabel('Velocity [ m/s
]','FontName','Arial','Fontsize',5,'FontWeight','Bold')
     title('Frequency Response of Y2')

     subplot(6,2,10),plot(f,P1Z1_dot,'r','LineWidth',1)
     xlabel('Frequency [ Hz
]','FontName','Arial','Fontsize',10,'FontWeight','Bold')
     ylabel('Velocity [ m/s
]','FontName','Arial','Fontsize',5,'FontWeight','Bold')
     title('Frequency Response of Z1')

     subplot(6,2,12),plot(f,P1Z2_dot,'r','LineWidth',1)
     xlabel('Frequency [ Hz
]','FontName','Arial','Fontsize',10,'FontWeight','Bold')
     ylabel('Velocity [ m/s
]','FontName','Arial','Fontsize',5,'FontWeight','Bold')
     title('Frequency Response of Z2')



     figure(4)
     subplot(6,2,1),plot(SimTime,Veloc_THETA1*180/pi,'r','LineWidth',1)
     xlabel('Time [ Seconds
]','FontName','Arial','Fontsize',10,'FontWeight','Bold')
     ylabel('Angular Velocity
[degree/s]','FontName','Arial','Fontsize',5,'FontWeight','Bold')
     title('Velocity Time Response of THETA1')

     subplot(6,2,3),plot(SimTime,Veloc_THETA2*180/pi,'r','LineWidth',1)
     xlabel('Time [ Seconds
]','FontName','Arial','Fontsize',10,'FontWeight','Bold')
     ylabel('Angular Velocity
[degree/s]','FontName','Arial','Fontsize',5,'FontWeight','Bold')
     title('Velocity Time Response of THETA2')

     subplot(6,2,5),plot(SimTime,Veloc_BETA1*180/pi,'r','LineWidth',1)
     xlabel('Time [ Seconds
]','FontName','Arial','Fontsize',10,'FontWeight','Bold')
     ylabel('Angular Velocity
[degree/s]','FontName','Arial','Fontsize',5,'FontWeight','Bold')
     title('Velocity Time Response of BETA1')

     subplot(6,2,7),plot(SimTime,Veloc_BETA2*180/pi,'r','LineWidth',1)
     xlabel('Time [ Seconds
]','FontName','Arial','Fontsize',10,'FontWeight','Bold')
     ylabel('Angular Velocity
[degree/s]','FontName','Arial','Fontsize',5,'FontWeight','Bold')
     title('Velocity Time Response of BETA2')

     subplot(6,2,9),plot(SimTime,Veloc_ALPHA1*180/pi,'r','LineWidth',1)
     xlabel('Time [ Seconds
]','FontName','Arial','Fontsize',10,'FontWeight','Bold')
     ylabel('Angular Velocity
[degree/s]','FontName','Arial','Fontsize',5,'FontWeight','Bold')
     title('Velocity Time Response of ALPHA1')

     subplot(6,2,11),plot(SimTime,Veloc_ALPHA2*180/pi,'r','LineWidth',1)
```

```
     xlabel('Time [ Seconds
]','FontName','Arial','Fontsize',10,'FontWeight','Bold')
     ylabel('Angular Velocity
[degree/s]','FontName','Arial','Fontsize',5,'FontWeight','Bold')
     title('Velocity Time Response of ALPHA2')

     subplot(6,2,2),plot(f,P1THETA1_dot,'r','LineWidth',1)
     xlabel('Frequency [ Hz
]','FontName','Arial','Fontsize',10,'FontWeight','Bold')
     ylabel('Angular Velocity
[degree/s]','FontName','Arial','Fontsize',5,'FontWeight','Bold')
     title('Frequency Response of THETA1')

     subplot(6,2,4),plot(f,P1THETA2_dot,'r','LineWidth',1)
     xlabel('Frequency [ Hz
]','FontName','Arial','Fontsize',10,'FontWeight','Bold')
     ylabel('Angular Velocity
[degree/s]','FontName','Arial','Fontsize',5,'FontWeight','Bold')
     title('Frequency Response of THETA2')

     subplot(6,2,6),plot(f,P1BETA1_dot,'r','LineWidth',1)
     xlabel('Frequency [ Hz
]','FontName','Arial','Fontsize',10,'FontWeight','Bold')
     ylabel('Angular Velocity
[degree/s]','FontName','Arial','Fontsize',5,'FontWeight','Bold')
     title('Frequency Response of BETA1')

     subplot(6,2,8),plot(f,P1BETA2_dot,'r','LineWidth',1)
     xlabel('Frequency [ Hz
]','FontName','Arial','Fontsize',10,'FontWeight','Bold')
     ylabel('Angular Velocity
[degree/s]','FontName','Arial','Fontsize',5,'FontWeight','Bold')
     title('Frequency Response of BETA2')

     subplot(6,2,10),plot(f,P1ALPHA1_dot,'r','LineWidth',1)
     xlabel('Frequency [ Hz
]','FontName','Arial','Fontsize',10,'FontWeight','Bold')
     ylabel('Angular Velocity
[degree/s]','FontName','Arial','Fontsize',5,'FontWeight','Bold')
     title('Frequency Response of ALPHA1')

     subplot(6,2,12),plot(f,P1ALPHA2_dot,'r','LineWidth',1)
     xlabel('Frequency [ Hz
]','FontName','Arial','Fontsize',10,'FontWeight','Bold')
     ylabel('Angular Velocity
[degree/s]','FontName','Arial','Fontsize',5,'FontWeight','Bold')
     title('Frequency Response of ALPHA2')


     figure(5)
     subplot(6,2,1), plot(SimTime,Accel_X1,'r','LineWidth',1)
     xlabel('Time [ Seconds
]','FontName','Arial','Fontsize',10,'FontWeight','Bold')
     ylabel('Acceleration [ m/s2
]','FontName','Arial','Fontsize',5,'FontWeight','Bold')
     title('Acceleration Time Response of X1')

     subplot(6,2,3),plot(SimTime,Accel_X2,'r','LineWidth',1)
     xlabel('Time [ Seconds
]','FontName','Arial','Fontsize',10,'FontWeight','Bold')
     ylabel('Acceleration [ m/s2
]','FontName','Arial','Fontsize',5,'FontWeight','Bold')
     title('Acceleration Time Response of X2')

     subplot(6,2,5),plot(SimTime,Accel_Y1,'r','LineWidth',1)
```

```
     xlabel('Time [ Seconds
]','FontName','Arial','Fontsize',10,'FontWeight','Bold')
     ylabel('Acceleration [ m/s2
]','FontName','Arial','Fontsize',5,'FontWeight','Bold')
     title('Acceleration Time Response of Y1')

     subplot(6,2,7),plot(SimTime,Accel_Y2,'r','LineWidth',1)
     xlabel('Time [ Seconds
]','FontName','Arial','Fontsize',10,'FontWeight','Bold')
     ylabel('Acceleration [ m/s2
]','FontName','Arial','Fontsize',5,'FontWeight','Bold')
     title('Acceleration Time Response of Y2')

     subplot(6,2,9),plot(SimTime,Accel_Z1,'r','LineWidth',1)
     xlabel('Time [ Seconds
]','FontName','Arial','Fontsize',10,'FontWeight','Bold')
     ylabel('Acceleration [ m/s2
]','FontName','Arial','Fontsize',5,'FontWeight','Bold')
     title('Acceleration Time Response of Z1')

     subplot(6,2,11),plot(SimTime,Accel_Z2,'r','LineWidth',1)
     xlabel('Time [ Seconds
]','FontName','Arial','Fontsize',10,'FontWeight','Bold')
     ylabel('Acceleration [ m/s2
]','FontName','Arial','Fontsize',5,'FontWeight','Bold')
     title('Acceleration Time Response of Z2')

     subplot(6,2,2),plot(f,P1X1_Ddot,'r','LineWidth',1)
     xlabel('Frequency [ Hz
]','FontName','Arial','Fontsize',10,'FontWeight','Bold')
     ylabel('Acceleration [ m/s2
]','FontName','Arial','Fontsize',5,'FontWeight','Bold')
     title('Frequency Response of X1')

     subplot(6,2,4),plot(f,P1X2_Ddot,'r','LineWidth',1)
     xlabel('Frequency [ Hz
]','FontName','Arial','Fontsize',10,'FontWeight','Bold')
     ylabel('Acceleration [ m/s2
]','FontName','Arial','Fontsize',5,'FontWeight','Bold')
     title('Frequency Response of X2')


     subplot(6,2,6), plot(f,P1Y1_Ddot,'r','LineWidth',1)
     xlabel('Frequency [ Hz
]','FontName','Arial','Fontsize',10,'FontWeight','Bold')
     ylabel('Acceleration [ m/s2
]','FontName','Arial','Fontsize',5,'FontWeight','Bold')
     title('Frequency Response of Y1')


     subplot(6,2,8),plot(f,P1Y2_Ddot,'r','LineWidth',1)
     xlabel('Frequency [ Hz
]','FontName','Arial','Fontsize',10,'FontWeight','Bold')
     ylabel('Acceleration [ m/s2
]','FontName','Arial','Fontsize',5,'FontWeight','Bold')
     title('Frequency Response of Y2')

     subplot(6,2,10),plot(f,P1Z1_Ddot,'r','LineWidth',1)
     xlabel('Frequency [ Hz
]','FontName','Arial','Fontsize',10,'FontWeight','Bold')
     ylabel('Acceleration [ m/s2
]','FontName','Arial','Fontsize',5,'FontWeight','Bold')
     title('Frequency Response of Z1')

     subplot(6,2,12),plot(f,P1Z2_Ddot,'r','LineWidth',1)
```

```
     xlabel('Frequency [ Hz
]','FontName','Arial','Fontsize',10,'FontWeight','Bold')
     ylabel('Acceleration [ m/s2
]','FontName','Arial','Fontsize',5,'FontWeight','Bold')
     title('Frequency Response of Z2')



     figure(6)
     subplot(6,2,1),plot(SimTime,Accel_THETA1*180/pi,'r','LineWidth',1)
     xlabel('Time [ Seconds
]','FontName','Arial','Fontsize',10,'FontWeight','Bold')
     ylabel('Angular Acceleration
[degree/s2]','FontName','Arial','Fontsize',5,'FontWeight','Bold')
     title('Acceleration Time Response of THETA1')

     subplot(6,2,3),plot(SimTime,Accel_THETA2*180/pi,'r','LineWidth',1)
     xlabel('Time [ Seconds
]','FontName','Arial','Fontsize',10,'FontWeight','Bold')
     ylabel('Angular Acceleration
[degree/s2]','FontName','Arial','Fontsize',5,'FontWeight','Bold')
     title('Acceleration Time Response of THETA2')

     subplot(6,2,5),plot(SimTime,Accel_BETA1*180/pi,'r','LineWidth',1)
     xlabel('Time [ Seconds
]','FontName','Arial','Fontsize',10,'FontWeight','Bold')
     ylabel('Angular Acceleration
[degree/s2]','FontName','Arial','Fontsize',5,'FontWeight','Bold')
     title('Acceleration Time Response of BETA1')

     subplot(6,2,7),plot(SimTime,Accel_BETA2*180/pi,'r','LineWidth',1)
     xlabel('Time [ Seconds
]','FontName','Arial','Fontsize',10,'FontWeight','Bold')
     ylabel('Angular Acceleration
[degree/s2]','FontName','Arial','Fontsize',5,'FontWeight','Bold')
     title('Acceleration Time Response of BETA2')

     subplot(6,2,9),plot(SimTime,Accel_ALPHA1*180/pi,'r','LineWidth',1)
     xlabel('Time [ Seconds
]','FontName','Arial','Fontsize',10,'FontWeight','Bold')
     ylabel('Angular Acceleration
[degree/s2]','FontName','Arial','Fontsize',5,'FontWeight','Bold')
     title('Acceleration Time Response of ALPHA1')

     subplot(6,2,11),plot(SimTime,Accel_ALPHA2*180/pi,'r','LineWidth',1)
     xlabel('Time [ Seconds
]','FontName','Arial','Fontsize',10,'FontWeight','Bold')
     ylabel('Angular Acceleration
[degree/s2]','FontName','Arial','Fontsize',5,'FontWeight','Bold')
     title('Acceleration Time Response of ALPHA2')

     subplot(6,2,2),plot(f,P1THETA1_Ddot,'r','LineWidth',1)
     xlabel('Frequency [ Hz
]','FontName','Arial','Fontsize',10,'FontWeight','Bold')
     ylabel('Angular Acceleration
[degree/s2]','FontName','Arial','Fontsize',5,'FontWeight','Bold')
     title('Frequency Response of THETA1')

     subplot(6,2,4),plot(f,P1THETA2_Ddot,'r','LineWidth',1)
     xlabel('Frequency [ Hz
]','FontName','Arial','Fontsize',10,'FontWeight','Bold')
     ylabel('Angular Acceleration
[degree/s2]','FontName','Arial','Fontsize',5,'FontWeight','Bold')
     title('Frequency Response of THETA2')

     subplot(6,2,6),plot(f,P1BETA1_Ddot,'r','LineWidth',1)
```

```
     xlabel('Frequency [ Hz
]','FontName','Arial','Fontsize',10,'FontWeight','Bold')
     ylabel('Angular Acceleration
[degree/s2]','FontName','Arial','Fontsize',5,'FontWeight','Bold')
     title('Frequency Response of BETA1')

     subplot(6,2,8),plot(f,P1BETA2_Ddot,'r','LineWidth',1)
     xlabel('Frequency [ Hz
]','FontName','Arial','Fontsize',10,'FontWeight','Bold')
     ylabel('Angular Acceleration
[degree/s2]','FontName','Arial','Fontsize',5,'FontWeight','Bold')
     title('Frequency Response of BETA2')

     subplot(6,2,10),plot(f,P1ALPHA1_Ddot,'r','LineWidth',1)
     xlabel('Frequency [ Hz
]','FontName','Arial','Fontsize',10,'FontWeight','Bold')
     ylabel('Angular Acceleration
[degree/s2]','FontName','Arial','Fontsize',5,'FontWeight','Bold')
     title('Frequency Response of ALPHA1')

     subplot(6,2,12),plot(f,P1ALPHA2_Ddot,'r','LineWidth',1)
     xlabel('Frequency [ Hz
]','FontName','Arial','Fontsize',10,'FontWeight','Bold')
     ylabel('Angular Acceleration
[degree/s2]','FontName','Arial','Fontsize',5,'FontWeight','Bold')
     title('Frequency Response of ALPHA2')
```